THE UNIVERSITY OF MICHIGAN
COLLEGE OF ENGINEERING
Department of Chemical and Metallurgical Engineering

Technical Report

THERMODYNAMIC MEASUREMENTS USING OPTICAL ABSORPTION IN METAL VAPORS

Philip A. Rice
David A. Ragone
James A. Craig

ORA Project 02668

under contract with:

U. S. ATOMIC ENERGY COMMISSION
CHICAGO OPERATIONS OFFICE
CONTRACT NO. AT(11-1)-543
LEMONT, ILLINOIS

administered through:

OFFICE OF RESEARCH ADMINISTRATION ANN ARBOR

August 1962

This report was also a dissertation submitted in partial fulfillment of the requirements for the degree of Doctor of Philosophy in The University of Michigan, 1962.

TABLE OF CONTENTS

LIST OF TABLES

LIST OF FIGURES

LIST OF APPENDICES

NOMENCLATURE

N	Concentration of the absorbing atoms in atoms/cc
N'	Concentration of excited atoms in atoms/cc
N_I	Concentration of the broadening gas in atoms/cc
I_t	Intensity of transmitted light
I_o	Intensity of light before absorption
I_ω	Intensity of light at wave number ω
P_ω	Absorption coefficient at wave number ω in cm^2/atom
ℓ	Length of the light absorption path, cm
X	Optical density in atoms/cm^2, equals $N\ell$
c	Velocity of light in cm/sec.
g_2/g_1	Ratio of the statistical weights of the excited and ground states
S	Integrated intensity, equals $\int P_\omega \, d\omega$
b_D	Doppler half-breadth: equals the half-breadth of the absorption line when P_ω is half its maximum value and only Doppler broadening is present. $$b_D = \left(\frac{2RT \ln 2}{mc^2}\right)^{\frac{1}{2}} \omega_o, \ cm^{-1}$$
b_N	Natural half-breadth arising from the inherent uncertainty in the energy levels. It equals the half-breadth of the absorption line when P_ω is half its maximum value and only natural broadening is present. $$b_N = \frac{1}{4\pi c\tau}, \quad cm^{-1}$$
b_C	Collision half-breadth due to interactions between the absorbing atoms and the other atoms present. It equals the half-breadth of the absorption line when P_ω is half its maximum value and only collision broadening is present. $$b_C = \frac{\sigma_I^2}{\pi c} N_I \times \left(2\pi RT \left(1/M1 + 1/M2\right)\right)^{\frac{1}{2}}, \ cm^{-1}$$
b_S	Self-broadening half-breadth resulting from interactions between the absorbing atoms themselves. It equals the half-breadth of the absorption line when P_ω is half its maximum value and only self-broadening is present $$b_s = \frac{\sigma_s^2}{\pi c} \ p \ a \left(\frac{2\pi}{RT} \times \frac{2}{M1}\right)^{\frac{1}{2}} \ cm^{-1}$$

b	$b_N + b_C$
M_1 or M	Molecular weight of the absorbing gas
M_2	Molecular weight of the broadening gas
T	Absolute temperature in °K
p	Vapor pressure of absorbing gas, atm
ΔH_V	Heat of vaporization of absorbing gas
Δc_p	Difference between the constant pressure heat capacities of the absorbing gas and its equilibrium liquid
R	Gas constant
C_I	Integration const for the Clapeyron Equation
ω	Wave-number = $1/\lambda$, cm^{-1}
λ	Wavelength
τ	Average lifetime in the excited state, sec
σ_I^2	Optical collision cross-section, sq. Å
β	The total energy absorbed over the incident intensity, cm^{-1}
σ_s^2	Optical Collision cross-section for self-broadening, sq. Å
T_R	The transmittance of an absorption band
f	Fugacity
a	Avagadro's number
A	Area of the absorption line
cu.	Chart Units
Sq. in.	Square inches

SUBSCRIPTS

self	Absorption data are self-broadened
no self	Absorption values are not affected by self-broadening
SQRT	Absorption data are proportional to the square root of the vapor concentration
LIN	Absorption data are directly proportional to the vapor concentration
t	Indicates data taken at 746 mm Hg helium pressure
0	Absorption data were taken at zero helium pressure
f	Absorption data have been corrected for self-broadening and hyperfine structure

ABSTRACT

The purpose of this study has been to investigate the amount and the reliability of the thermodynamic information which can be obtained by measuring the absorption of light in spectral lines and bands by metal vapors. The technique involves measuring the amount of light absorbed in particular small wavelength regions corresponding to the electronic transitions of gaseous atoms and molecules. The relationships existing between the amount of light absorbed by the equilibrium vapor and the vapor pressure were ascertained as a function of temperature. These were then used to deduce relationships from which activities of an element in solution and its heat of solution were calculated.

Optical absorption measurements were made for pure lead, pure bismuth, a test lead-bismuth alloy, and a uranium-bismuth alloy. From these measurements, the activities of lead and bismuth in the lead-bismuth alloy, the activity of bismuth in U-Bi, and the heats of vaporization of lead and atomic and diatomic bismuth were calculated.

The values of the heats of vaporization at 298°K obtained in this work are given in the table below along with appropriate values obtained by other workers.

	THIS WORK	BRACKETT AND BREWER
$\Delta H_{V_{Bi},\ 298°K}$	$49{,}600 \pm 1100$ cal/gm mole	$49{,}500 \pm 1000$ cal/gm mole
$\Delta H_{V_{Bi_2},298°K}$	$49{,}430 \pm 2000$ cal/gm mole	$52{,}500 \pm 2000$ cal/gm mole
		STULL AND SINKE
$\Delta H_{V_{Pb},\ 298°K}$	$47{,}240 \pm 850$ cal/gm mole	$46{,}800 \pm 300$ cal/gm mole

Also calculated from the measurements of the 3067Å Bi and 2833Å Pb absorption lines were the vapor pressure of atomic bismuth, the lifetimes of the excited states and the optical collision cross sections for He-Bi and

He-Pb and self collision cross sections for bismuth and lead.

The method is a useful one for measuring thermodynamic properties of alloys, if one is careful to correct for or mask out unwanted contributions to the absorption lines and bands. It is more accurate for determining activities and heats of vaporization than for determining absolute vapor pressures or heats of solution. It is relatively quick and allows independent measurements of a number of species in the vapor.

CHAPTER I

INTRODUCTION

The thermodynamic properties of alloys are commonly determined by effusion cell, gas transport, ebulition, or electrochemical techniques. All but the electrochemical method measure the vapor pressure of a particular element above an alloy and use this parameter to calculate the thermodynamic properties of the element in the alloy. Effusion cell and gas transport techniques are generally only applicable to systems which have vapor pressures between 10^{-8} - 10^{-5} mm Hg., since above these pressures bulk flow becomes a significant factor. On the other hand, ebulition point techniques are accurate only for vapor pressures above 0.1 mm Hg. For all three of these vapor pressure methods the relative amounts of each species must be known if there is more than one specie in the vapor. Electrochemical measurements are also often impossible in metal alloy systems because potential cells cannot be constructed at the necessary high temperatures. A technique which is especially applicable in the vapor pressure range of 10^{-5} - 1 mm Hg and which can easily measure more than one specie in the vapor is needed. Optical absorption is a likely candidate since the spectra of different absorption species are independent of one another. The method has not been widely used because of the difficulties in relating the optical absorption data to the vapor pressures of the elements of interest. Thus, the purpose of this work has been to examine more fully optical absorption as a method for determining the thermodynamic properties of alloys. To do this the thermodynamic information which can be obtained by measuring optical absorption parameters was defined and the reliability of this information, once it had been obtained, was estimated. Also, because the possibility became apparent during the course of the investigation, both

the lifetime in the excited state of the Bi 3067Å line and the vapor pressure of atomic bismuth were determined simultaneously, using the Clapeyron Equation and proper optical absorption measurements.

CHAPTER II

DESCRIPTION OF THE METHOD

Optical absorption utilizes the fact that atoms and molecules absorb radiation at certain characteristic frequencies. Every kind of atom has a particular set of absorption frequencies which correspond to a particular set of energy levels. Briefly the method consists of directing a parallel beam of continuous-spectrum light through an absorption cell which contains the absorbing atoms in a certain concentration. The light radiation is absorbed in certain narrow frequency ranges by the atoms or molecules in the vapor. The amount of absorption is then recorded by a spectrometer in the form of an intensity versus frequency trace. Auxiliary equipment is used to control the temperature and the total pressure at which the absorption takes place. The principal components of the experimental apparatus are shown in Figure 1 with a more complete description given in Appendix A.

Using optical absorption to measure thermodynamic properties involves two general steps: the calculation of the concentration of absorbing atoms or molecules in the vapor from the measured optical absorption parameters and the calculation of the thermodynamic properties of the condensed alloy phase from the vapor concentration. In this dissertation the two calculations are discussed in terms of the measurements which must be made and the errors which may arise. Then the experimental results of a number of example systems are compared with those which are predicted by theory and with those obtained by other experimental techniques. In conclusion the advantages and disadvantages of the method are discussed, the possible experimental results which may be obtained using the method are summarized, and the magnitude of the errors involved when the method is used are estimated.

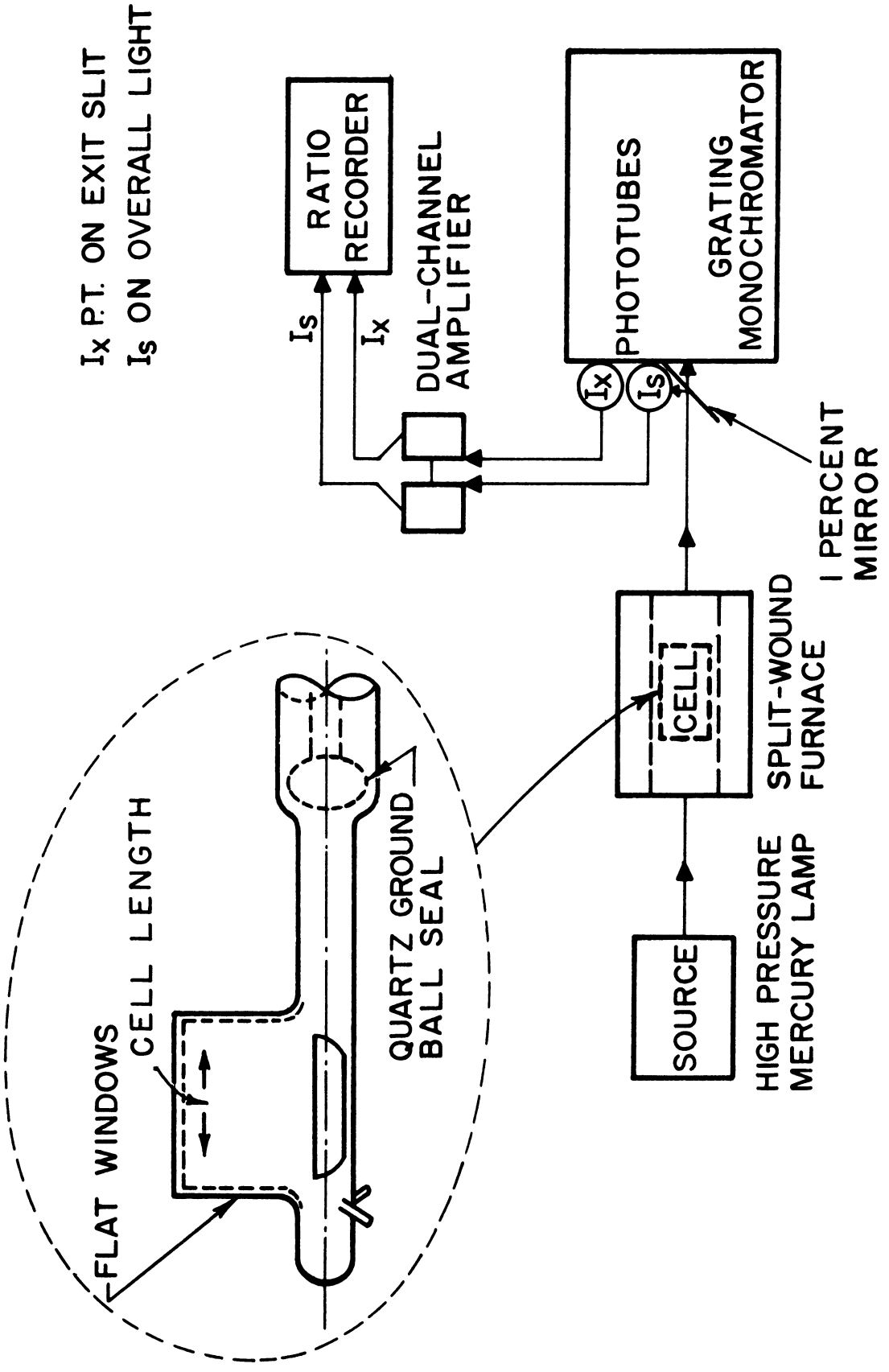

Figure 1. Schematic of Experimental Apparatus

CHAPTER III

HISTORY OF METHOD

Optical absorption has most commonly been used to determine the lifetimes of the excited states of elements which have known vapor pressures[2]. The method was first used for thermodynamic measurements in 1929 by Hirst and Olson[11], who measured the thermodynamic properties of certain mercury amalgams using mercury vapor as their absorbing species. In 1941, Herbenar, Siebert, and Duffendack[10], using zinc as the absorber, determined the thermodynamic properties of zinc in alpha brasses. Scatchard and Westland[21] in 1953, again using zinc as the absorbing species, measured the thermodynamic properties in alpha silver-zinc alloys. Scatchard and Boyd[22] in 1956, using cadmium as the absorber, determined the thermodynamic properties of alpha silver-cadmium alloys. In 1959, Cosgarea, Ragone, and Hucke[5] used the optical absorption of atomic and diatomic bismuth vapor to determine the thermodyanmic properties of uranium-bismuth alloys. Finally, Vidale[25], in 1960 used optical absorption to determine the heat of formation of silicon carbide, the heat of vaporization of sodium in sodium silicate glass, and the f-value of copper 3247$\mathring{A}$ line. In all of these measurements, Beer's law was used to relate the ratio of the incident and transmitted intensities to the concentration of the absorbing species in the vapor. Except where zinc or diatomic bismuth had been used as the absorbing species, the absorption coefficient varied with the concentration of the absorbing species.

Until Vidale made his measurements in 1960, no one corrected their atomic absorption data for the line distortion of the spectrometer grating and slits, the hyperfine structure of the absorption line, and the total pressure in the absorption cell. Because these effects can greatly alter the absorption line size and shape, Beer's Law cannot reliably be directly applied to monatomic absorption data.

The atomic absorption measurements made in this study differ from those discussed above in that the measure of light absorption is the area of the absorption line divided by the incident intensity rather than the ratio of the incident intensity to the transmitted intensity. (See Figure 2.) This measure, called the total absorption, has the advantage of being relatively insensitive to the resolution of the spectral instrument. The diatomic bismuth absorption measurements of this study were correlated using Beer's Law since this relationship had been successfully applied previously and is predicted theoretically for absorption bands.

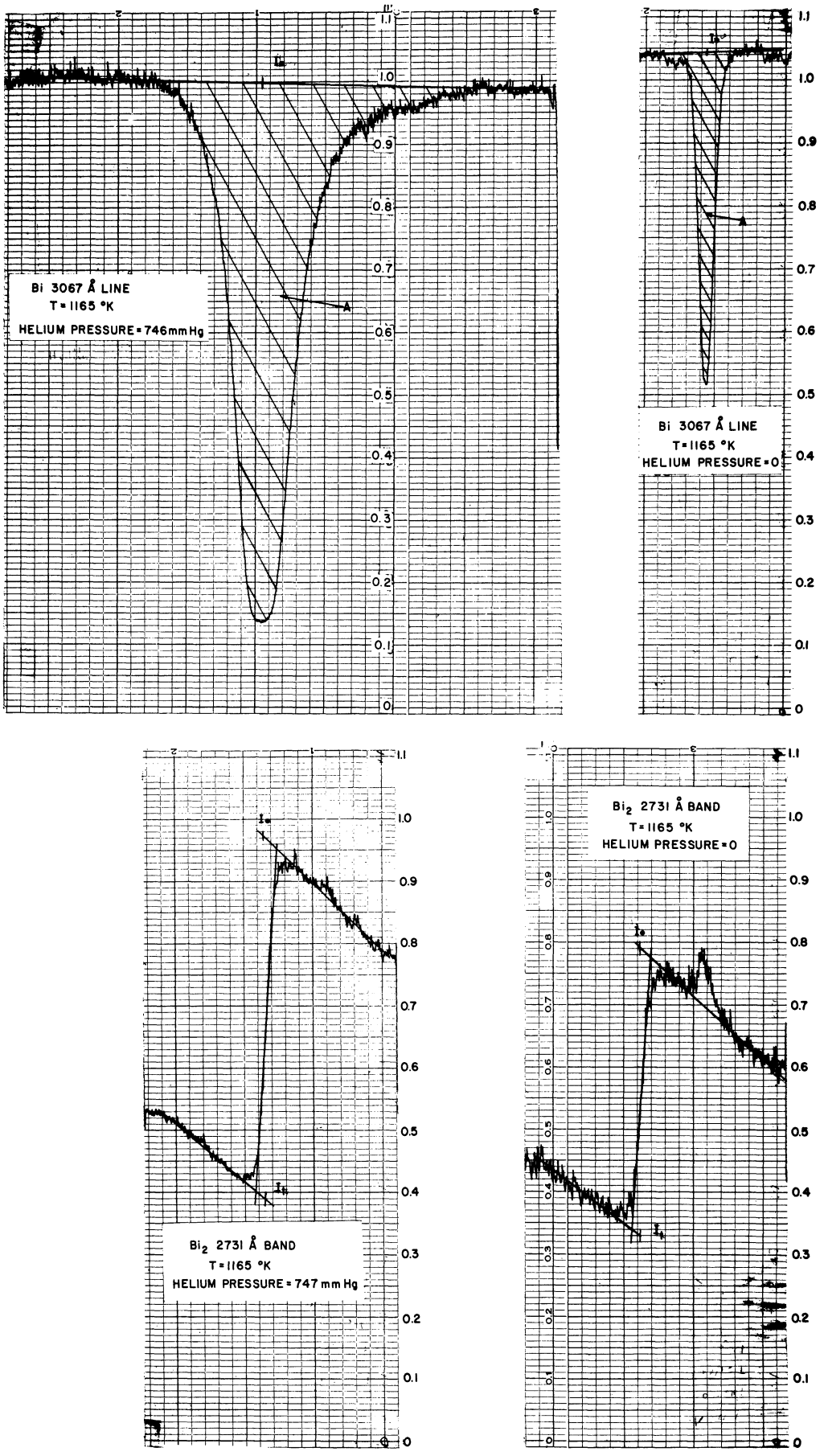

Figure 2. Representative Absorption Lines and Bands

CHAPTER IV

OPTICAL ABSORPTION THEORY

A. Introduction

Optical absorption theory describes the interaction of light quanta with atoms and molecules and relates the amount of light absorbed as a function of frequency to the concentration of the absorbing atoms or molecules. The bases of the description of this interaction are the electromagnetic theory of light and the quantum theory of matter. The first step in the description of light absorption by atoms or molecules is to calculate the probability of photons being absorbed at a wave number, ω, for light of intensity I_ω incident on the absorbing atom or molecule. An absorption coefficient can be defined in terms of this probability. When the absorption coefficient is known as a function of the light frequency, the absorption line or band is then fully described. The absorption coefficients for the various processes contributing to light absorption by gaseous atoms and dimers have been derived for some time[9], and the final forms of these coefficients are used without proof in this presentation.

B. Absorption by Atoms

General. The simplest case of light absorption is by gaseous atoms. If the absorbing atoms were motionless and the energy levels associated with these atoms were infinitely narrow, then light would be absorbed only at a particular set of frequencies. The energy change associated with one of these frequencies, corresponds to the energy of the photon absorbed, i.e., it equals Planck's constant, h, times ν_o, the frequency of the light absorbed. Because of the thermal motion and the Heisenberg uncertainty in the energy levels, absorption takes place in a narrow frequency range about the characteristic frequency, ν_o. If collisions also occur between the absorbing

atoms and other absorbing atoms or any other gaseous atoms which are present, the average uncertainty of the energy levels is increased and the permissible frequency range for absorption is broadened further. All of the above processes predict absorption lines which have a narrow frequency width. In practice the theoretical widths of these lines are ordinarily greatly increased by the distortion resulting from the finite slit widths and finite resolution of the recording spectrometer. Figure 2 shows several experimental absorption lines at 3067Å for atomic bismuth vapor. The widths of these experimental lines are approximately 65 times the theoretical widths calculated for the same lines.

Figure 1, the schematic diagram of the apparatus, shows light from a continuous-spectrum source passing through the absorption cell to a spectrometer where it is recorded as the ratio of I_ω (intensity at wave number ω out of the cell) to I_o (the intensity incident on the cell).

The change of intensity of light at wave number, ω, as it passes through a medium of optical density X is given by Beer's Law:

$$\frac{dI_\omega}{I_\omega} = -P_\omega dX \qquad (1)$$

where:

I_ω = intensity at wave number ω

P_ω = absorption coefficient at wave number ω in cm^2/atom

X = optical density in atoms/cm^2 = Nℓ

N = concentration of absorbing atoms in atoms/cm^3

ℓ = length of the absorption path in cm

The amount of energy absorbed by the vapors divided by the incident intensity is given by β, the total absorption, as follows:

$$\beta = \int_0^\infty \frac{I_o - I_\omega}{I_o} \, d\omega \tag{2}$$

$$\beta = \int_0^\infty \left(1 - e^{-P_\omega X}\right) d\omega \tag{3}$$

β is related to the number of atoms in the path of the light beam. If we assume an ideal gas, then the number of atoms is directly proportional to the pressure of the gaseous species through which the light is being passed.

If we define a parameter S (a constant for a given absorption species)* as:

$$S = \int_0^\infty P_\omega d\omega, \tag{4}$$

the various contributions to absorption line width from Doppler broadening (due to thermal motion), natural broadening (Heisenberg uncertainty in energy levels), and collision broadening are expressed in terms of the absorption coefficient as follows:

For Doppler broadening:

$$P_\omega = \frac{S}{b_D} \sqrt{\ell n 2} \quad \exp\left(-\frac{\omega-\omega_o}{b_D} \sqrt{\ell n 2}\right)^2 \tag{5}$$

where:

b_D = Doppler half-breadth

ω_o = wave number at center of line.

For natural and collision broadening: (also called dispersion broadening):

$$P_\omega = \frac{Sb}{\pi} \quad \frac{1}{(\omega-\omega_o)^2+b^2} \tag{6}$$

where:

$b = b_N + b_C$

b_N = natural half-breadth

b_C = collision half-breadth = $\frac{\sigma_I^2}{\pi c} N_I \left[2\pi RT \left(1/M_1 + 1/M_2\right)\right]^{\frac{1}{2}}$

σ_I^2 = optical collision cross section

N_I = concentration of broadening gas

M_1 = molecular weight of absorbing species

M_2 = molecular weight of the broadening gas

*Appendix C

A total absorption coefficient, incorporating both Doppler and dispersion broadening, can be found by superimposing equations (5) and (6).* The resulting expression can then be substituted into equation (3) and the total absorption evaluated as a function of the optical density.

Two limiting cases result. When $P_\omega X$ is small enough so that $e^{-P_\omega X} \approx 1-P_\omega X$, then

$$\beta = \int_0^\infty P_\omega X d\omega = SX \qquad (7)$$

In this case the energy absorbed is proportional to the first power of the number of atoms present in the vapor. On the other hand, when $P_\omega X$ is so large that the center of the line is completely absorbed, then:*

$$\beta = \sqrt{2\ SbX} \qquad (8)$$

and the total absorption is proportional to the square root of the vapor concentration. This law is referred to as the square root absorption law.

The total absorption has also been evaluated for intermediate values of optical density.(23), (24) The results are presented in Figure 3 in the form of a plot of:

$$\frac{\beta}{2b_D}\sqrt{\ln 2} \qquad \text{vs.} \qquad \frac{6\ SX\sqrt{\ln 2}}{b_D}$$

It can be seen from this figure that in the square root absorption law region the measured parameter, β, for any optical density, X, can be increased markedly by increasing α. In turn, α can be increased by increasing b_C, the collision half-breadth, which can be accomplished by introducing a foreign gas, such as helium. This property is often useful since it allows the amplification of weak absorption lines and also provides a means of identifying the particular absorption law to apply to a set of experimental data.

Note here also that the two limiting abosrption laws can be predicted from dispersion (natural + collision) broadening alone. Examination of

*Appendix D

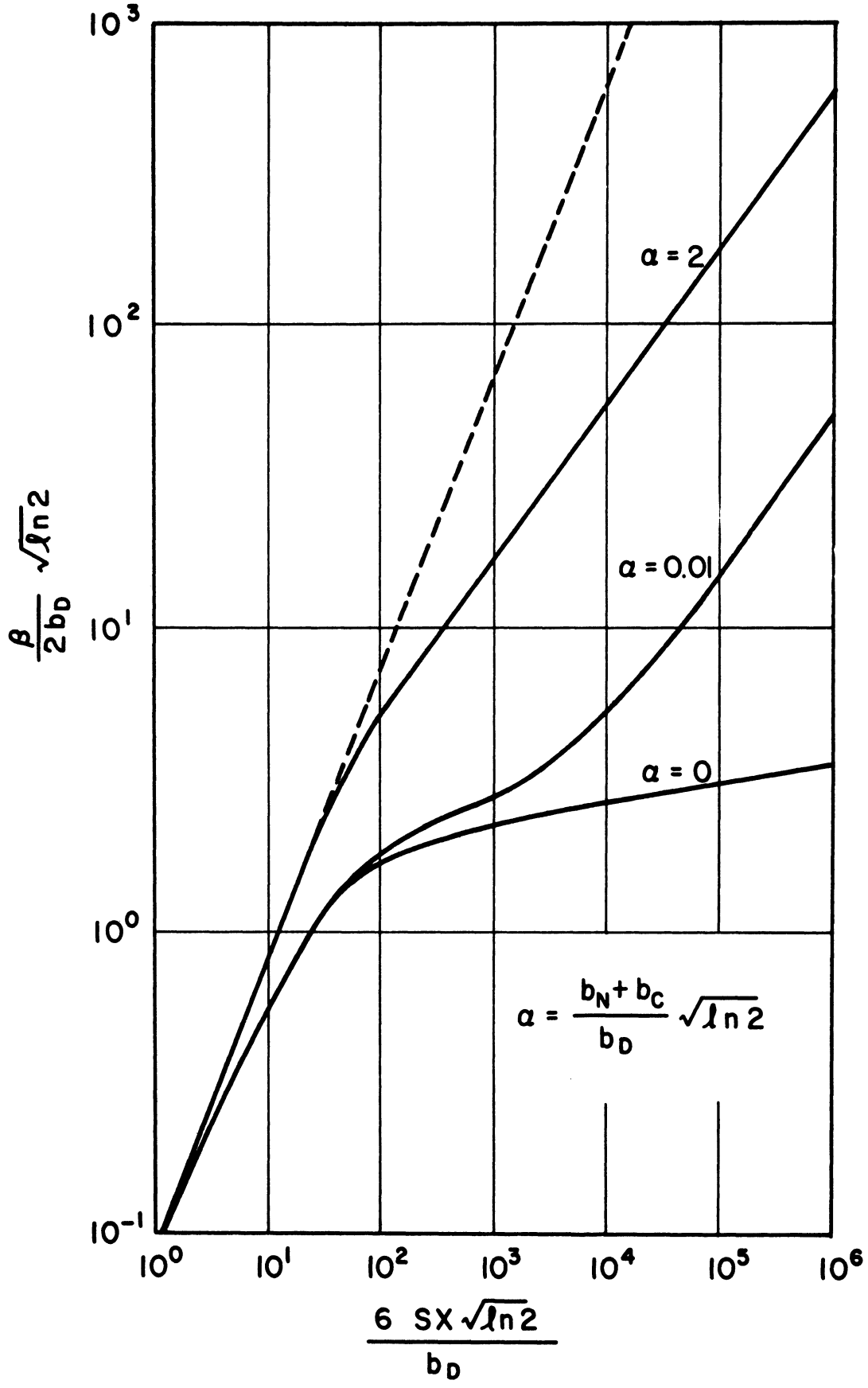

Figure 3. Van der Held Plot

Figure 3 shows that these two limiting cases account for all the portions of the graph except for the almost horizontal curves which appear at low α's and low optical densities. Only in this region is Doppler broadening an important factor in determining the integrated area of the absorption line.

Hyperfine Structure and Self-Broadening. In addition to Doppler, natural, and foreign gas collision broadening, two other phenomena often significantly influence the shape of the absorption line. They are the hyperfine structure of the absorption line and the collision broadening of the line resulting from the collisions between the absorbing atoms themselves (called self-broadening).

The hyperfine structure of the line results from various isotopes of an element or from the different nuclear spin states of a single isotope. This means that what is ordinarily seen as a single absorption line can really be a series of several lines very close together. When the total line width is so great that all the hyperfine components completely overlap, the hyperfine structure has no effect on the magnitude of the total absorption.* It can also be shown that the hyperfine structure has no effect, regardless of the component separation, when the total absorption is proportional to the first power of concentration of absorbing atoms since the contributions of the various hyperfine components add linearly.

Hyperfine structure has its maximum effect when the total absorption is not proportional to the first power of concentration and the hyperfine components are completely separate. For example, if the total absorption is proportional to the square root of the concentration, then, for n equally intense, completely separate components, the total absorption is increased by a factor, $\sqrt{n}$.* On the other hand, if the absorption line has a Doppler shape, the effect of the hyperfine components on the total absorption may

*Appendix F

be determined using the δ factors calculated by Landenburg and Levy[13] and tabulated by Mitchell and Zermansky[15] and Penner[16].

Important for this work is the case when the total absorption follows the square root law for any single hyperfine component and the various components are neither completely separated nor completely overlapped.

To evaluate the effect of hyperfine structure in this case, an expression for the absorption coefficient, which accounts for the absorption by each hyperfine component, must be substituted into the expression for the total absorption and the integral evaluated numerically. Of particular interest here is the effect of hyperfine structure on the Bi 3067Å line and the Pb 2833Å line. The bismuth line has six hyperfine components spread over a distance of 1.06 cm^{-1} and the lead line has a fine component structure spread over 0.54 cm^{-1}. The spacings and relative strengths of the components of these two lines are shown in Figure 4.

The absorption coefficient for an absorption line made up of n hyperfine components, each of which follows the square root absorption law and has its center at a particular ω_{oi}, is written as:

$$P_\omega = \frac{Sb}{\pi X} \sum_{i=1}^{n} \frac{X_i}{(\omega-\omega_{oi})^2} \qquad (9)$$

Where X_i is the optical density of associated with component i. This coefficient can be introduced into the expression for the total absorption, β, and the integral divided by the expression for the total absorption in the square root region if there were no hyperfine structure. The resultant expression, shown below, represents a correction factor which can be applied to absorption data taken in the square root region.

$$F(\beta) = \frac{1}{\beta_{NH}} \int_{-\infty}^{\infty} \left[1 - \exp(-P_\omega X)\right] d\omega \qquad (10)$$

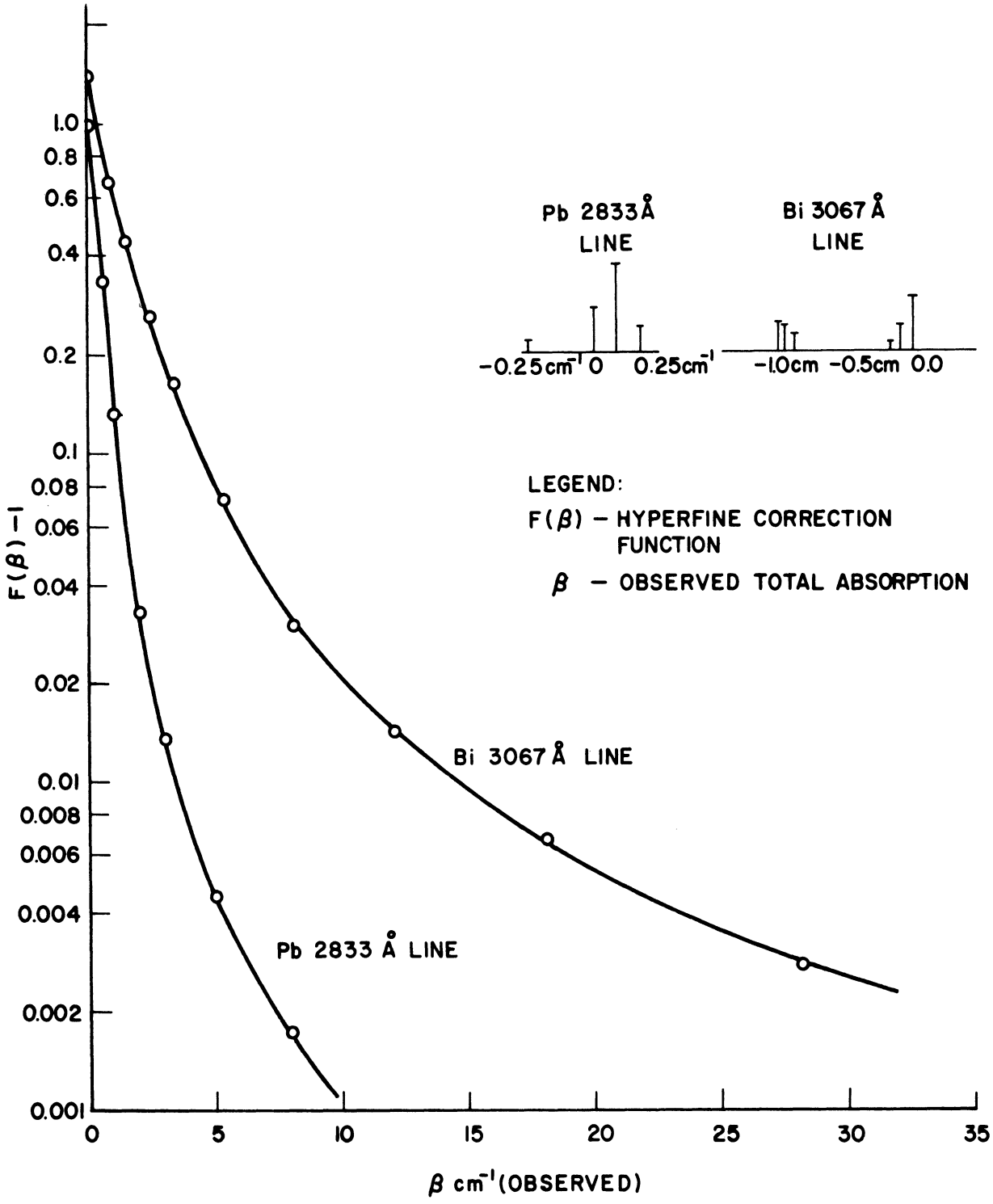

Figure 4. Hyperfine Correction Function

where:

β_{NH} = the total absorption if no hyperfine structure were present

The preceding integral was evaluated numerically as a function of β_{NH} for the hyperfine structures of the 3067Å line and the Pb 2833Å line using an IBM 709 digital computer. The resulting values of $F(\beta)$ are plotted as a function of β (the observed total absorption) in Figure 4. The limits of complete separation and complete overlap of the hyperfine components can be calculated from $\sum_{i=1}^{n} \sqrt{X_i} \Big/ \sqrt{\sum_{i=1}^{n} X_i}$ * and are shown also on the graph. Note also that the hyperfine contribution to the total absorption decreases markedly with increasing optical density for the smaller hyperfine separation of the Pb 2833Å line.

The second broadening process to be considered in this section, self broadening, influences the line shape in the same way as collision broadening by a foreign gas. In this case, however, the concentration of broadening gas in the expression for the collision half-breadth is also the concentration of the absorbing gas. Thus, if self-broadening is significant, total absorption data, taken at concentrations where the center of the absorption line is totally absorbed, is no longer proportional to the square root of the concentration, but follows the relationship shown below:

$$\beta = 2\sqrt{SbX + SC_S X^2} \qquad (11)$$

where: $b_S = C_S X$

and: $C_S = \frac{\alpha_S^2}{\pi c} (2\pi RT(2/M_1))^{\frac{1}{2}}$

Equation 11 also shows that, if self-broadening dominates ($C_S X^2 >> bX$) over all other broadening effects, then the total absorption becomes directly proportional to the concentration of absorbing atoms.

* Appendix F

The ratio of the square of the observed total absorption (with self-broadening) to the square of the total absorption with no self-broadening can be used to directly calculate the self-collision cross-section if the lifetime of the excited state of the observed line and the number density of the absorbing atoms are known. In a system where the absorbing gas is in equilibrium with a condensed phase, the total absorption with no self-broadening and the self-collision cross-section can be calculated from the observed total absorption data using the lifetime of the excited state and the heat of vaporization of the absorbing gas. The method for doing this is discussed in Appendix G.

The effects of both hyperfine structure and self-broadening can be controlled to an extent by varying the amount of foreign gas collision broadening, since the introduction of a foreign gas can greatly increase the line size. In the case of hyperfine structure, this leads to a greater overlapping of the hyperfine components and consequently a reduced contribution to the total absorption. In the case of self-broadening, the foreign gas collision broadening can increase the line size to such an extent that the contribution from self-broadening can often be neglected.

The contribution to the total absorption data from natural and self-broadening can also be subtracted from total absorption measurements made at some inert gas pressure, p. Subtracting the natural, and self-broadening contributions yields total absorption values which would result from foreign gas collision broadening alone. This is done for absorption data following the square root law in the following way:

$$\beta_{\text{collision}} = \left(\beta^2_{\substack{\text{natural + self} \\ \text{+ collision}}} - \beta^2_{\text{natural + self}} \right)^{\frac{1}{2}} \qquad (12)$$

Simultaneous Determination of τ and N. From a set of absorption measurements, the lifetime of an atom in the excited state corresponding to an absorption line can be determined directly if the concentration of atoms is known or the concentration can be determined directly if the lifetime is known. Both cannot be determined simultaneously, however, unless another independent relationship exists between the concentration (N) and the lifetime (τ). If the absorbing gas is in equilibrium with a condensed phase, the two limiting absorption laws which arise for high and low atomic concentrations, respectively, can be used as two independent relationships between N and τ. This is permitted because the absorption measurements made in the different concentration regions can be tied together with the Clapeyron Equation.* If absorption measurements are also made under an inert gas pressure, the optical collision cross-section between the absorbing and inert atoms may be calculated.

In order to carry out the above scheme, absorption data must be obtained as a function of temperature in both the temperature range where the total absorption is proportional to the first power of the optical density and in the temperature range where the total absorption is proportional to the square root of the optical density. The data following the square root absorption law is then extrapolated, using the Clapeyron Equation, to the temperature range where the total absorption is directly proportional to the concentration. Comparing the two absorption laws at constant temperature (constant number density) implies the following relationship:

$$r = \beta^2_{SQRT}/\beta_{LIN} = \frac{4SbX}{SX} = 4b \qquad (13)$$

If the square root data has not been significantly affected by collision broadening or the hyperfine structure of the absorption line, the dispersion

*See section on the Use of the Calpeyron Equation.

half-breadth, b, is b_N, the natural half-breadth. The lifetime, τ, and the integrated intensity, S, can now be calculated since:

$$b_N = \frac{1}{4\pi c\tau} \tag{14}$$

and

$$S = \frac{\lambda\sigma^2}{8\pi c} \quad \frac{g_2}{g_1} \quad \frac{1}{\tau} \tag{15}$$

Once b_N and S are known, the density of absorbing atoms can be calculated either from Equation (8), using the data following the square root law, or from Equation (7), using the data following the linear absorption law.

The optical collision cross-section can also be determined if additional total absorption data following the square root law is taken under a particular inert gas pressure. From the ratio of the total absorption at pressure, p_I to the total absorption at zero inert gas pressure (at the same concentration of absorbing atoms), the collision half-breadth, b_C, can be calculated since:

$$\frac{\beta^2_{SQRT,\ p_I}}{\beta^2_{SQRT,\ 0}} = \frac{b_C + b_N}{b_N} = 1 + \frac{b_C}{b_N} \tag{16}$$

Since the collision cross-section σ_I^2, is related to b_C by:

$$b_C = \frac{\sigma_I^2}{\pi c} \quad N_I \quad \times \quad \left[2\pi RT\ (1/M_1 + 1/M_2)\right]^{\frac{1}{2}} \tag{17}$$

σ_I^2 can also be calculated since all the other parameters in the above equation have been previously determined.

The accuracy of the above procedure depends largely on the accuracy of the extrapolation of the data following one absorption law to a concentration region where another absorption law holds. Consequently, it is important that the square root absorption data taken at zero inert gas pressure be corrected for self-broadening and hyperfine structure, when these effects are significant.

C. Absorption By Molecules

If the absorption species are molecules rather than atoms, then light is absorbed in frequency bands. These absorption bands are made up of very closely spaced absorption lines, which arise because the absorbing molecules not only change their electronic energy states but their vibrational and rotational energy states as well. Often associated with these bands are band heads. These occur at the maximum frequencies at which absorption takes place in a band and correspond to the frequencies where the absorption line density is the highest. While the individual lines which make up the band can be treated by the same theories which apply to atomic absorption lines, the situation is generally such that the individual lines of the band are so closely spaced that they are unresolved by the spectrometer or they are so broad as to completely overlap each other. The experimental result in either case is a continuous band of absorption such as is shown in Figure 1 for the 2731Å absorption band of the bismuth dimer in the vapor.

The theoretical treatment for absorption lines has been extended by Elasser [6] to an absorption band made up of an infinite number of equally spaced equally intense dispersion broadened absorption lines. For this kind of band, the absorption coefficient P_ω is given by:

$$P_\omega = \sum_{n=1}^{\infty} \frac{Sb}{\pi} \frac{1}{(\omega - nd)^2 + b^2} \qquad (18)$$

where:

d = distance between lines in cm^{-1}

b = half-breadth of the individual lines in cm^{-1}

An absorption coefficient of this form leads to a series of limiting cases* for the transmittance of the band as a function of the optical density, X. The transmittance is the average ratio of the transmitted

*Appendix E

intensity to the incident intensity for the absorption band and is equal to $\frac{1}{\Delta\omega} \int_{\Delta\omega} I_\omega / I_o \, d\omega$.

This absorption coefficient permits the transmittance of the absorption band to be expressed in terms of the optical density. Three limiting absorption laws* can be derived depending upon the magnitude of the optical density and the ratio of the line breadth to the line spacing. Since the transmittance is defined as:

$$T_R = \frac{1}{\Delta\omega} \int_{\Delta\omega} I\omega / I_o \, d\omega, \tag{19}$$

then, if $b << d$

$$T_R = 1 - \frac{SX}{d} \qquad \text{when } \frac{SX}{2\pi b} << \frac{2}{\pi} \tag{20}$$

and

$$T_R = 1\text{-erf}\left(\frac{\sqrt{\pi SbX}}{d}\right) \qquad \text{when } \frac{SX}{2\pi b} >> \frac{2}{\pi} \tag{21}$$

On the other hand if $b >> d$,

$$T_R = \exp(-\frac{SX}{d}) \tag{22}$$

Since the second expression above depends on the half-breadth of the absorption lines, and the half-breadth can be increased by collision broadening, the effect on the transmittance of an added inert gas indicates whether $b << d$ or vice-versa.

When $b >> d$ in an Elasser band, Beer's law is predicted. Beer's law is also predicted when $b >> d$ for an absorption band made up of a large number of absorption lines which have completely random spacings and intensities[17] (in direct contrast to the regularity of an Elasser band). Therefore, it is reasonable to assume that Beer's law should also hold for a real absorption band (which is neither completely regular or random) whenever $b >> d$.

*Appendix E

D. Other Effects

Several other effects which may contribute to total absorption also deserve comment. Light absorption by adsorbed gases on the windows of the absorption cell has been suggested by Cosgarea [5] to explain the invalidity of Beer's law for atomic absorption. The basis of this suggestion was the non-zero intercept of a plot of $T\log_{10} I_o/I_t$ vs ℓ at constant number density for atomic absorption data. Two considerations make this theory suspect. In the first place, the adsorption bonds between the absorbing atoms and the atoms which make up the window material almost certainly would disturb the energy levels of the absorbing atoms to such an extent that absorption would no longer take place around the same characteristic frequency as before. The disturbances in the energy levels of the adsorbed atoms would have to be on the order of the disturbances which give rise to the hyperfine splitting if the adsorbed atoms were to absorb light in a frequency range indistinguishable from the frequency range of absorption for the gaseous atoms. Secondly, neglecting the effects of hyperfine structure and self-broadening as Cosgarea did, can lead to a non-zero intercept on a plot of light absorbed versus the absorption cell length since these effects become increasingly important as the size of the absorption line decreases. Thus, what has been interpreted as an effect due to adsorbed gases is probably entirely due to the neglected hyperfine structure and self-broadening effects.

The adsorbed gases on the absorption cell walls and the gases trapped in the alloy which are released as the absorption cell is heated can pressure broaden absorption lines, if a sufficient amount of gas is released. For a considerable period of time, variation in the values of the total absorption was noticed for runs made at zero inert gas pressure even though the concentration of absorbing atoms was the same. The results obtained when the absorption cell was evacuated at comparatively low

temperatures and closed off were always higher than those obtained when a dynamic vacuum was maintained across the quartz to quartz seal of the cell at each temperature where absorption data were taken. Also, runs with sealed cells, i.e. cells evacuated at room temperature and sealed off, gave high total absorption values, by a factor of 1.5 - 2.0, than all runs made with absorption cells closed off with the quartz to quartz seal. That this effect did not result from a non-equilibrium vapor concentration in the absorption cell was assured by a comparison of the rate of mass lost across the quartz to quartz seal to the rate of evaporation of mass in the cell. Measurement of the amount of mass lost during a run and an estimate of the rate of evaporation from kinetic theory indicated that the evaporation rate was more than 1000 times greater than the diffusion rate across the quartz to quartz seal. These results indicated that the increase in observed total absorption in the sealed cell was due to the collision broadening of the absorption line by the adsorbed gases on the quartz and the trapped gases in the alloy which were released as the absorption cell was heated. The total absorption data for the subsequently discussed thermodynamic measurements were taken from runs where a dynamic vacuum was maintained on the quartz to quartz seal of the absorption cell during the readings made at zero inert gas pressures. This procedure eliminated the previously observed run-to-run variation in the total absorption values.

Calculations of the effect of the slit width and the finite resolution of the spectrometer on the absorption line shape have been made be a number of investigators [4], [12]. These workers have been concerned with the errors resulting in the observed line breadth, peak absorption coefficient,

and the integrated intensity of an emission line ($\int P_\omega X d\omega$). It is generally concluded that the errors increase as the resolution of the spectral instrument decreases and that the errors in line breadth and peak absorption coefficient are much greater than those in the integrated intensity. Minkowski [14] found that the resolution of the spectrometer had no effect on the total absorption measurements following the square root absorption law for a range of slit widths which varied by a factor of 10. Total absorption measurements at several spectrometer slit widths which were made for this work confirm Minkowski's results. These measurements were made in the concentration region where the total absorption is proportional to the square root of the concentration of absorbing atoms. No additional measurements of absorption line sizes as a function of spectrometer slit widths were made in the concentration region where the total absorption is proportional to the first power of the concentration. It was assumed that, in this case also, the slit width and spectrometer resolution do not affect the ratio of absorption line area to incident intensity.

CHAPTER V

THERMODYNAMIC MEASUREMENTS

A. Introduction

Optical absorption measurements of the Bi 3067Å line, the Pb 2833Å line, and the Bi_2 2731Å band were made for Bi vapor pressures from 2×10^{-8} to 10^{-3} atm., Bi_2 vapor pressures from 10^{-5} to 10^{-3} atm, and Pb vapor pressures from 3×10^{-8} to 2×10^{-3} atm. Both the atomic and diatomic vapor species were measured in equilibrium with pure liquid bismuth, a 47.4 mole % Bi lead-bismuth alloy, and the two phases, uranium and UBi in a uranium-bismuth alloy. Lead vapor measurements were made for the vapor in equilibrium with pure liquid lead and the 47.4 mole % Bi lead-bismuth alloy mentioned above. From these optical absorption measurements, the heats of vaporization of atomic bismuth, diatomic bismuth, and lead, the activities of lead and bismuth in the lead-bismuth alloy, and the activity of bismuth in U-UBi were calculated. The activities of lead and bismuth in the lead-bismuth alloy and the heats of vaporization of lead, atomic bismuth, and diatomic bismuth were compared with previously measured values and the agreement obtained indicates the validity of the absorption laws which were used. The measurement of the activity of bismuth above U-UBi serves as an example of the way pressure broadening can be used to extend the range of applicability of the method.

For atomic absorption, the actual measure of the total absorption was the area of the absorption curve in square inches divided by the incident intensity in chart units (cu.). This is related to the total absorption in cm^{-1} by an instrumental constant which depends upon the scanning rate of the spectrometer and the original units of the measurements. The constant for the spectrometer used in this work is 0.568 sq.in./cu./cm^{-1}.

The absorption measure for diatomic absorption is the ratio of the transmitted intensity, I_t, to the incident intensity, I_o, where both have

been extrapolated to the frequency where the absorption at the band head is half its maximum value. Since these values represent intensities averaged over the frequency range of the spectrometer resolution width,

$$\frac{I_t}{I_o} = \frac{1}{\Delta\omega} \int_{\Delta\omega} I_\omega / I_o \, d\omega = T_R \qquad (23)$$

B. The Use of the Calpeyron Equation and the Calculation of Activities

In the preceding section of this paper, the relationships between the amount of light absorbed and the concentration of the absorbing gas were discussed for atomic and diatomic gases. When the absorbing gas is in equilibrium with some condensed phase, another relationship between the condensed phase and the absorbing gas can be applied, namely the Clapeyron equation. It is through the Clapeyron equation that the absorption parameters can be expressed in terms of the temperature of the system instead of the vapor concentration.

Since in various concentration ranges different absorption laws apply, the relationship between the absorption parameters and the temperature, which can be derived by introducing the Clapeyron equation, will be different for each absorption law. Two examples of the results of the introduction of the Clapeyron equation are shown below. The first is for atomic absorption in the concentration range where β is proportional to the square root of X and the second is for molecular absorption which follows Beer's law.

Assuming that the vapor pressure is related to the vapor concentration by the ideal gas law, the total absorption in the square root region can be expressed as follows:

$$\beta = 2\sqrt{SbX} = 2\sqrt{\frac{Sb\ell pa}{RT}} \qquad (24)$$

If the dispersion half-breadth, b, is a constant

$$\log_{10}(T^{\frac{1}{2}}\beta) = \tfrac{1}{2}\log_{10} p + \tfrac{1}{2}\log_{10}\left(\frac{4Sb\ell a}{R}\right) \qquad (25)$$

Introducing the Calpeyron Equation,

$$\log_{10} p = \frac{-\Delta Hv}{2.303RT} + C_I \text{ yields}$$

$$\log_{10}(T^{\frac{1}{2}}\beta) = \frac{-\Delta Hv}{2 \times 2.303RT} + \frac{C_I}{2} + \tfrac{1}{2}\log_{10}\frac{4Sb\ell a}{R} \qquad (26)$$

If Δc_p is constant, $(\Delta H_v - \Delta c_p T)$ is constant, and

$$\log_{10}(T^{(\frac{1}{2} - \frac{\Delta c_p}{2R})}\beta) = \frac{-SLOPE}{T} + \frac{C_I}{2} + \tfrac{1}{2}\log_{10}\frac{4Sb\ell a}{R} \qquad (27)$$

where: $$SLOPE = \frac{\Delta Hv - \Delta c_p T}{2 \times 2.303 R},$$

C_I = the integration constant for the Clapeyron Equation,

and $c_p = c_p(v) - c_p(\ell)$

If b is inversely proportional to the square root of T, (the case when foreign gas collision broadening dominates) and the foreign gas pressure is constant, data may be correlated by:

$$\log_{10}(T^{(3/4 - \frac{\Delta c_p}{2R})}\beta) = \frac{-SLOPE}{T} + \frac{C_I}{2} + \tfrac{1}{2}\log_{10}\frac{4SC_p p_I \ell a}{R} \qquad (28)$$

where the substitution $b = C_p \frac{p_I}{\sqrt{T}}$ has been made and it has been assumed that p_I, the inert gas pressure, is constant.

These equations allow simple linear correlations of the total absorption data following the square root law.

For molecular absorption following Beer's law,

$$-\log_{10} T_R = \frac{SX}{2.303\ d} = \frac{S\ell pa}{2.303\ dRT}$$

or

$$T\log_{10}(I_o/I_t) = \frac{S\ell a}{2.303\ dR}\ p \qquad (29)$$

Again introducting the Clapeyron equation and assuming Δc_p is constant yields:

$$\log_{10} T^{(1 - \frac{\Delta c_p}{R})} \log_{10}(I_o/I_t) = - \frac{(\Delta Hv - \Delta c_p T)}{2.303\ R\ T} + C_m \qquad (30)$$

where C_m is the sum of the integration constant from the Clapeyron Equation and $\log_{10} (\frac{S\ell a}{2.303\ dR})$.

Again a linear semi-log plot can be used to correlate the absorption data.

The relative thermodynamic properties of the element in the alloy can be calculated if the activity of the condensed phase is know as a function of temperature. The activity can be determined directly from optical absorption measurements of either the atomic of diatomic species in the vapor. When the equilibrium vapor is atomic:

$$A_{(pure)} \rightarrow A_{(alloy)}$$

$$a(c) = f(c)/f(c)^*$$

but since

$$A(c) \rightarrow A(v),$$

$$f(c) = p_1(v)$$

and it follows that

$$a_{(c)} = p_1(v)/p_1^*(v)$$

Thus if the total absorption, β, is proportional to p_1

$$a_{(c)} = (\beta/\beta^*)^2 \qquad (31)$$

where β = the value of the total absorption measured above the alloy and β^* = the value of the total absorption measured above pure A.

When the equilibrium vapor is diatomic:

$$A_{(pure)} \rightarrow A_{(alloy)}$$

$$a_{(c)} = f(c)/f^*(c)$$

but since

$$A_{(c)} \rightarrow \tfrac{1}{2} A_2 (v),$$

$$f(c) = p_2^{\frac{1}{2}} (v)$$

it follows that

$$a_{(c)} = \left(p_2 (v) / p_2 (v) \right)^{\frac{1}{2}}$$

Thus if $T\log_{10} (I_o/I_t)$ is proportional to p_2

$$a_{(c)} = \left(\frac{\log_{10} (I_o/I_t)}{\log_{10} (I_o/I_t)^*} \right)^{\frac{1}{2}} \qquad (32)$$

where I_o/I_t = the value of the transmittance measured above the alloy and $(I_o/I_t)^*$ = the value of the transmittance measured above pure A.

Since total absorption and transmittance measurements can be made at different temperatures, the activity of an element in an alloy can be determined as a function of temperature from optical absorption measurements. Thus, all the other relative thermodynamic properties of the element in the alloy can be determined.

C. Activity Measurements in a Lead-Bismuth Alloy

Optical absorption measurements of lead, atomic bismuth, and diatomic bismuth vapor in equilibrium with a 0.474 mole fraction Bi lead-bismuth alloy were taken under helium pressures of zero and 746 mm Hg. These measurements were used, in conjunction with measurements above pure lead and pure bismuth, to calculate the activity of lead and bismuth in the alloy. The activity of liquid bismuth was calculated four ways since both bismuth species were measured at two different helium pressures. The activity of lead was determined two ways since the measurements were made at the two helium pressures. All of the optical absorption data were taken in the concentration range where the total absorption follows the square root law if the amount of collision broadening is a constant. The atomic

bismuth data above pure bismuth and the lead-bismuth alloy taken at zero and 746 mm Hg helium pressure are shown in Figures 5 and 6 respectively. The corresponding diatomic bismuth data, taken at zero and 746 mm Hg helium pressure, are shown in Figure 7.

Although the Bi_2 data taken at 746 mm Hg do not differ significantly from the data taken at zero helium pressure, separate activity calculations were made at each helium pressure. The lead data taken at 746 mm Hg helium pressure above pure lead and the lead-bismuth alloy are shown in Figure 8 while similar data taken at zero helium pressure is shown in Figure 9. Figures 10 and 11 show the activities of bismuth and lead in the lead- bismuth alloy calculated from the data taken under 746 mm Hg of helium pressure. At this helium pressure, the atomic absorption measurements above pure lead, pure bismuth, and the lead-bismuth alloy were corrected for the effects of hyperfine structure using the functions plotted in Figure 4. The effects of self-broadening were also subtracted out using Equation (12). Least square lines were calculated from the corrected pure atomic lead and bismuth data. The activities of lead and bismuth in the lead-bismuth alloy were then calculated from the corrected absorption data taken above the alloy and the least-square lines through the corrected data for the pure elements.

The activities of bismuth calculated from the diatomic bismuth measurements are shown in Figure 12. A single least-square line was calculated from both the pure diatomic measurements at zero and at 746 mm Hg helium pressure, using only that data which plotted linearly on a semi-log Clapeyron plot (data shown on Figure 7 taken at temperatures below 1145° K). The activities at zero and 746 mm Hg helium pressure were calculated from the diatomic data taken above the alloy and the least-square line through data for pure bismuth.

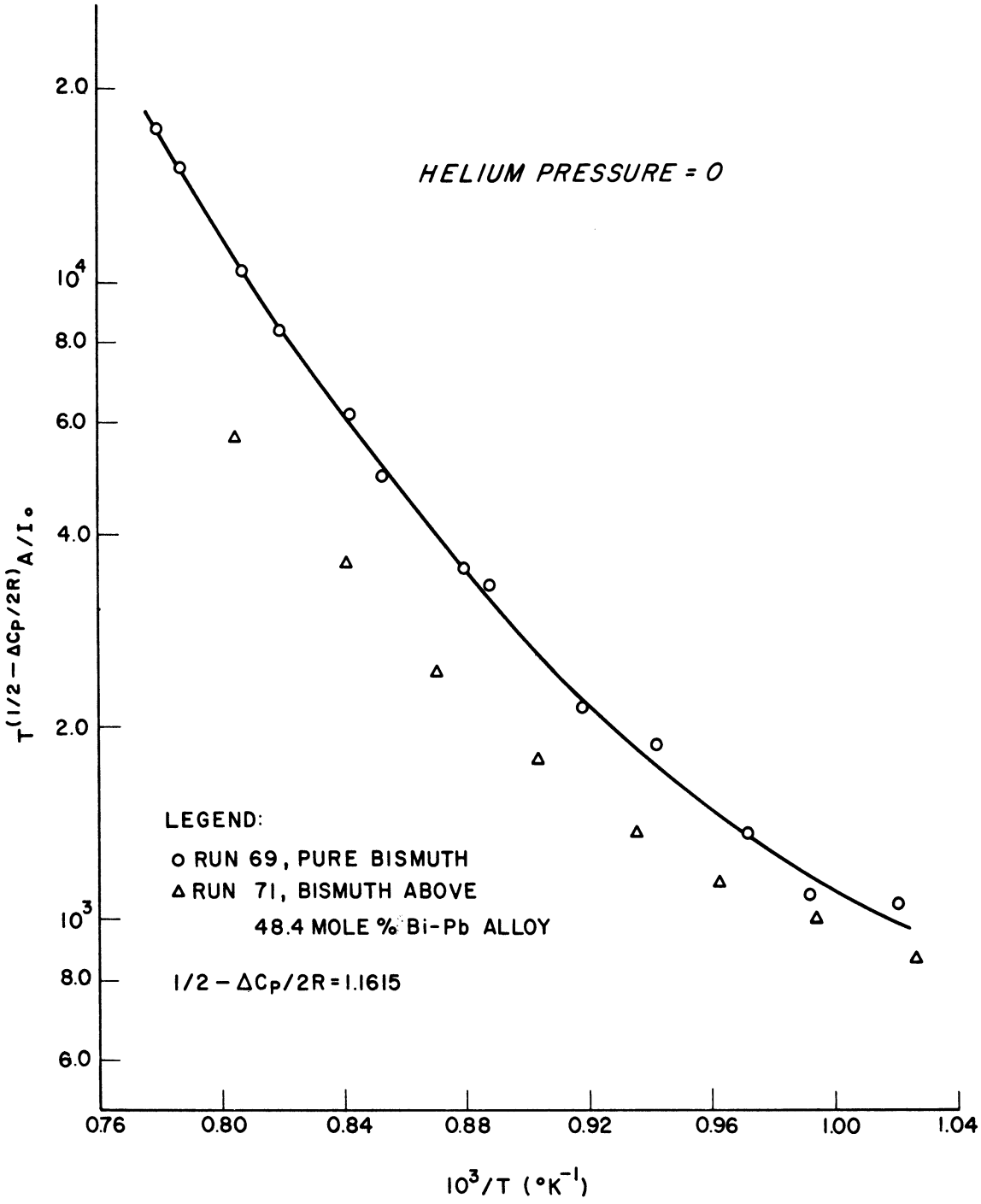

Figure 5. Bismuth Absorption Data, Helium Pressure = 0

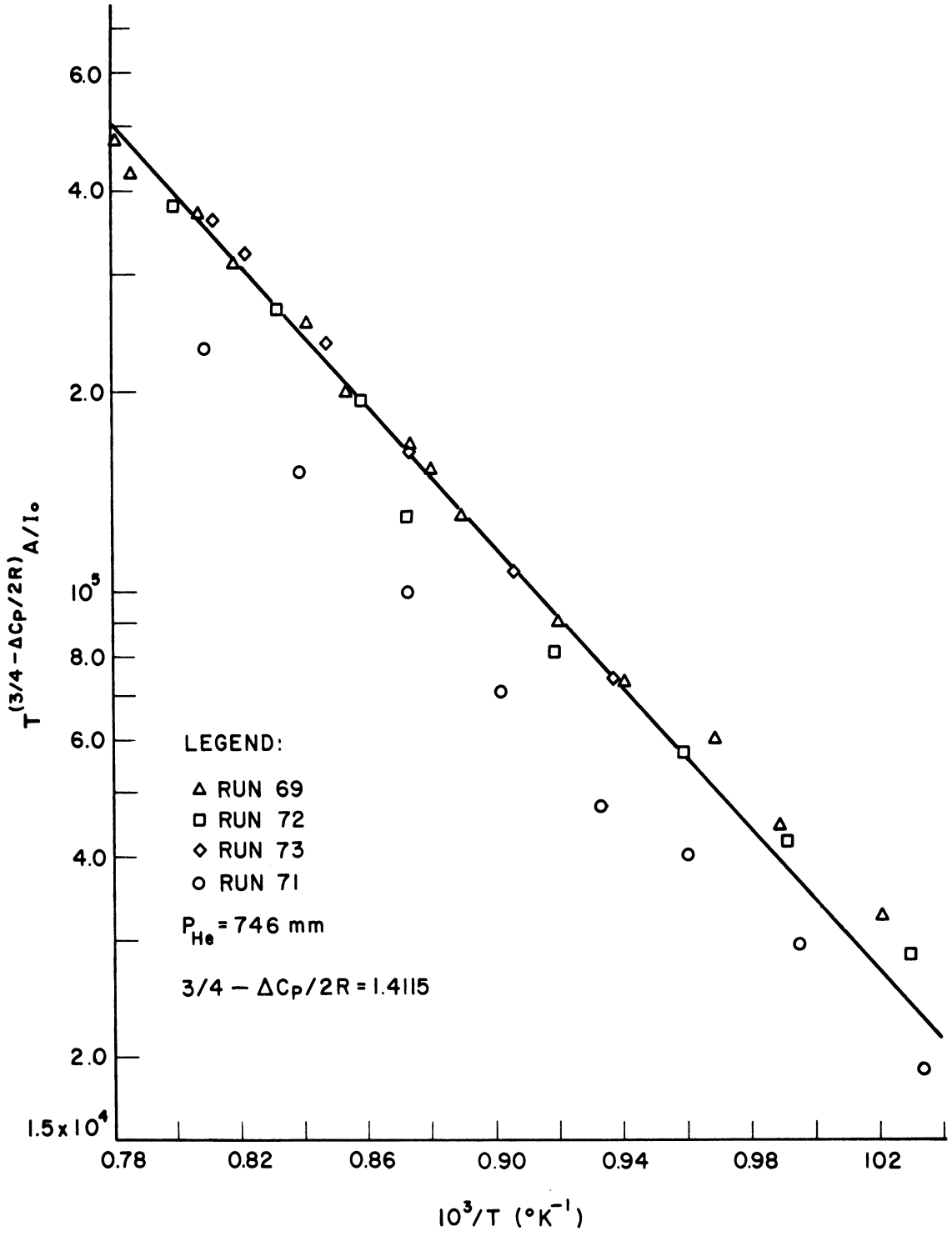

Figure 6. Atomic Bismuth Absorption Data, Helium Pressure = 746 mm Hg

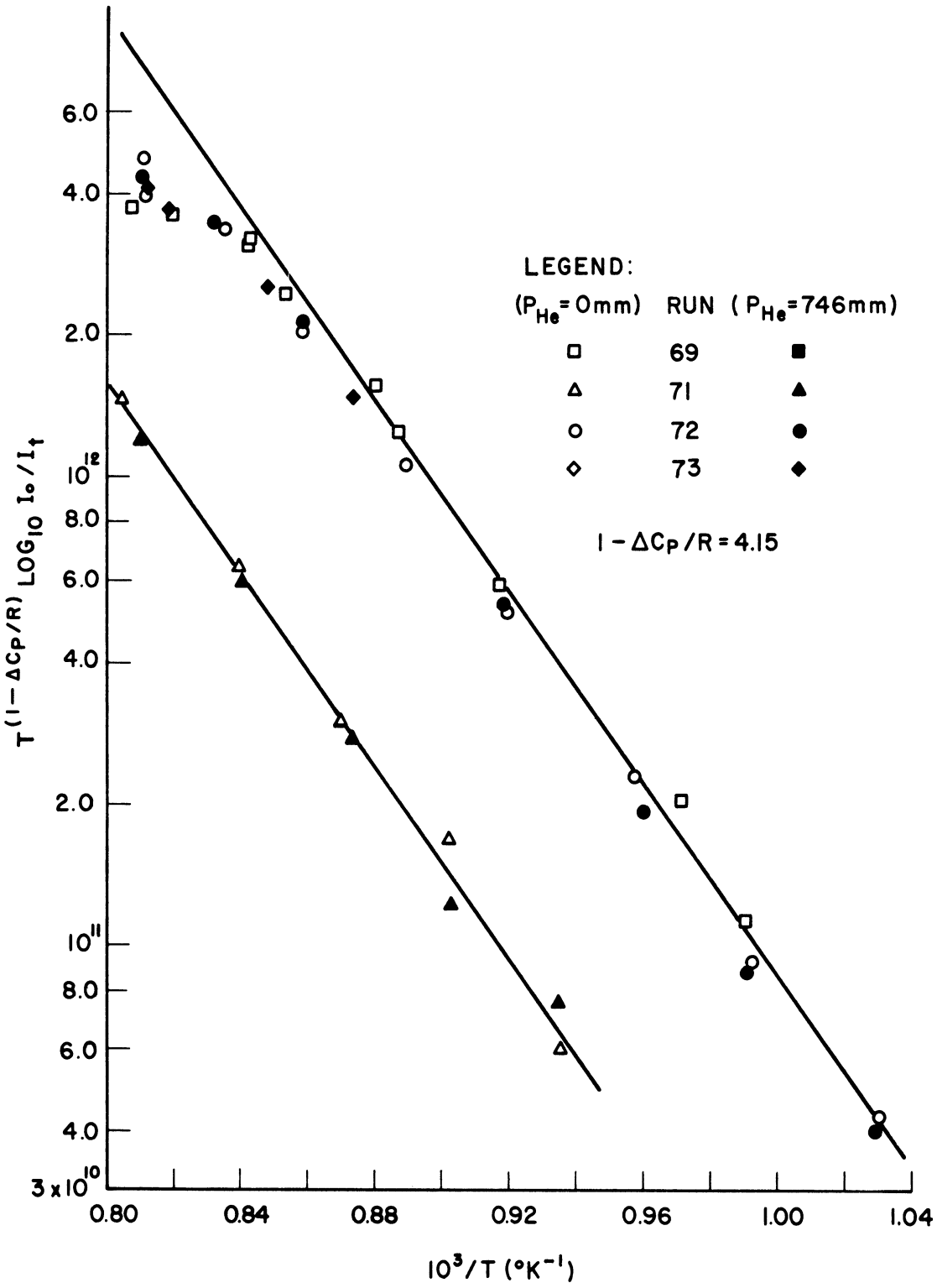

Figure 7. Diatomic Bismuth Absorption Data

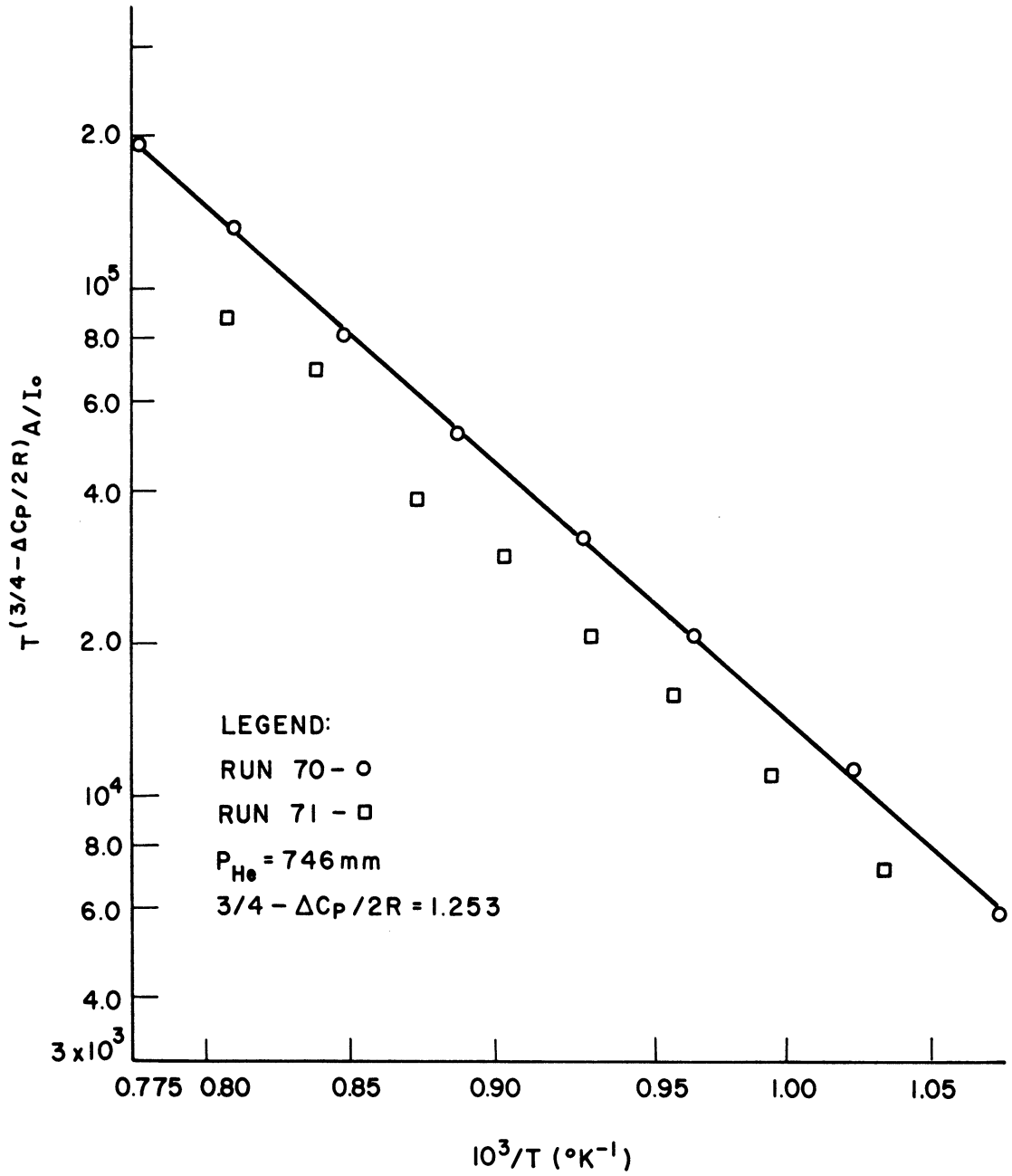

Figure 8. Atomic Lead Absorption Data,
Helium Pressure = 746 mm Hg

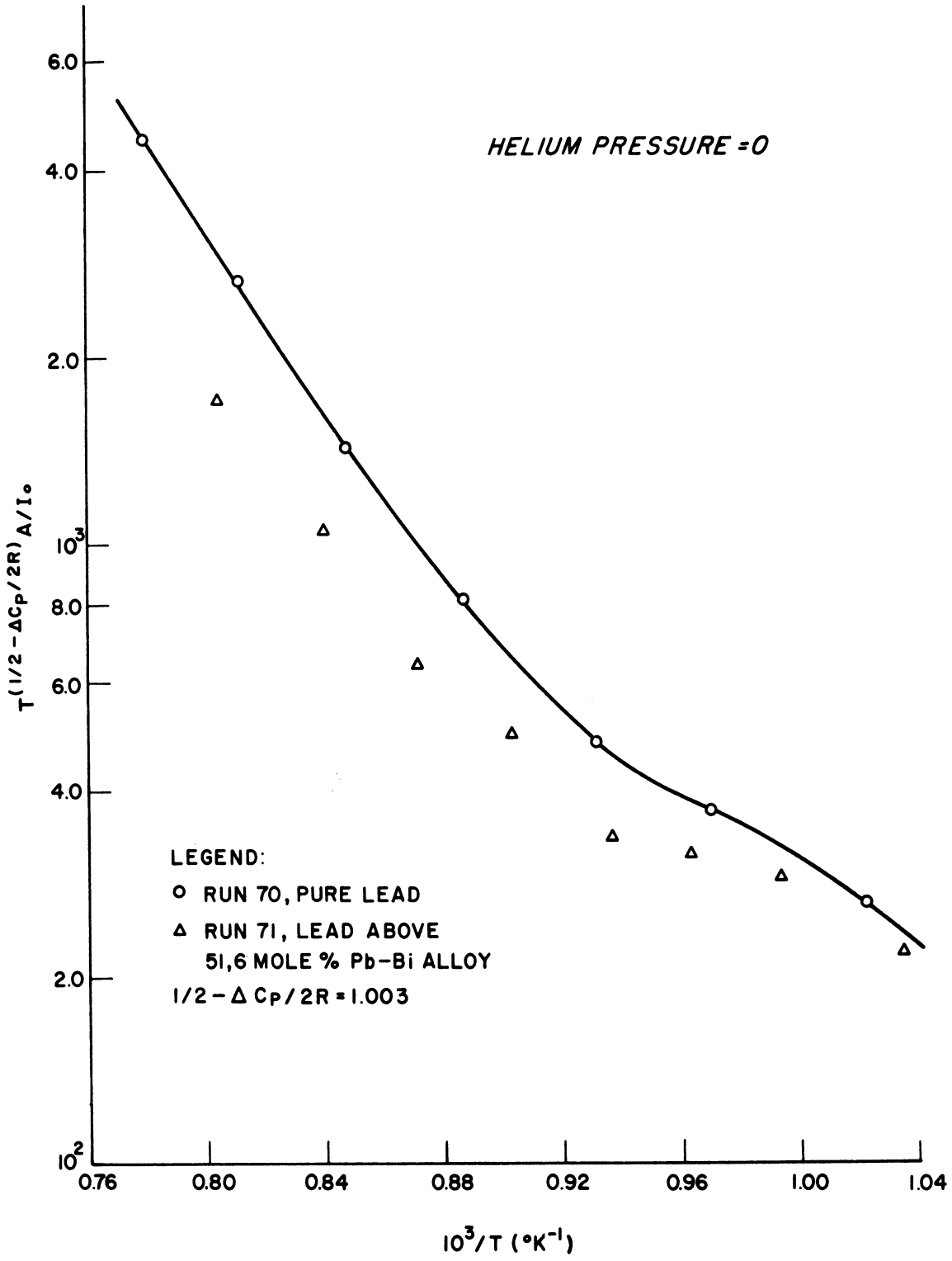

Figure 9. Lead Absorption Data, Helium Pressure = 0

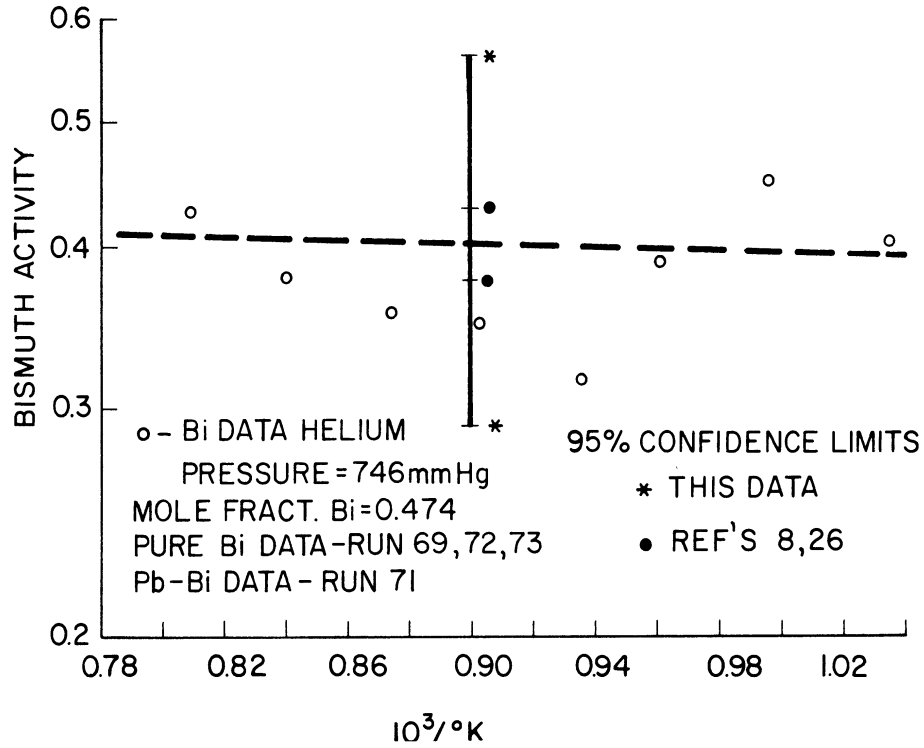

Figure 10. Activity of Bismuth in Lead-Bismuth Alloy, Helium Pressure = 746 mm Hg, using Bi

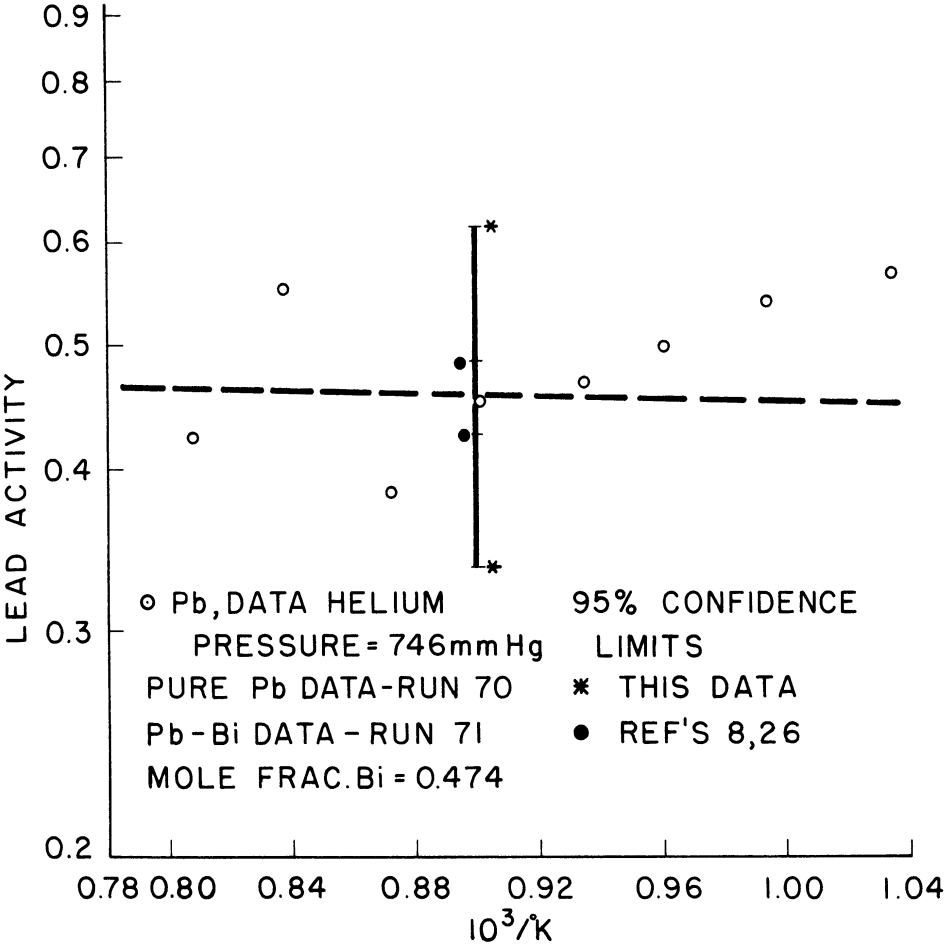

Figure 11. Activity of Lead in Lead-Bismuth Alloy, Helium Pressure = 746 mm Hg

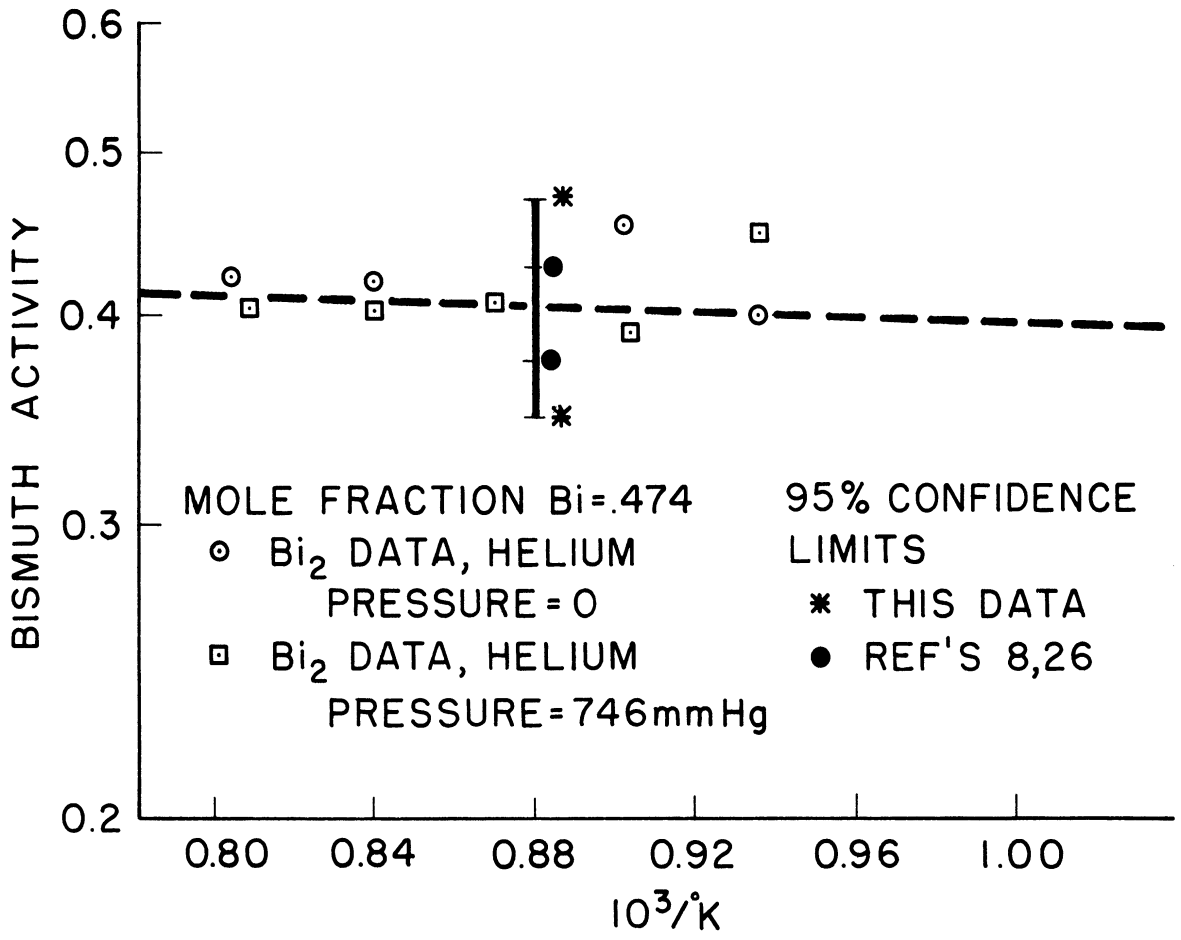

Figure 12. Activity of Bismuth in Lead Bismuth Alloy, Using Bi_2

The activities of lead and bismuth calculated from the data taken at zero helium pressure are shown in Figures 13 and 14. These activities were calculated directly from lines drawn by eye through the pure lead and bismuth data and the actual lead and bismuth data taken above the lead-bismuth alloy. With all these results are shown the activity versus 1/T lines predicted using Gonser's [8] and Wagner and Engelhardt's [26] emf data. All of activities of lead and bismuth were calculated in the manner described in a previous section, assuming the atomic absorption data followed the square root absorption law and the diatomic data followed Beer's law.

D. Discussion of Lead-Bismuth Activities

Figure 12 indicates that activities calculated from the diatomic bismuth absorption data agree well with the emf values. The activities calculated from the atomic bismuth and lead measurements made at 746 mm Hg helium pressure agree also with the emf values, although the precision of the data is not good. The atomic data taken under zero helium pressure, however, indicate a trend in the deviation of the calculated activities from those determined previously from emf measurements, the calculated activities being too low at the higher temperatures and too high at the lower temperatures.

For the atomic bismuth and lead data, taken at zero helium pressures, no corrections were made for the hyperfine structure and self-broadening contributions to the total absorption. The significance of self-broadening in both the lead and atomic bismuth zero helium pressure measurements is apparent from the non-linearity of the data on the semi-log Clapeyron plot and the fact that the slope of the zero helium pressure data is increasingly steeper than the slope of the 746 mm Hg helium pressure data.

Since the effect of self-broadening is directly proportional to the vapor density and the vapor density above the Pb-Bi alloy is less than the

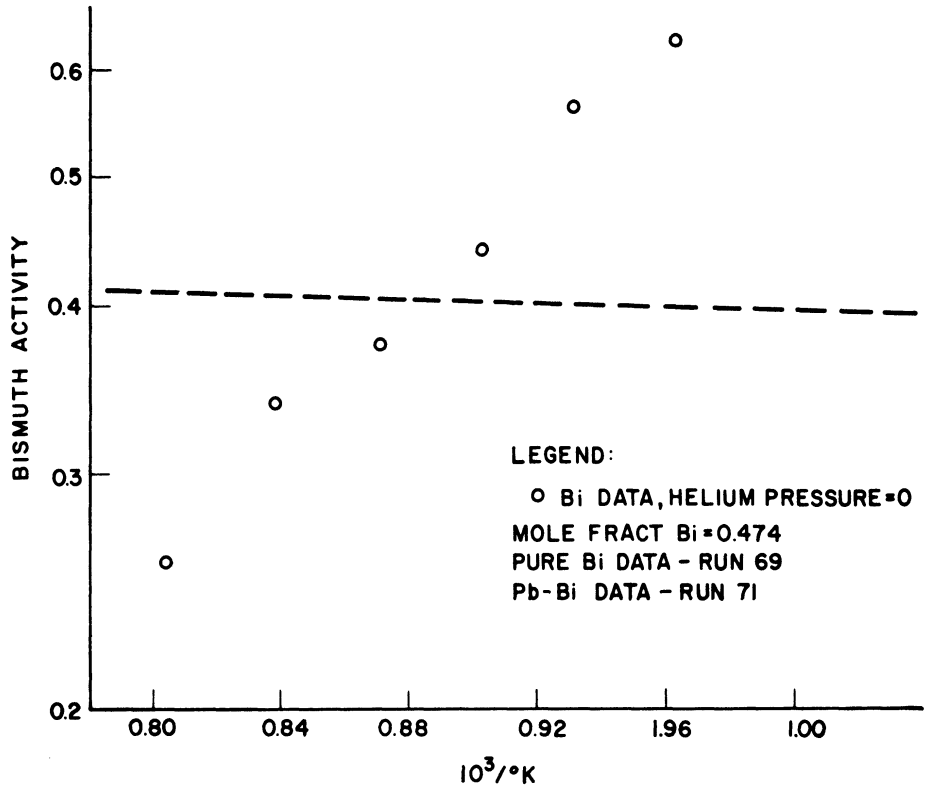

Figure 13. Activity of Bismuth in Lead-Bismuth Alloy, Helium Pressure = 0

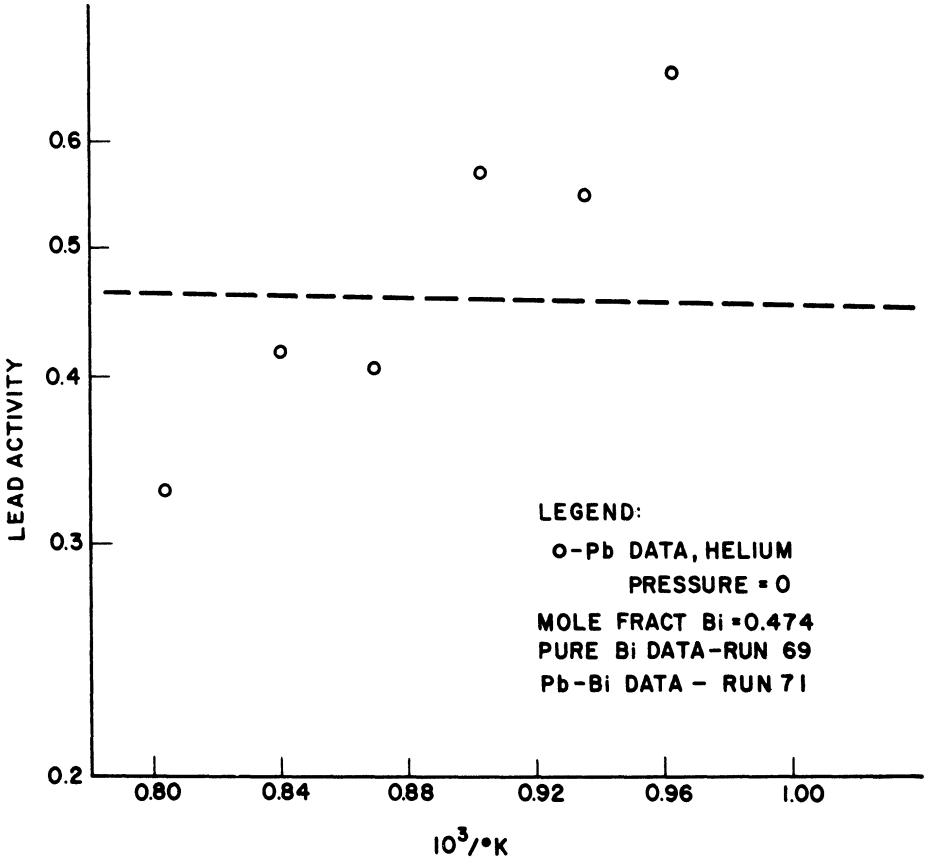

Figure 14. Activity of Lead in Lead-Bismuth Alloy, Helium Pressure = 0

vapor density above pure lead or bismuth, the effect of self-broadening on the total absorption data of the alloy is less than the effect on the total absorption data of pure lead and bismuth. This leads to the low activities calculated at the higher temperatures.

Hyperfine structure also affects the zero helium pressure atomic lead and bismuth data, increasing the observed total absorption as much as 48 per cent for the lead data and as much as 65 per cent for the bismuth data. Because the total absorption values above the alloy are smaller than those measured above pure lead and bismuth, neglecting hyperfine structure would lead to high than expected calculated activities. The high activities for the zero helium pressure measurements made at the lower temperatures result both from this hyperfine effect and the deviation of the total absorption data from the square root absorption law at the lower temperatures.

Self-broadening does not affect the activities calculated from the 746 mm Hg helium pressure data because the total absorption data taken under zero helium pressure was subtracted from the 746 mm Hg data according to Equation (12). Self-broadening was practically negligible anyway compared to the collision broadening from the 746 mm Hg helium pressure, since it contributed less than 1% to the total absorption. Hyperfine structure corrections were made for the 746 mm Hg helium pressure lead and bismuth data using the hyperfine correction function plotted in Figure 4. These corrections decreased the observed total absorption values, at most, 18 per cent for the bismuth data and 3.9 per cent for the atomic lead data.

The lead and bismuth activity determinations using the data taken at helium pressures of zero and 746 mm Hg contrast each other. The activities derived from the zero helium pressure measurements demonstrate the inaccuracies which can arise if the effects of hyperfine structure and self-broadening

are neglected while the activities determined from the data taken at 746 mm Hg show how correct activities may be measured if these effects are accounted for.

The insensitivity of the diatomic bismuth data to pressure broadening is predicted theoretically when the widths of the band's absorption lines are much greater than the line spacing. That this condition is met can be shown by calculating the rotational line spacing using an approximate atomic spacing estimated by Almy and Sparks [1] and the Doppler breadth of the line.

The 95% confidence limits of the activities calculated from the atomic lead and bismuth data taken at 746 mm Hg helium pressure and the diatomic bismuth data taken at zero and 746 mm Hg helium pressure are shown also in Figures 10, 11, and 12 along with the expected error of the values determined by Wagner and Engelhardt [26] and Gonser [8]. No estimate of error was made for the activities calculated from the atomic zero helium pressure data since least square lines for this data were not computed. The error limits are such that the activities determined by optical absorption agree within the precision of the measurements with those of Gonser and Wagner and Engelhardt. Note that, if the precision of the absorption data is the same for the diatomic band measurements and the atomic line measurements following the square root law, the precision of the calculated activities is much greater for the diatomic measurements. The activity equals the square root of the ratio of the transmittances, in the diatomic instance, while it equals the square of the ratio of the total absorptions for atomic absorption. The smaller 95% confidence limits for the activities determined from the diatomic measurements indicate that this effect is observable for the absorption measurements of this work.

While diatomic activity measurements are inherently more precise, much lower activities can be measured using atomic absorption measurements which follow the square root law. The proportional decrease in the absorption parameter with vapor concentration is less for atomic absorption. The total absorption decreases only as the square root of the concentration decrease whereas the decrease in the transmittance is directly proportional to the decrease in vapor concentration. This advantage of atomic absorption is augmented by the shift in the equilibrium between the molecular and atomic species toward the atomic specie as the total pressure decreases.

E. The Activity of Bismuth in U-UBi

Cosgarea, Ragone, and Hucke [5] have recently reported the activity of bismuth across the uranium-bismuth phase diagram (Figure 15). These activities were calculated from diatomic bismuth absorption measurements made above the liquid, liquid-UBi_2, and UBi_2-U_3Bi_4 concentration regions. The diatomic specie was unobservable in the U_3Bi_4-UBi and U-UBi regions because of the decreased vapor pressure and the shift in the vapor equilibrium toward the atomic specie. To calculate the bismuth activity in these concentration regions, Cosgarea used an empirical correlation of his atomic absorption data which had been processed using Beer's law. Because of the lack of theoretical basis for the above correlation, the activity of bismuth in the U-UBi region was remeasured for this dissertation using atomic absorption lines which were broadened with 746 mm Hg helium pressure. These measurements serve also as an example of how pressure broadening can be used to amplify weak absorption lines to the point where accurate activity determinations can be made. The bismuth absorption data above U-UBi is shown in Figure 16. The activities of bismuth in U-UBi calculated from this data and the least square line through the pure bismuth data are

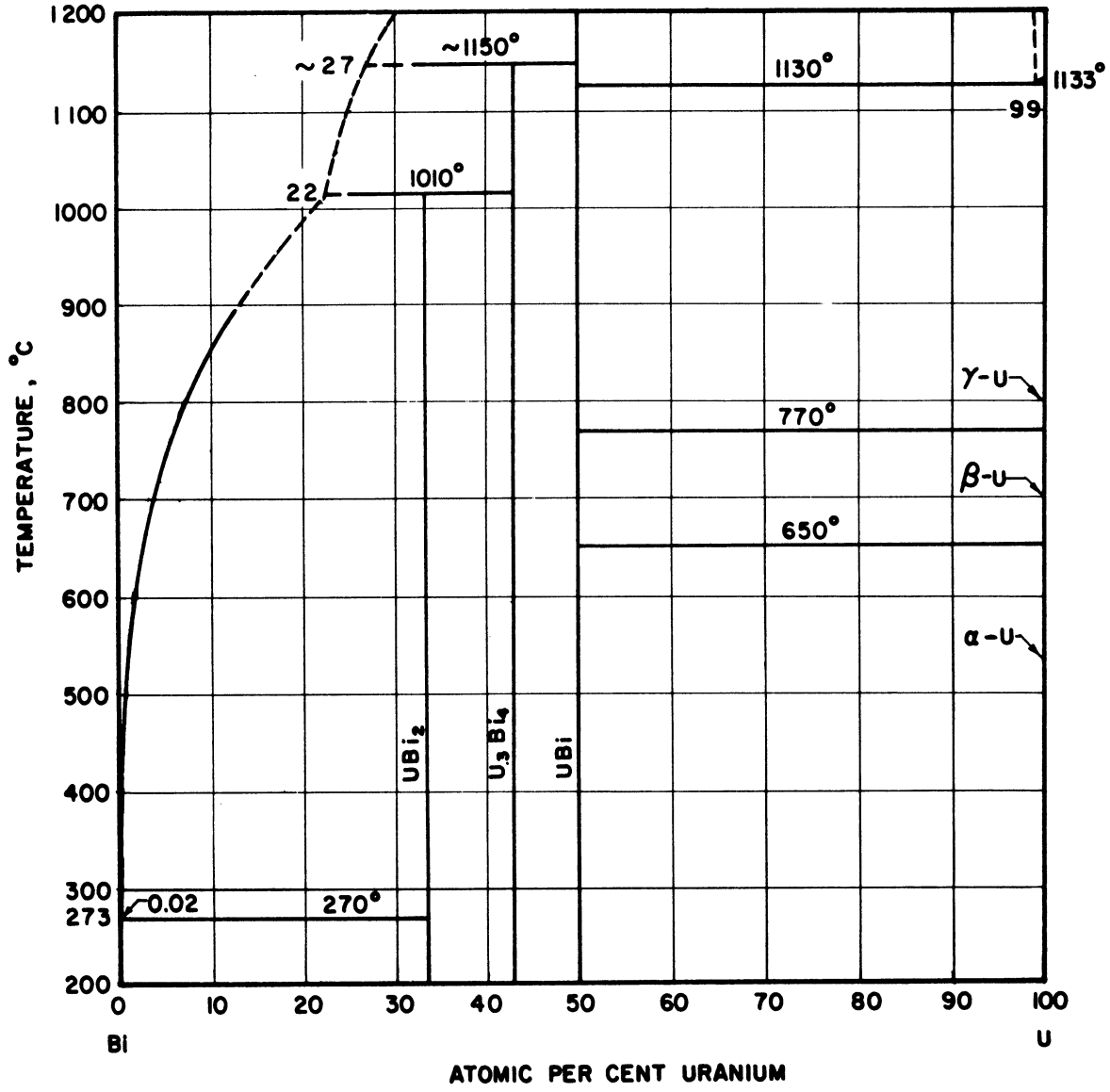

Figure 15. Uranium-Bismuth Phase Diagram

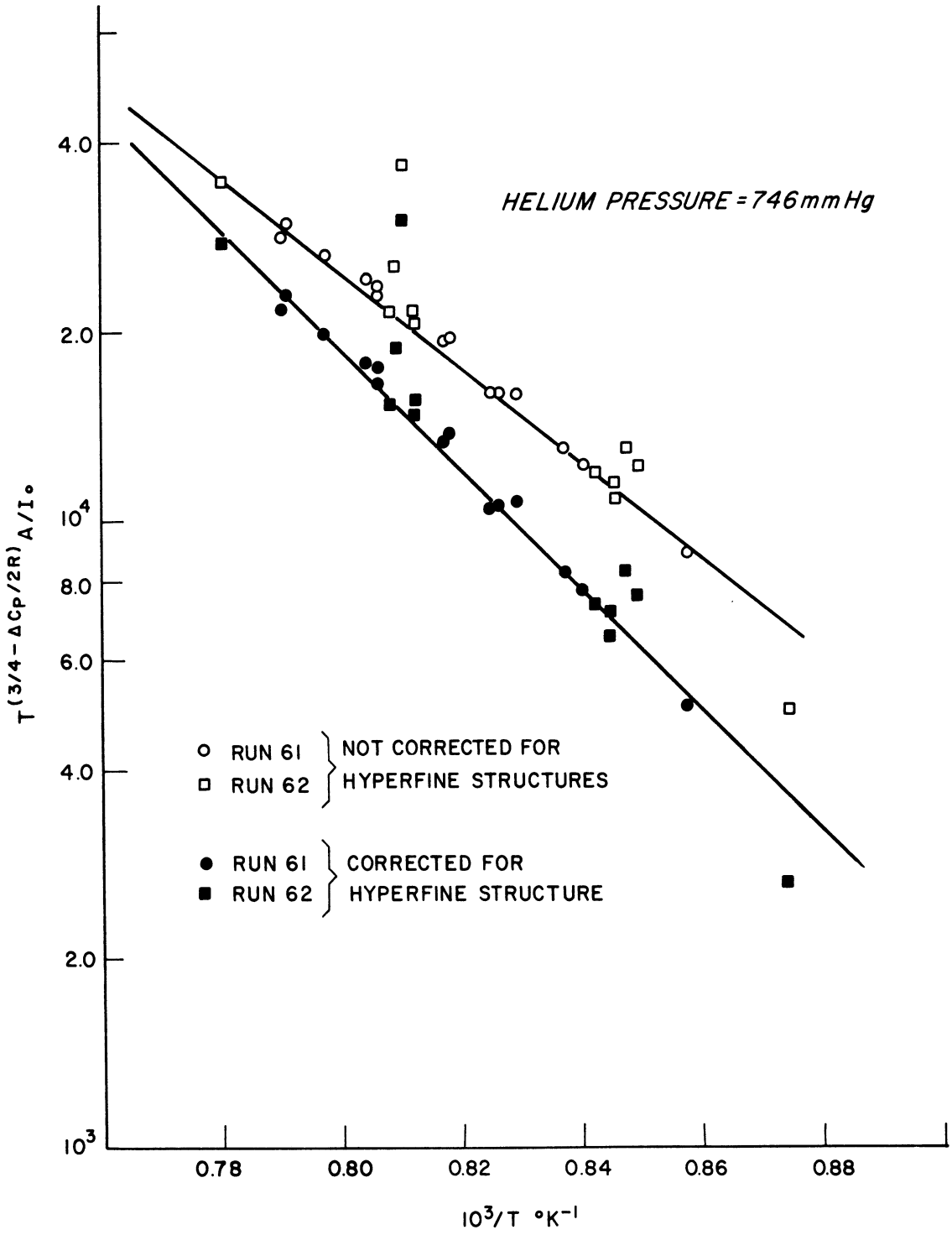

Figure 16. Bismuth Absorption Data Above U-Ubi

plotted as a function of temperature in Figure 17. For these measurements as for the activity measurements for the lead-bismuth alloy, both the pure bismuth data and the bismuth data above the alloy were corrected for the hyperfine structure of the bismuth 3067Å line. The corrections were much larger for the U-UBi data (as large as 60 per cent) than for the lead-bismuth data because the total absorption values are much smaller. An estimate of the 95% confidence limits for these activities values is also given in this figure.

The uranium-bismuth alloys were prepared by putting chunks of bismuth and very fine helical spirals of uranium into an alumina boat, inserting the boat into the absorption cell, heating the cell to temperature, and allowing the liquid bismuth to react with the solid uranium. The magnitude of the total absorption decreases stepwise with time as the bismuth diffuses into the uranium. Each step corresponds to one of the two-phase regions of the uranium-bismuth systems (see Figure 15). In this way one has an indication as to when the bismuth has diffused completely into the uranium and the U-UBi two phase equilibrium has been reached.

F. Discussion of U-UBi Measurements

From Figure 17, it is apparent that difficulty was experienced in attaining equilibrium above the U-UBi alloy. Small amounts of water vapor or oxygen would immediately cause a marked increase in the observed total absorption. This increase would be followed by a slow decrease in the total absorption if the precipitating condition was corrected and a hard vacuum was maintained on the absorption cell. Any oxygen present probably reacted to form small amounts of UO_2. This released bismuth from the UBi compound yielding the observed high bismuth pressures. As time passed, however, the free bismuth diffused through the alloy and reacted

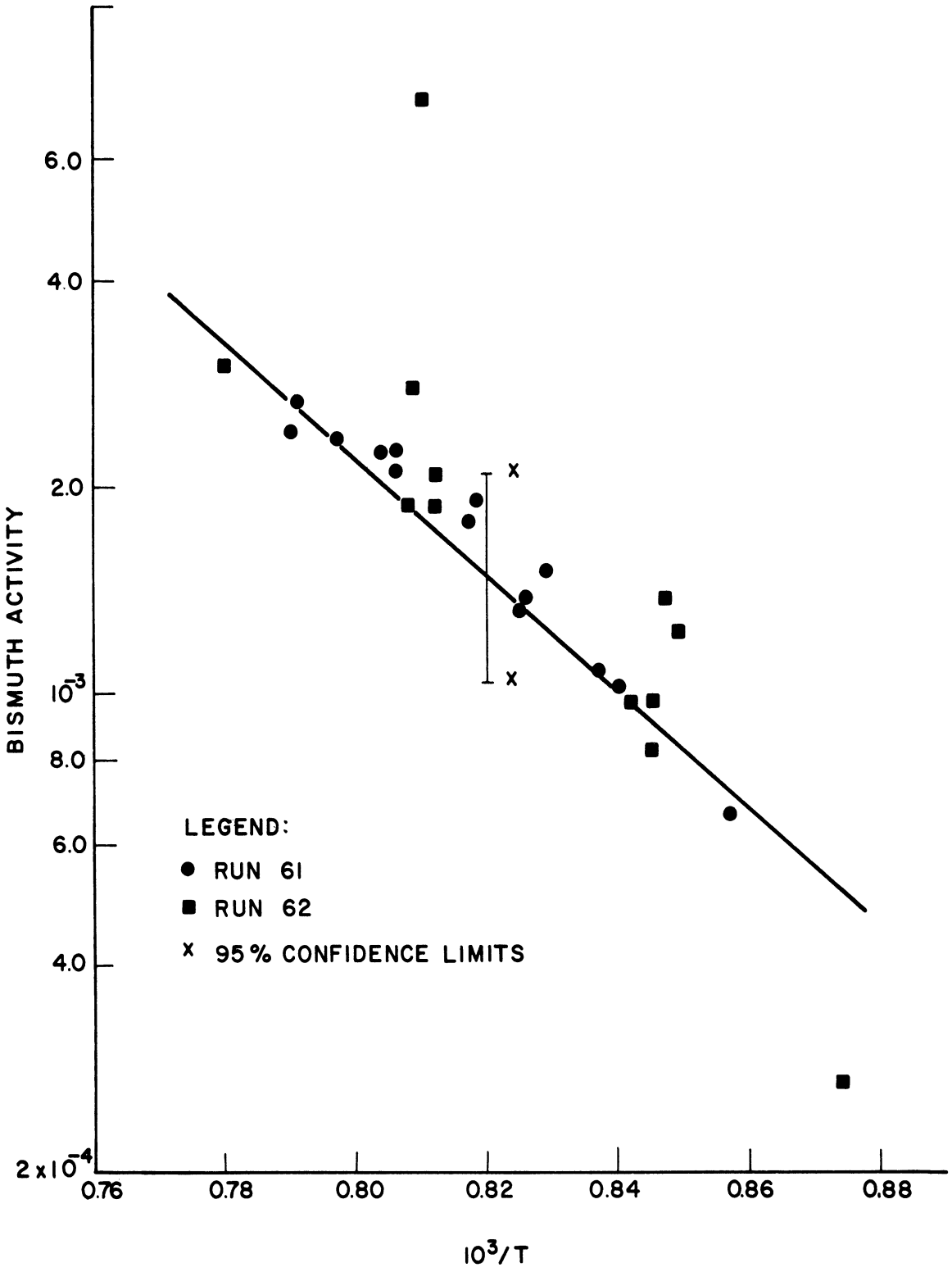

Figure 17. Activity of Bismuth in U-UBi

with free uranium to again form the compound UBi. A liquid nitrogen cold trap on the helium inlet line to the absorption cell and the presence of titanium chips in the hot inlet portion of the cell (not in the absorption chamber proper) were used to control the oxygen level and consequently eliminated the variation of the total absorption. Because of the possible competing UO_2 reaction, only the lower data points were used to determine the activity versus temperature lines shown in Figure 17.

The bismuth absorption data above U-UBi were also corrected for the effect of hyperfine structure. This effect changes the bismuth activites in U-UBi much more significatly than it changed the bismuth activities in the lead-bismuth alloy. Correcting the U-UBi total absorption data for hyperfine structure, using the hyperfine correction function yields the second group of absorption data in Figure 16. It is from these corrected data and the least square line through the corrected pure bismuth data that the activities in Figure 17 were calculated.

G. Heats of Vaporization Measurements

Bismuth. Optical absorption measurements at helium pressures of zero, 350, and 746 mm Hg were made for bismuth vapor above pure bismuth and for lead vapor above pure lead. A plot of the data for atomic bismuth over the entire temperature range of measurement is shown in Figure 18. The two optical density regions in which the limiting absorption laws hold are apparent for the data taken at each helium pressure. The nearly horizontal transition region between the two limiting absorption regions is also present for the absorption data taken at zero helium pressure. The 746 mm Hg helium pressure data at the higher temperatures were corrected both for the hyperfine structure and for the self-broadening contribution, and are shown in Figure 19. The contribution from self-broadening was removed by subtracting out the zero helium

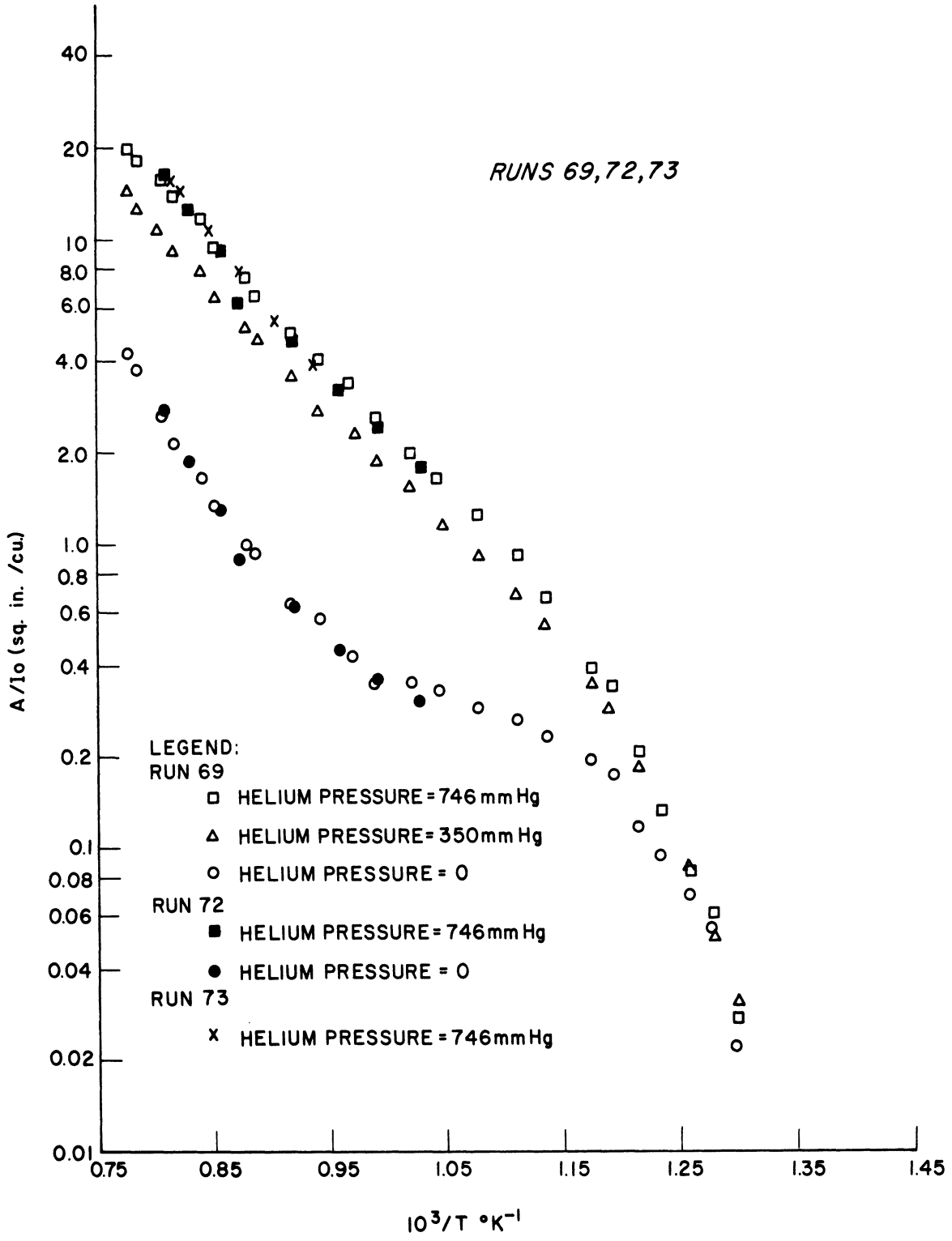

Figure 18. Bismuth Absorption Data

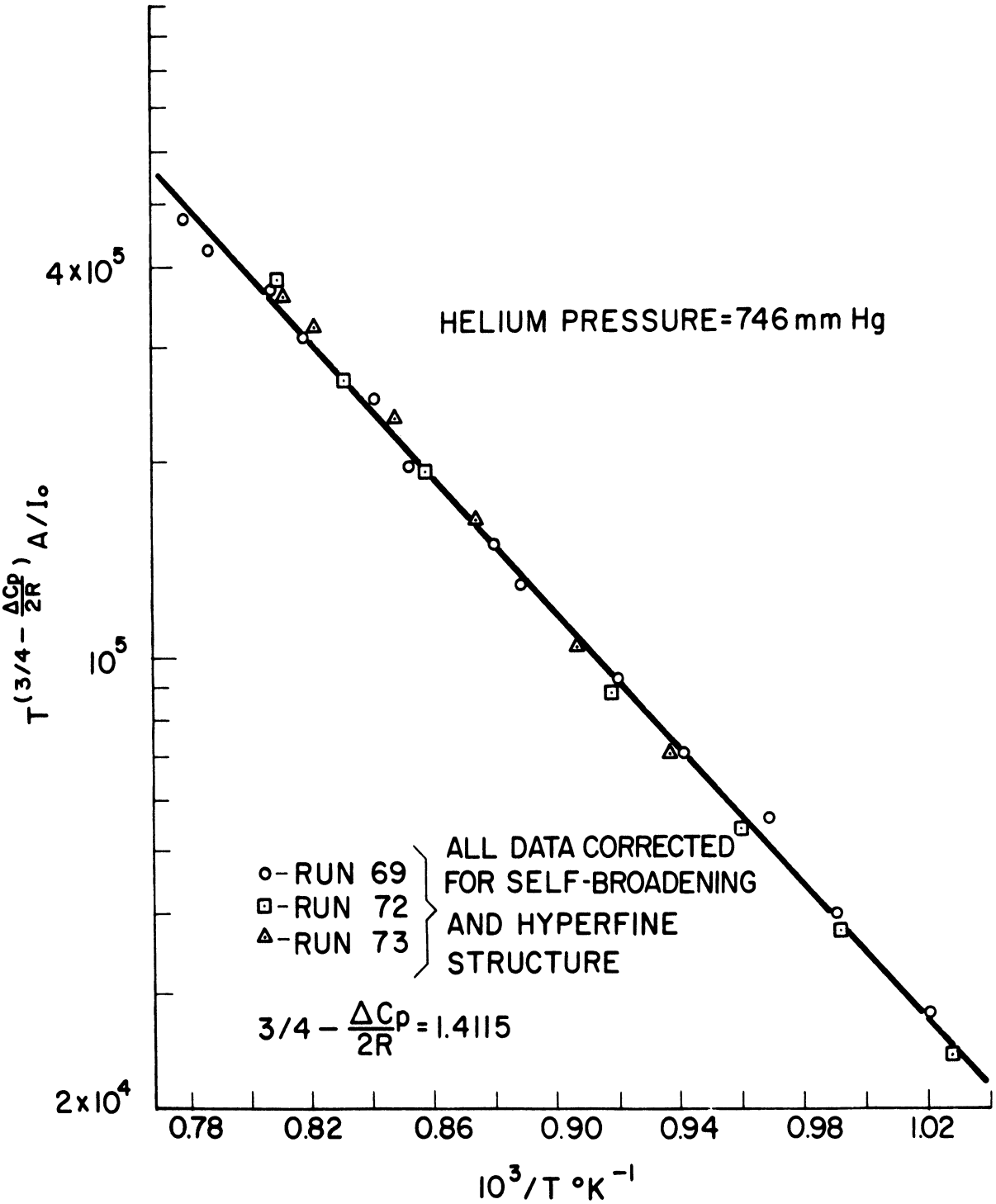

Figure 19. Corrected Bismuth Absorption Data

pressure contribution to the total absorption, using Equation (12) while the hyperfine structure correction was made using the hyperfine correction function for the Bi 3067Å line, plotted in Figure 4. As a result of these two corrections, the data of Figure 19 follow the square root absorption law exactly.

The heat of vaporization of bismuth was found by calculating the least square line through this 746 mm Hg helium pressure data. The heat of vaporization, obtained from the slope of the least square line, is given by the equation:

$$\Delta H_{v,\,Bi,\,T} = 48{,}100 - 2.63T \pm 1100^{*} \text{ cal/mole} \qquad (33)$$

$$800 < T < 1250^{\circ}K$$

and $\Delta H_{v,Bi,298^{\circ}K}$ is compared to the recalculated value of Brackett and Brewer[3] in Table I. The table shows that the values obtained from the optical absorption data agree within the experimental precision of the data with the recalculated value obtained from effusion data.

TABLE I

Heats of Vaporization

	OUR VALUE	RECALCULATED BY BRACKETT AND BREWER
$\Delta H_{v,\,Bi,\,298^{\circ}K}$	49,600 ± 1100 cal/gm mole	49,500 ± 1000 cal/gm mole
$\Delta H_{v,\,Bi_2,\,298^{\circ}K}$	49,430 ± 2000 cal/gm mole	52,500 ± 2000 cal/gm mole
		STULL AND SINKE
$\Delta H_{v,\,Pb,\,298^{\circ}K}$	47,240 ± 850 cal/gm mole	46,800 ± 300 cal/gm/ mole

A plot of the diatomic absorption data taken at zero and 746 mm Hg helium pressure is shown in Figure 7. Only those data points which fell on the straight line portion of Figure 7 were used to calculate the least square line and the heat of vaporization of Bi_2. The $\Delta H_{v,\,Bi_2,\,298^{\circ}K}$ obtained from the least square slope is given by the equation below and is compared with

*95% Confidence Limits

Brackett and Brewer's recalculated value in Table I.

$$\Delta H_{v,Bi_2,T} = 46{,}800 - 6.26\,T \pm 2000^{*} \text{ cal/mole} \qquad (34)$$
$$970 < T < 1150^{\circ}K$$

Discussion of Bismuth Heats of Vaporization Calculation. The contribution to the total absorption from the hyperfine structure was calculated from a knowledge of the hyperfine structure and the hyperfine correction function shown in Figure 4. The size of this correction varied from 18% for the lowest temperature data point to 0.2% for the highest temperature data point. The correction for self-broadening was less than 1%.

The bending away of the diatomic absorption measurements at the higher temperatures was not expected and is not predicted by either Elasser's or Plass's theoretical models. This anomaly would be explained if the intensity of the re-emitted light which can be seen by the spectrometer became a significant percentage of the transmitted light or the number of excited molecules in the vapor became a significant proportion of the total number of molecules. Approximate calculations of the magnitude of either of the two above effects indicate that they are completely negligible. The anomaly could also result from the overlapping absorption of another nearby band, if this absorption caused the baseline of the measured absorption band to deviate from linearity. The data show some indication of this. The slope of the intensity versus frequency trace before absorption begins increases with the temperature over the whole temperature range of measurement. On the other hand, the slope of the intensity versus frequency plot during absorption increases with temperature only until that temperature is reached where the bending away of the absorption curve begins; then it begins to decrease. This

*95% Confidence Limits

behavior indicates that the intensity versus frequency plot of the unabsorbed light is no longer a straight line, thus leading to errors in the computed value of the transmittance. Also it is important to realize, in this regard, that for larger absorption values small errors in the value of the transmitted intensity at the band head lead to considerable errors in the transmittance since I_t has such a small value (0.07 - 1.10 cu.).

Another possible source of error is the estimate of the average value of the transmittance used. Alternatively, the value of I_o could have been extrapolated to the frequency of maximum absorption and the values of I_o and I_t read there. The procedure used in this work was chosen because it gives the same value of I_o/I_t regardless of the slope of the baseline (assuming it is linear) while the above procedure does not.

Table I shows that the heat of vaporization values obtained from this work agree well within the limits of the precision of the data with the values recalculated by Brackett and Brewer. The only possible significant difference exists between the two values of the diatomic heat of vaporization.

This difference may result from discrepancies which exist in the earlier bismuth vapor pressure measurements. Brackett and Brewer's general success in making these earlier measurements consistent does not insure that the compiled result is not in error.

The third law of thermodynamics allows the calculation of the vapor pressure from the heat of vaporization using the entropy of vaporization. Heat capacity measurements for the condensed phase for temperatures from absolute zero to the temperature of interest determine the entropy of the liquid. Thus, if the vapor phase can be assumed an ideal gas, the entropy of vaporization can be calculated. This is the principle which Brackett and Brewer used to correlate the bismuth vapor pressure data which had been

obtained by that time. By using this technique, the vapor pressure of Bi and Bi_2 at 1000°K were predicted from the heats of vaporization determined in this work. By using the ΔH_v's and the Δc_p's to extrapolate these pressures to higher temperatures, the boiling point of bismuth can also be predicted. The heat of vaporization values from this work, together with the entropies of vaporization from Stull and Sinke, were used to predict the boiling point of bismuth to be 1830° ± 5°K. This compares with 1852°K predicted by Brackett and Brewer and 1832°K predicted by Stull and Sinke.

Lead. Optical absorption measurements of the lead 2833Å absorption line were also taken for pure lead vapor in equilibrium with liquid lead at helium pressures of zero and 746 mm Hg. Figure 20 shows the lead data over the whole temperature range of measurements. The higher temperature lead data which follow the square root absorption law were corrected for hyperfine structure and self-broadening and plotted in figure 21. The $\Delta H_{v,Pb}$ of lead was determined from the slope of the least square line through the data of Figure 21. For this calculation, Δc_p was assumed to be constant over the temperature range of measurement although in reality it decreases from 7.17 to 6.95 as the temperature changes from 800 to 1200°K. The results of the least square fit are given in the equation below and the $\Delta H_{v,Pb,298°K}$ is compared with that reported by Stull and Sinke[28] in Table I.

$$\Delta H_{v,Pb,T} = 46,700 - 2.0\ T \pm 850 \text{ cal/mole} \qquad (35)$$

The two values agree well within their respective precision limits.

H. Discussion of Lead Heat of Vaporization Determination

All of the lead data at the higher temperatures were used to compute the least square line. The hyperfine correction involved for

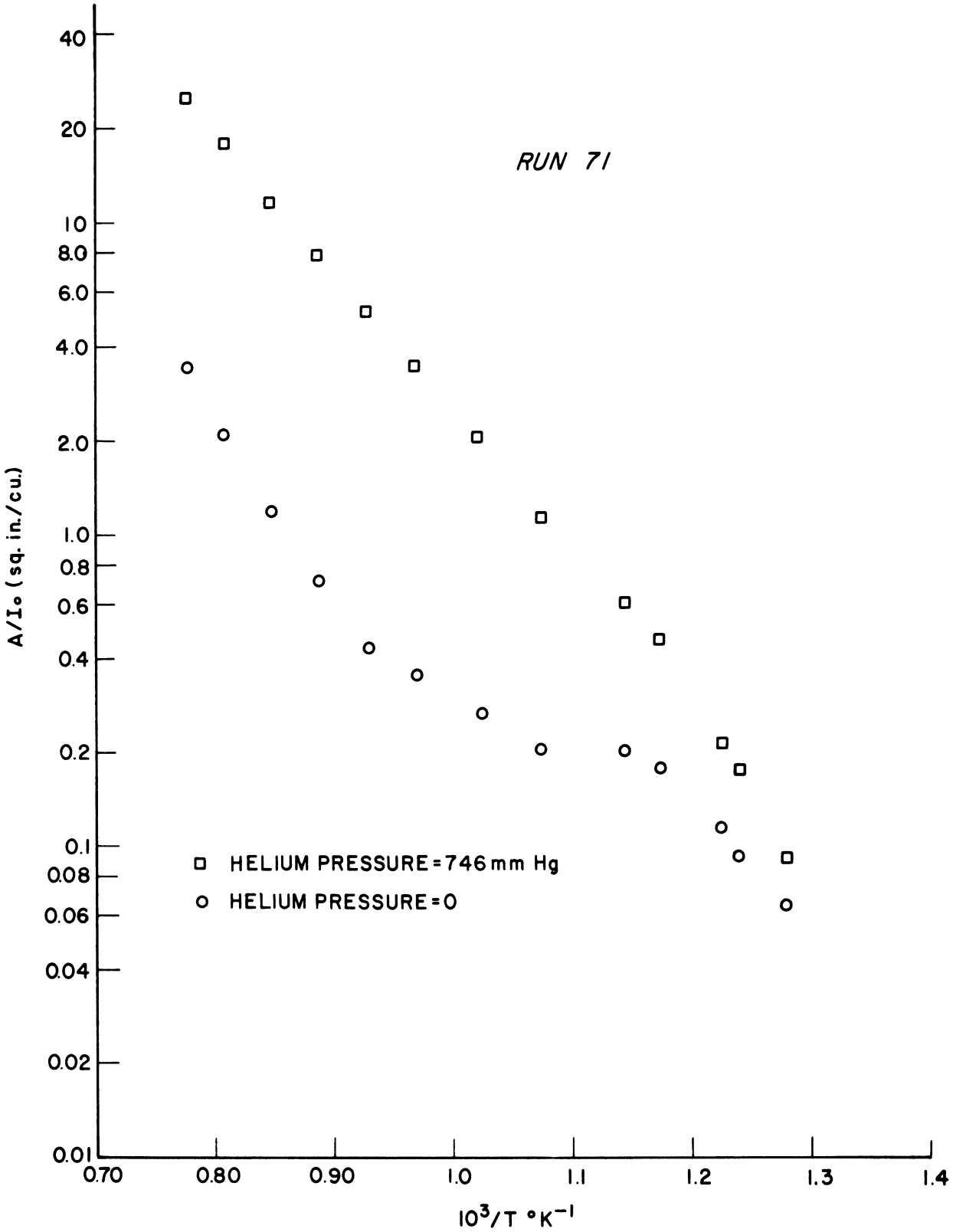

Figure 20. Lead Absorption Data

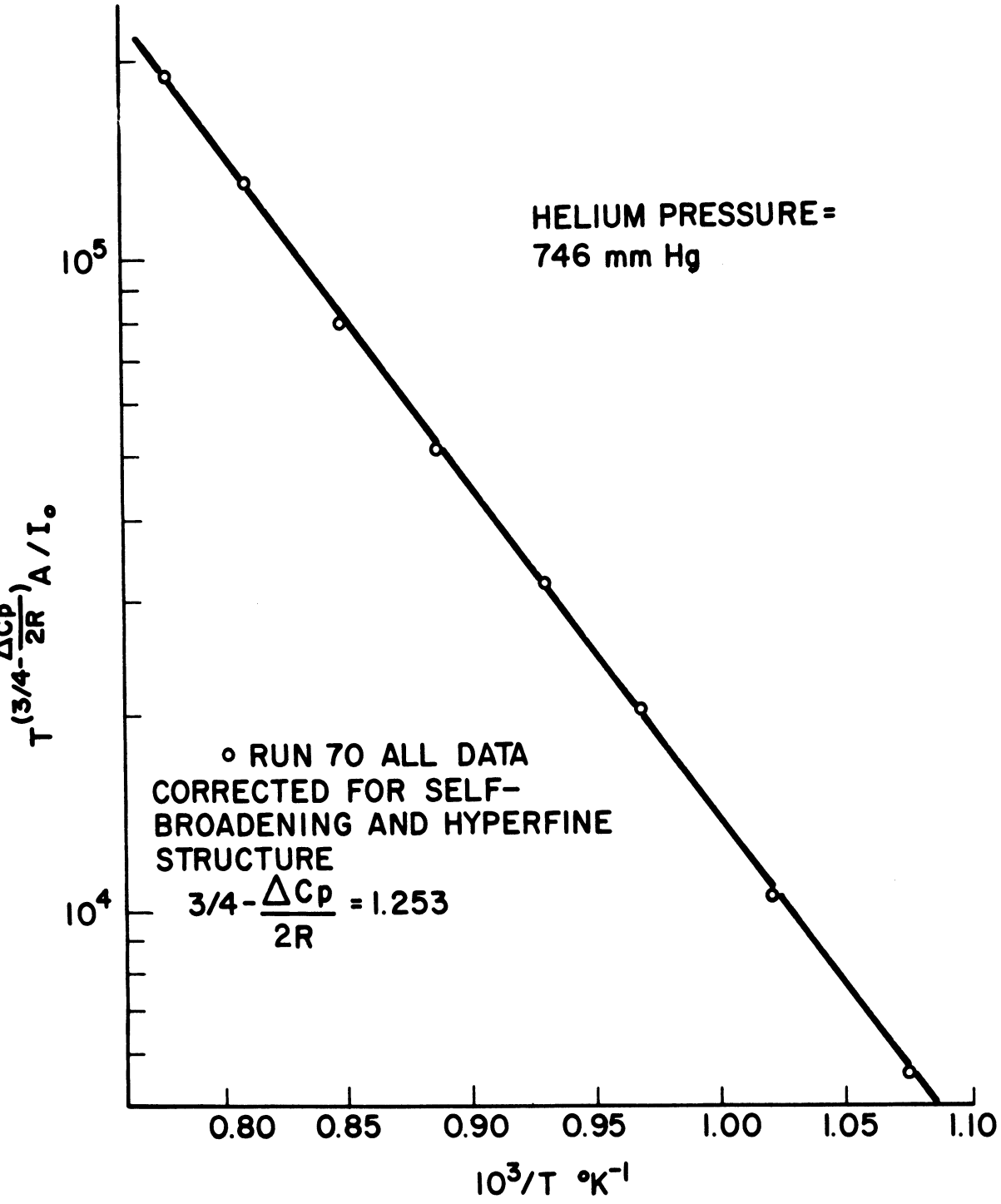

Figure 21. Corrected Lead Absorption Data

the experimental values of total absorption is practically negligible except for the data point taken at the lowest temperature. The correction for that point was 3.9%.

The optical absorption data for lead indicate the reliability of the method for the determination of heats of vaporization when hyperfine structure is not an important factor. The data also demonstrate the validity of the square root absorption law.

CHAPTER VI

SPECTROSCOPIC MEASUREMENTS

A. Introduction

The atomic optical absorption measurements of the lead 2833Å and the bismuth 3067Å lines were also used to calculate the vapor pressure of bismuth, the lifetimes of the excited states of the absorption lines, the collision cross-sections of the absorbing vapor with helium, and the self-collision cross sections. The vapor pressure of bismuth and the lifetime of the excited state of the bismuth 3067Å line were determined simultaneously in the manner described in chapter IV, B. The resulting vapor pressures were compared with Brackett and Brewer's recalculated vapor pressure values. Sufficient data were not taken to simultaneously determine the vapor pressure of lead and the lifetime of the excited state of the Pb 2833Å line. The lifetime of the lead line was calculated, however, from the absorption measurements using Stull and Sinke's compilation of lead vapor pressure based primarily on the data of Rodebush and Dixon [19], [20].

For both the Bi 3067Å line and the Pb 2833Å line, the self-collision cross-sections were determined from the zero helium pressure absorption data using the heat of vaporization values determined previously from the 746 mm Hg helium pressure data. This method was discussed earlier in the text of this report and described more fully in Appendix G. The helium collision cross-sections were obtained from the ratio of the total absorptions measured at 746 mm Hg helium pressure to those measured at zero helium pressure which were corrected for self-broadening and hyperfine structure.

B. Calculations for the Bi 3067Å Line

Figure 18 shows the Bi 3067Å absorption data over the whole range

of measurements. Data was taken in the linear absorption law region primarily under 746 mm Hg helium pressure while the data in the square root law region were taken at zero, 350, and 746 mm Hg helium pressure. As was pointed out earlier, the total absorption data at zero helium pressure are significantly affected by contributions from the hyperfine structure of the line and self-broadening resulting from the collisions between the absorbing atoms. To determine simultaneously the lifetime in the excited state and the vapor pressure the contributions of the hyperfine structure and self-broadening must be subtracted from the absorption data taken at zero helium pressure. These corrections are necessary for an accurate extrapolation of the square root absorption data to the linear absorption region. The data were corrected for hyperfine structure using the hyperfine correction function chart (Figure 4). The self-broadening corrections for the zero helium pressure total absorption data were made using the slope of the Clapeyron plot of the total absorption data taken at 746 mm Hg helium pressure, $(-\frac{\Delta H_V - \Delta c_p T}{2 \times 2.303 R})$. The proper corrections were determined by trying various intercept values for an assumed corrected zero helium pressure $T^{(\frac{1}{2} - \frac{\Delta c_p}{2R})} A/I_o$ versus $1/T$ line, until the slope of the $T^{(\frac{1}{2} - \frac{\Delta c_p}{R})}(r_b - 1)$ versus $1/T$ line equalled $-\frac{\Delta H_V - \Delta c_p T}{2.303 R}$ *. Once the line representing the corrected zero helium pressure total absorption data following the square root absorption law was determined it was extrapolated to the lower temperatures where the total absorption is proportional to the first power of the vapor concentration. The natural breadth, b_N, the lifetime, τ, and the integrated intensity, S, were then calculated from Equations (13), (14), and (15). The intercept of the bismuth vapor pressure equation was also calculated using Equation (12) of Appendix G and the previously calculated intercept

*See Appendix G

of the least square line through the corrected zero helium pressure total absorption data.

The self collision cross-section (bismuth atoms with both bismuth atoms and bismuth dimers) was determined from the intercept of Equation (8) in Appendix G, since the intercept for the bismuth Clapeyron equation, C_I, and b_N have been previously determined. The collision cross-sections for bismuth by helium was calculated from Equations (16) and (17) of the text, using the corrected zero helium pressure absorption data.

The resulting vapor pressure equation is given below and a representative value of the vapor pressure at 1000°K is compared in Table II with corresponding values from Yoshiyama,[27] Brackett and Brewer, and a value obtained using the third law. The self-collision and helium collision cross-sections are listed together with the lifetime of the excited state of the 3067Å bismuth line in Table III.

$$\log_{10} p = \frac{-10521}{T} + 9.5380 - 1.323 \log_{10} T \qquad (36)$$

The estimated 95% confidence limits for the lifetime, collision cross-sections and vapor pressure values are also given in Tables II and III.

TABLE II

Estimated Vapor Pressures in Atm at 1000°K

	ABSORPTION DATA ALONE	THIRD LAW USING ΔH_V FROM ABSORPTION MEASUREMENTS	BRACKETT AND BREWER	YOSHIYAMA USING THIS ΔH_V
Bi	$1.1^{+0.7}_{-0.5} \times 10^{-5}$ atm	$1.8^{+1.3}_{-0.7} \times 10^{-5}$ atm	$2.07^{+1.3}_{-0.8} \times 10^{-5}$	1.35×10^{-5}
Bi_2	----	$1.1^{+2.0}_{-0.7} \times 10^{-4}$ atm	$2.8^{+4.8}_{-1.8} \times 10^{-5}$ atm	
Pb	----	$1.2^{+0.6}_{-0.4} \times 10^{-5}$ atm	STULL AND SINKE 1.51×10^{-5}	

TABLE III

Spectral Constants

	τ(sec)	σ_s^2 (Å^2)	σ_{He}^2 (Å^2)
Bi 3067Å line	$5.4^{+2.3}_{-1.7} \times 10^{-9}$	3100^{+3000}_{-1000}	$25.3^{+12.2}_{-8.5}$
Pb 2833Å line	$1.39^{+0.13}_{-0.13} \times 10^{-8}$	626^{+320}_{-210}	$14.2^{+3.8}_{-3.0}$
Engler	6×10^{-9}		

τ = lifetime in the excited state

σ_{He}^2 = optical collision cross-section for absorbing atoms with helium

σ_s^2 = optical collision cross-section for the absorbing atoms with other absorbing atoms (in the case of bismuth, collisions also occur with the diatomic species in the vapor).

C. Discussion of Bismuth Calculations

Brackett and Brewer's recalculated vapor pressures are 88% higher than the vapor pressures calculated from this optical absorption data. However, the uncertainty in both values is large enough so that they are not significantly different. The previous vapor pressure data which were taken in the temperature range most closely corresponding to the temperature range of these optical absorption measurements were the data of Yoshiyama[27]. His bismuth vapor pressure measurements, using a torsion effusion cell in the temperature range, 912-962°K, agree very well with the vapor pressures calculated from the optical absorption data if the slope of the Clapeyron plot of Yoshiyama's data is made to agree with the heat of vaporization value obtained from this absorption data.

No previously measured values of the lifetime in the excited state and the self-broadening and helium collision cross-sections were found in the literature for the Bi 3067Å line so no comparison could be made for the values obtained in this work.

The 95% confidence limits for the lifetime, τ, and the vapor pressure were estimated from the confidence limits of the slope of the zero helium pressure total absorption data following the square root absorption law and the error limits of the total absorption values following the linear absorption law. These error limits amount to $^{+39\%}_{-29\%}$ for the value of τ and to $^{+60\%}_{-40\%}$ for the vapor pressure of bismuth. These error limits reflect for the most part the uncertainties in the zero helium pressure total absorption data which are amplified by the extrapolation to the linear absorption region. The error limits for the helium collision cross-section, σ_I^2, were calculated from the 95% confidence limits of the 746 mm Hg and the zero helium pressure total absorption data and the previously calculated confidence limits of τ. The error limits on the self-broadening cross-sections, σ_S^2, were calculated from an estimated possible error in $(r_b - 1)$ line and the error limits in the lifetime, τ. All of these error calculations were made assuming that the logarithms of the total absorption data are normally distributed.

D. Calculations for the Lead 2833Å Line

An attempt was made to obtain lead absorption data in the linear absorption region in order to also determine simultaneously the vapor pressure of lead and the lifetime of the excited state of the 2833Å line of lead. Absorption data at 746 mm Hg helium pressure could not be taken at temperatures low enough so that the total absorption values varied with the first power of the concentration. This is indicated by the lead absorption data plotted in Figure 20. Consequently, the lifetime in the excited state was calculated from the zero helium pressure lead data taken in the concentration region where the total absorption

varies with the square root of the concentration. The atomic lead data were corrected for self-broadening in the same way as was the atomic bismuth data discussed earlier, using the heat of vaporization of lead determined from the 746 mm Hg helium pressure data. Corrections for hyperfine structure were also made using the hyperfine correction function plot. Once the corrected total absorption is known for the hypothetical non-self-broadened absorption lines, τ, the lifetime in the excited state, can be calculated from $A/I_o = 0.568\beta = 1.136\sqrt{Sb_N X} = 1.136\sqrt{\frac{\lambda_o^2}{32\pi^2 c^2 \tau^2} g_2/g_1 X}$. The self-broadening collision cross-section for helium on lead was calculated from Equation(8)of Appendix G using the value of τ calculated above and the known intercept of the lead Clapeyron equation. The helium collision cross-section was calculated from Equations (16) and (17) of the text using the total absorption data taken at zero and 746 mm Hg helium pressure and the value of τ calculated above. These values of τ, σ_s^2, and σ_I^2 are given in Table III with estimates of the 95% confidence limits of the values.

E. Discussion of Lead Calculations

The lifetime of the excited state of the Pb 2833Å line has previously been measured by Engler[7]. His value, also given in Table III, is about half the value determined for this work. Neglecting the corrections for self-broadening and hyperfine structure would still yield a value for the lifetime which would be higher than that determined by Engler. One might suspect that vapor-liquid equilibrium was not attained within the cell because of the diffusion of lead atoms across the quartz to quartz seal. This possibility was checked, however, by calculating the diffusion rate across the quartz to quartz seal from the amount of lead condensed in the cold end of the absorption cell at the end of a run. This rate was calculated to be more than 1000 times less than the evaporation rate in the cell

estimated from kinetic theory. On the other hand, Engler's value may be in error since he made measurements using a narrow emission line as the light source. Errors in the observed integrated absorption of this source, resulting from the distortion of the true line shape, would lead to a value of the lifetime which would be too low[12].

The error limits of the lifetime in the excited state were calculated from the estimated uncertainty in the corrected zero helium pressure total absorption data which follow the square root absorption law. The error limits of the helium collision cross-section were determined from the above uncertainty and the 95% confidence limits of the 746 mm Hg helium pressure total absorption data. The uncertainties in the self-broadening cross-section were estimated from the error limits of $(r_b - 1)$ and those previously calculated for the lifetime. These error calculations are based on a log-normal distribution of the total absorption data.

CHAPTER VII

SUMMARY AND CONCLUSIONS

The avowed purpose of this work was to investigate optical absorption as a means of measuring the thermodynamic properties of metal alloys. The scope of the work was later expanded to include the calculation of vapor pressures and certain spectroscopic constants (lifetimes, cross-sections, etc.).

The heat of vaporization determinations made from the pure lead and pure bismuth optical absorption measurements demonstrate the validity of the square root law for atomic absorption measurements and Beer's law for diatomic absorption measurements. They also point out the necessity of taking into account the effects of the hyperfine structure and self-broadening on the atomic absorption lines.

The activity measurements in the lead-bismuth alloy demonstrate that optical absorption can be used to measure activities, again confirming the optical absorption laws and indicating the importance of correcting for or masking out the effects of hyperfine structure and self-broadening. These activity measurements also show the inherently lower statistical error of the diatomic measurements and, moreover, show how a number of species in the vapor above an alloy can be monitored independently.

The bismuth activity measurements in U-UBi point up the extended range of activity measurements available when atomic absorption following the square root absorption law is used. They also demonstrate the use of inert gas pressure broadening for amplifying absorption line size.

The calculation of the lifetimes of the excited state of the Pb 2833Å line and the collision cross-sections of this line between helium and lead and between lead and lead show how spectroscopic data can be obtained from

optical absorption measurements if the vapor concentration is already known.

Finally, the simultaneous determination of the vapor pressure of bismuth and the lifetime of the excited state of the Bi 3067Å line demonstrate how the Clapeyron equation, derived from the conditions for liquid-vapor equilibrium, may be used to tie together two different absorption laws corresponding to two different vapor concentration regions. This technique provides a way of obtaining both the lifetime in the excited state and the vapor pressure exclusively from optical absorption measurements.

As a technique for measuring thermodynamic properties, optical absorption has the advantage over other vapor pressure measuring techniques of allowing the experimenter to observe any number of individual species in the vapor independently since the spectra of each specie is independent. It is also a relatively quick method of measurement and can cover a considerable temperature range since data points over a 200 - 300°K temperature range may be obtained in a single run. The accuracy of the atomic absorption measurements is dependent largely upon the accuracy of the corrections for or the completeness of the masking out of unwanted contributions to the total absorption from hyperfine structure and self-broadening. Generally speaking diatomic absorption activity measurements are more precise, if they can be made, but the range of measurement is limited since $\log_{10} (I_o/I_t)$ decreases as the square of the activity. On the other hand, atomic absorption offers more flexibility for activity determinations than diatomic absorption since the size of the total absorption can be regulated by orders of magnitudes through foreign gas collision

broadening and total absorption measurements following the square root absorption law decrease only as the square root of the activity.

The maximum temperature at which measurements can be made is determined by the absorption cell material. For quartz cells, such as those used for this work, the maximum working temperature was about 1000°C. If measurements at higher temperatures are desired, they can be made with a cell similar to the one used by Vidale[25].

In general it can be concluded that optical absorption is most useful for measuring thermodynamic properties when there are multiple species in the vapor, the temperature of measurement is less than 1000°C, and the hyperfine and self-broadening contributions to atomic absorption are small.

APPENDIX A

EQUIPMENT

The light source used to supply a continuum in the desired frequency range was a high-pressure mercury lamp, H3FE, manufactured by General Electric. The lamp was contained in a water-cooled jacket and the power input was stabilized by two ballast transformers. The maximum fluctuation of the light intensity was not greater than 2%. The lamp emits an approximately continuous intensity over the wavelength region from 2600 to approximately 4000Å except in the vicinity of mercury emission lines. The cell used for the absorption measurements was made entirely of quartz with optically flat, polished windows. Quartz cells were procured from the Euclid Glass Engineering Laboratory, Cleveland, Ohio and the Superior Glass Apparatus Company, Ann Arbor, Michigan. The window spacing employed for this work was 4.6 cm.

The furnace used to heat the quartz cell was a split-wound, resistance furance. The furnace had two main windings and two end windings, separately controlled to offset the effect of end-cooling. By regulating the power input to the various windings, it was possible to control the temperature in the immediate vicinity of the cell to $\pm$2°C. The necessary isothermal volume in the furance was a cylinder 5 cm in diameter and 10 cm in length. A small crucile, containing absorbing material, and the absorption cell proper were located in the center of this isothermal range. Temperatures were measured in four different positions along the cylinder with calibrated chromel-alumel thermocouples. The thermocouples were placed in the immediate vicinity of the cell.

The total pressure in the absorption cell was regulated by a helium dispensing unit. High purity helium was slowly released from a

high pressure cylinder through a liquid nitrogen cold trap into the vacuum line. The quartz to quartz seal in the absorption cell served the dual purpose of containing the absorbing atoms while allowing the helium atoms to pass back and forth freely. The seal worked remarkably well, allowing almost instantaneous changes of helium pressure in the cell proper while keeping the diffusion rate of the absorbing atoms from the cell to less than one thousandth that of the evaporation rate calculated from kinetic theory. The helium pressure in the system was measured by a mercury manometer.

A plano-convex lens was placed at its focal distance from the mercury lamp source to give a parallel beam of light through the absorption cell. After passage through the cell, the light was condensed with another plano-convex lens before it reached the spectrometer. The mercury lamp source was not a point source and hence some divergence was still present. This did not affect the measurements, however, since the path length through the cell was less than 5 cm. In this length the beam of light was essentially parallel. The absorbed radiation was analyzed by means of a Leeds and Northrup spectrochemical analyzer. The unit contains a small plane grating monochromator. The spectrometer is 30 inches long and uses a 3 inch wide grating with 30,000 lines per inch. Spectra were obtained which demonstrate a second-order resolution of 0.1Å in the visible and ultraviolet region.

Approximately 1% of the light through the cell was reflected by a mirror in front of the entrance slit to a reference phototube called I_s. The remaining radiation passed through the spectrograph and was recorded by the phototube marked I_x which was at the exit slit. The radiation striking the I_s tube has wavelengths from approximately 2500-4000Å. The light striking the I_x phototube corresponds to radiation in a small wavelength region.

The signals from the two phototubes were fed into a dual-channel amplifier. The power input to the phototubes could be adjusted so that at any particular reading the intensity of the two signals in the amplifier could be balanced. The output from the dual-channel amplifier was recorded on a ratio recorder, which displayed the intensity ratio I_x/I_s as a function of wavelength. Splitting the radiation before it entered the monochromator helped stabilize the recorded intensity trace. The instrument was set to scan in a particular wavelength region at a speed of 2.9Å/min.

APPENDIX B

EXPERIMENTAL PROCEDURE

The general aspects of the experimental procedure are described below. In particular experimental instances, deviations from the general procedure were made. These deviations are discussed in the text of the report.

1. Two to six grams of the element or elements of interest were placed in an alumina boat and the boat placed inside the absorption cell in the position shown in Figure 2.
2. The absorption cell and the helium apparatus were evacuated to a pressure of less than three microns of mercury.
3. The furnace was turned on, the temperature controller set, and heating continued until the cell reached equilibrium at the desired temperature. The end windings were then adjusted so the four thermocouples butted against the cell read within 2°C of each other.
4. If the absorption measurements were to be taken under a particular helium pressure, the vacuum line was closed off and helium released slowly into the system until the desired pressure was reached. The absorption measurements were taken at this point.
5. After an absorption measurement had been taken, the cell was re-evacuated, the temperature controller reset, and the cell allowed to come to equilibrium at a different temperature.

Steps 4 and 5 are repeated until all the desired absorption data has been taken.

It was necessary to heat the absorption cell under vacuum in order to remove the outgas which was released from the walls of the quartz cell, the alumina boat, and the element or alloy in the boat. For experimental runs made with sealed cells which were evacuated at room temperature, the amount of pressure broadening resulting from the outgas caused increases in the size of the absorption lines of up to 100%.

APPENDIX C

THERMODYNAMIC ENERGY BALANCE

From Mitchell and Zermonsky pp. 93-95

Consider a parallel beam of light of wave-number between ω and $\omega + d\omega$ at intensity I_ω traveling in the positive x direction through a layer of atoms bounded by planes at x and x + dx. Suppose also that there are normal atoms of which the fraction $\frac{\delta N_\omega}{N}$ are capable of absorbing and N' excited atoms of which the fraction $\frac{\delta N'_\omega}{N'}$ are capable of emitting in this wave number range. Let:

$B_{1\rightarrow 2}$ = the probability per second that an atom in state 1 when exposed to parallel radiation traveling in a given direction x with wave number between ω and $\omega + d\omega$ and intensity I_ω will absorb a quantum $h\omega$ and pass to state 2.

A = the probability per second that an atom in state 2 will spontaneously emit in a random direction, a quantum $h\omega$ and pass to state 1 ($A = \frac{1}{\tau}$).

$B_{2\rightarrow 1}$ = the probability per second that an atom will when exposed to parallel radiation traveling in a given direction x with wave number between ω and $\omega + d\omega$, and intensity I_ω will emit a quantum $h\omega$ in the same direction as the stimulating quantum.

If the effects of spontaneous remission are neglected in view of the fact that they take place in all directions, then an energy balance written around the optical length increment dx yields:

$$-d\left[I_\omega\, d\omega\right] = \delta N_\omega\, dx\, h\omega\, B_{1\rightarrow 2}\, \frac{I_\omega}{4\pi} - \delta N'_\omega\, dx\, h\omega\, B_{2\rightarrow 1}\, \frac{I_\omega}{4\pi} \qquad (1)$$

Rewriting the above equation,

$$-\frac{1}{I_\omega N}\, d\omega\, \frac{dI_\omega}{dx} = -\frac{1}{I_\omega} d\omega\, \frac{dI_\omega}{dX} = \frac{h\omega}{4\pi N}\left(B_{1\rightarrow 2}\, \delta N_\omega - B_{2\rightarrow 1}\, \delta N'\omega\right) \qquad (2)$$

where X is the optical density in atoms/cm^2. Recognizing that the left hand member of the equation is P_ω, and integrating over all wave numbers, neglecting the slight variation of ω over the line,

$$\int_0^\infty P_\omega \, d\omega = \frac{h\omega_o}{4\pi} \left(B_{1 \to 2} - B_{2 \to 1} \frac{N'}{N}\right) \tag{3}$$

But from the thermodynamic equilibrium between the radiation and atoms, Einstein showed that:

$$\begin{aligned} A/B_{1 \to 2} &= 2hc\omega^3 \, g_1/g_2 \\ B_{2 \to 1}/B_{1 \to 2} &= g_1/g_2 \end{aligned} \tag{4}$$

Substituting these relations and the fact that $A = \frac{1}{\tau}$ into equation (3) yields

$$\int_0^\infty P_\omega \, d\omega = \frac{\lambda_o^2}{8\pi c} \frac{g_2}{g_1} \frac{1}{\tau} \left(1 - \frac{g_1}{g_2} \frac{N'}{N}\right) \tag{5}$$

APPENDIX D

ATOMIC ABSORPTION THEORY

The absorption coefficient of a material is defined by the equation

$$\frac{dI_\omega}{I_\omega} = -P_\omega dX \tag{1}$$

From the energy balance around a parallel beam of light traveling over length ℓ through N normal atoms and N' excited atoms, it can be shown (Appendix C) that regardless of the form of the absorption coefficient

$$\int_o^\infty P_\omega \, d\omega = \frac{\lambda_o^2}{8\pi c} \frac{g_2}{g_1} \frac{1}{\tau} \left(1 - \frac{g_1}{g_2} \frac{N'}{N}\right) \tag{2}$$

If $N'/N \ll 1$, as in the case at normal temperatures when the gas is not electrically excited,

$$\int_o^\infty P_\omega \, d\omega = \frac{\lambda_o^2}{8\pi c} \frac{g_2}{g_1} \frac{1}{\tau} = S \tag{3}$$

The shape of P_ω is the result of the superposition of its possible functional forms. For the line broadening effect due to the motion of the atoms, Doppler broadening,

$$P_\omega = \frac{S}{b_D} \sqrt{\ln 2} \; e^{-\left(\frac{\omega - \omega_o}{b_o} \sqrt{\ln 2}\right)^2} \tag{4}$$

For the broadening due to the inherent uncertainty in the energy levels (natural broadening) and the uncertainty in the energy levels resulting from interatomic collisions (collision broadening),

$$P_\omega = \frac{Sb}{\pi} \frac{1}{(\omega - \omega_o)^2 + b^2} \tag{5}$$

The probability that an absorption will take place at ω-ω_o for either broadening process is given by P_ω/S. If both broadening processes are present, the probability that an absorption will take place at ω-ω_o is given by the superposition of the probabilities for each process. Consequently, if both broadening process are present the total probability

that an absorption will take place at $\omega-\omega_o$ is:

$$\frac{P_\omega}{S} = \frac{b}{\pi b_D}\sqrt{\frac{\ln 2}{\pi}} \int_{-\infty}^{\infty} \frac{e^{-(\delta/b_D\sqrt{\ln 2})^2}}{(\omega - \omega_o - \delta)^2 + b^2}\, d\delta \qquad (6)$$

The above equation represents the sum of all the possible Doppler broadenings of an infinitesimal wave number band at a distance $\omega-\omega_o$ from the center of a line showing only dispersion broadening.

By considering the ratio of the dispersion absorption coefficient to the Doppler absorption coefficient, it can be shown that the dispersion absorption coefficient becomes much greater than the Doppler absorption coefficient if $(\omega-\omega_o)^2$ becomes large enough. Consequently, the shape of the edges of an absorption line are determined only by the dispersion absorption coefficient. Now if X is large enough so the intensity of the absorption line in a region about its center is practically zero, i.e., the center region of the line is totally absorbed, then the entire shape of the line is determined by the dispersion absorption coefficient. Furthermore, if the width of this totally absorbed region is much greater than the dispersion half-breadth, b, then the absorption coefficient may be written as:

$$P_\omega = \frac{Sb}{\pi} \frac{1}{(\omega - \omega_o)^2} \qquad (7)$$

Since absorption lines are generally very narrow, i.e., half-breadths are on the order of a few hundredths of an angstrom, the true shape of the absorption line is not seen with ordinary spectrometers. Consequently, a measure of absorption which does not depend strongly on the resolution of the instrument is needed. Such a quantity is the ratio of the total energy absorbed by the line to the incident intensity. It is represented by:

$$\beta = \int_0^{\infty} \frac{I_o - I_\omega}{I_o}\, d\omega \qquad (8)$$

or

$$\beta = \int_0^\infty (1 - e^{-P_\omega X})\, d\omega \tag{9}$$

If $P_\omega X$ is small, the exponential term can be replaced by $1-P_\omega X$ and

$$\beta = \int_0^\infty P_\omega X\, d\omega = SX \tag{10}$$

as a consequence of the energy balance discussed earlier.

In the case that $P_\omega X$ is large enough so that the center of the line is totally absorbed over a sufficiently wide region for Equation (7) to hold,

$$\beta = \int_0^\infty \left(1 - e^{-\frac{SbX}{\pi} \frac{1}{(\omega - \omega_o)^2}}\right) d\omega \tag{11}$$

By letting $\mu = \omega-\omega_o$ and introducing a multiplicative factor $\lim_{q^2 \to 0} e^{-q^2\mu^2}$ Equation (11) becomes:

$$\beta = \lim_{q^2 \to 0} \int_{-\infty}^{\infty} \left(e^{-q^2\mu^2} - e^{-q^2\mu^2 - \frac{SbX}{\pi\mu^2}}\right) d\mu$$

$$\beta = \lim_{q^2 \to 0} \sqrt{\frac{\pi}{q}} \left[1 - e^{-2q\sqrt{\frac{SbX}{\pi}}}\right]$$

$$\beta = \lim_{q^2 \to 0} \sqrt{\frac{\pi}{q}} \left[1 - 1 + 2q\sqrt{\frac{SbX}{\pi}}\right]$$

$$\beta = 2\sqrt{SbX} \tag{12}$$

Thus, two limiting regions arise, one when $P_\omega X$ is small and β is independent of the broadening and is proportional to X, and another when $P_\omega X$ is large and β is proportional to the square root of bX.

If both sides of Equation (9) are divided by $2b_D$, multiplied by $\sqrt{\ln 2}$ and the logarithms of both sides are taken, the two limiting equations become:

$$\log \left(\frac{\beta}{2b_D} \sqrt{\ln 2}\right) = \log \left(\frac{SX}{2b_D} \sqrt{\ln 2}\right) \tag{13}$$

and

$$\log\left(\frac{\beta}{2b_D}\sqrt{\ln 2}\right) = \tfrac{1}{2}\log\left(\frac{SX}{2b_D}\sqrt{\ln 2}\right) + \tfrac{1}{2}\log\left(\frac{2b}{b_D}\sqrt{\ln 2}\right) \qquad (14)$$

In the first case a log-log plot of $\frac{\beta}{2b_D}\sqrt{\ln 2}$ vs $\frac{SX}{2b_D}\sqrt{\ln 2}$ yields a single line for all dispersion broadenings. In the second case a similar plot yields a series of lines which depend on the ratio of dispersion to Doppler broadening. The traditional way of presenting Equation (9) is to present a series of calculated values of curves on a log-log plot [23], [24] of $\frac{\beta}{2b_D}\sqrt{\ln 2}$ vs $6\,\frac{SX}{b_D}\sqrt{\ln 2}$. Such a set of curves is shown in Figure 3.

APPENDIX E

MOLECULAR ABSORPTION THEORY

From S. S. Penner, pp. 178-182

Consider a vibration-rotation band with equally spaced, equally intense spectral lines. The lines are a distance, d cm^{-1}, apart with centers at nd, where n is an integer. For lines which have a dispersion contour with half-breadth, b, it follows from Equation (5) of Appendix D that the absorption coefficient at wave number ω, is:

$$P_\omega = \sum_{n=-\infty}^{\infty} \frac{Sb}{\pi} \frac{1}{(\omega - nd)^2 + b^2} \qquad (1)$$

P_ω is a periodic function and can be expressed in terms of trigometric functions* as follows:

$$\text{If } s = \frac{2\pi\omega}{d} \quad \text{and} \quad \beta = \frac{2\pi b}{d}$$

then Equation (1) becomes

$$P_s = \frac{S}{d} \frac{\sinh \beta}{\cosh\beta - \cos s} \qquad (2)$$

Now let

$$\cos\phi = \frac{1-(\cos\beta)\cos s}{\cosh\beta - \cos s}$$

From which it follows that

$$\sin\phi = \frac{(\sinh\beta)(\sin s)}{\cosh\beta - \cos s},$$

$$\frac{\sinh\beta}{\cosh\beta - \cos s} = \frac{\sin\phi}{\sin s} = \frac{\cosh\beta - \cos\phi}{\sinh\beta} \qquad (3)$$

and

$$ds = \frac{\sinh\beta}{\cosh\beta - \cos\phi} d\phi \qquad (4)$$

The transmittance averaged over wave number interval, d, is given by:

$$T_R = \frac{1}{d} \int_{-d/2}^{d/2} \left[\exp(-P_\omega X)\right] d\omega$$

* See E. T. Whittaker and G. N. Watson, A Course in Modern Analysis, Chapter 7.4, 4th ed., Cambridge University Press.

Since the absorption pattern is repetitive, the integration may be also performed over an integral multiple of d.

Using the relation, $s = 2\pi\omega/d$,

$$T_R = \frac{1}{2\pi} \int_{-\pi}^{\pi} \left[\exp\left(-P_s X\right)\right] \, ds \qquad (5)$$

Substituting for P_s and expressing the result in terms of ϕ from Equations (3) and (4) yields:

$$T_R = \frac{\sinh\beta}{2\pi} \int_{-\pi}^{\pi} \frac{\exp(-y\,(\cosh\beta) + y\,(\cos\phi))}{\cosh\beta - \cos\phi} \, d\phi \qquad (6)$$

where:

$$y = \frac{SX}{d\sinh\beta} \qquad (7)$$

Differentiation of (6) with respect to y yields:

$$\frac{dT_R}{dy} = \frac{\sinh\beta}{2\pi} \int_{-\pi}^{\pi} \exp\left[-y(\cosh\beta) + y(\cos\phi)\right] \, d\phi$$

using the fact that $\cos\phi$ is an even function of ϕ.

But

$$\frac{1}{2\pi} \int_{-\pi}^{\pi} \left[\exp(y\cos\phi)\right] \, d\phi = J_o\,(iy),$$

the zeroth order Bessel function of (iy).

Therefore

$$\frac{dT_R}{dy} = \sinh\beta \left[\exp(-y\cos\beta)\right] \quad J_o(iy)$$

and

$$T_R = \sinh\beta \int_{y}^{\infty} \left[\exp(-y\cosh\beta)\right] \quad J_o\,(iy)\,dy \qquad (8)$$

The limits of integration have been taken such that $T_R \to 1$ as $y \to 0$ or $X \to 0$, and $T_R \to 0$ as $y \to \infty$ or $X \to \infty$.

If $b << d$, then β is $<< 1$, and $\sinh \beta \approx \beta$. Then $y = \frac{SX}{d\beta} = \frac{SX}{2\pi b}$. If y is large, then the integration in Equation (8) is limited to large values of y. Since $\lim_{y \to \infty} J_o(iy) = \frac{e^y}{\sqrt{2\pi y}}$ and $\sinh \beta \approx \beta$ and $\cosh\beta - 1 \approx \beta^2/2$ for small β, Equation (8) becomes:

$$T_{R_{b << d,\ y \text{ large}}} = \beta \int_y^\infty \exp\left(\frac{-y\beta^2}{2}\right) \frac{dy}{\sqrt{2\pi y}}$$

Since the error integral is defined by

$$\phi(z) = \frac{2}{\sqrt{\pi}} \int_o^z \exp(-t^2)\, dt, \qquad \phi(\infty) = 1,$$

$$\left(T_R\right)_{b << d,\ y \text{ large}} \approx 1 - \phi\left(\sqrt{\frac{y\beta^2}{2}}\right) \tag{9}$$

If $\sqrt{\frac{y\beta^2}{2}}$ is also small,

$$\phi\left(\frac{y\beta^2}{2}\right) = \frac{2}{\sqrt{\pi}} \left(\sqrt{\frac{y\beta^2}{2}} - \frac{\left(\sqrt{\frac{y\beta^2}{2}}\right)^3}{3} + \ldots\right)$$

and

$$\left(T_R\right)_{b << d,\ y \text{ large},\ \sqrt{\frac{y\beta^2}{2}} << 1} = 1 - \sqrt{\frac{2y\beta^2}{\pi}}$$

$$= 1 - 2\sqrt{\frac{SbX}{d}} \tag{10}$$

If $b << d$ and $X << 1$, then y is not unusually large compared with 1.

Now $\beta >> 1$, $\cos\beta \approx 1$, and $\sinh \beta \approx \beta$, and Equation (8) reduces to:

$$\left(T_R\right)_{b << d,\ X << 1} = \int_y^\infty e^{-y} J_o(iy)\, dy$$

But:

$$\frac{dJ_o(z)}{dz} = -J_1(z), \quad \frac{dJ_1(z)}{dz} = -\frac{J_1(z)}{z} + J_o(z)$$

whence:

$$\left[\exp(-y)\right] J_o(iy) = \frac{d}{dy}\left\{ y \left[\exp(-y)\right] \left[J_o(iy) - i\, J_1(iy)\right]\right\}$$

and

$$\left(T_R\right)_{b << d,\ X << 1} = 1 - \frac{2\pi b}{d} \times y \times \left[\exp(-y)\right] \left[Jo(iy) - i\, J_1(iy)\right]$$

For small $y << \frac{2}{\pi}$,

$$\left(T_R\right)_{b << d,\ X << 1} \rightarrow 1 - \frac{2\pi b}{d}\ y = 1 - \frac{SX}{d} \qquad (11)$$

For large $y >> \frac{2}{\pi}$,

$$T_{R_{b << d,\ X << 1}} \rightarrow 1 - \frac{2\pi b}{d}\ \sqrt{\frac{2y}{\pi}} = 1 - 2\sqrt{\frac{SbX}{d}} \qquad (12)$$

Note that Equations (10) and (12) are equivalent. This results since the condition that X must necessarily be less than one for Equations (11) and (12) to be valid, assures that $\sqrt{\frac{y\beta^2}{2}}$ will be $<< 1$ as long as $b << d$ in equation (10).

For $b >> d$, $\beta >> 1$, $\sinh \beta \approx \cosh \beta$, and $\cosh \beta >> 1$. Hence, the exponential in Equation (8) decreases more rapidly with increasing y than $J_o(iy)$ increases. The transmittance,

$$T_R = 1 - \sinh\beta \int_o^\gamma \left[\exp(-y \cosh \beta)\right]\ J_o(iy)\ dy,$$

is now determined by contributions to the integrand from small values of y. Using the approximation, $J_o(iy) \approx J_o(0) = 1$, the transmittance becomes:

$$T_{R_{b >> d}} = 1 - \cosh \beta \int_o^\gamma \left[\exp(-y \cosh \beta)\right]\ dy$$
$$= \exp\left(-\frac{SX}{d}\right) \qquad (13)$$

The relation:

$$P_{\omega\ b >> d} = \frac{S}{d}$$

follows more directly from Equation (2), for $\cosh \beta \approx \sinh \beta >> 1 >> \cos s$ and constitutes a reasonable approximation for $\beta \geq 2$.

APPENDIX F

EFFECT OF HYPERFINE STRUCTURE ON ABSORPTION LINES

Consider an absorption line which is made up of n hyperfine components. Each of these components arises from a group of atoms, N_i, having a particular nuclear spin or isotopic structure. If the absorption coefficient for the ith hyperfine component is given by P_{ω_i} and P_ω represents the overall absorption coefficient, then the total dimunition in light intensity over a path length $d\ell$ is given by:

$$\frac{dI_\omega}{I_\omega} = P_\omega \, dX = \sum_{i=1}^{n} P_{\omega_i} \, dX_i \tag{1}$$

or when N is constant along ℓ,

$$P_\omega X = \sum_{i=1}^{n} P_{\omega_i} X_i \tag{2}$$

If the optical density, $X = N\ell$ is small enough so that

$$\exp(-P_\omega X) \approx 1 - P_\omega X \tag{3}$$

Then the total absorption, β, is given by:

$$\beta = \int_0^\infty P_\omega X \, d\omega = \int_0^\infty \sum_{i=1}^{n} P_{\omega_i} X_i \, d\omega$$

$$= \sum_{i=1}^{n} X_i \int_0^\infty P_{\omega_i} \, d\omega$$

By assuming that all the hyperfine components have the same lifetimes in their excited states, it follows that:

$$\int_0^\infty P_{\omega_i} d\omega = \int_0^\infty P_{\omega_2} d\omega = \cdots = \int_0^\infty P_{\omega_n} d\omega = \int_0^\infty P_\omega d\omega = S$$

and

$$\beta = SX, \tag{4}$$

the result expected for a line with no hyperfine splitting.

If the center of the line is totally absorbed, the absorption coefficient is written as:

$$P_\omega X = \sum_{i=1}^{n} \frac{Sb}{\pi} \frac{X_i}{(\omega - \omega_{oi})^2} \tag{5}$$

Again assuming that the integrated absorption, S, and the line half-breadth, b, are the same for every hyperfine component, the total absorption, β, becomes:

$$\beta = \int_0^\infty \left[1 - \exp\left(- \sum_{i=1}^{n} \frac{SbX_i}{\pi} \left(\frac{1}{\omega - \omega_{o_i}}\right)^2\right)\right] \quad d\omega \qquad (6)$$

If X is so large that the exponential term is approximately zero except for wave numbers much different than any ω_{o_i}, then negligible error is introduced by setting

$$\omega_{o_i} = \omega_{o_2} = \cdots = \omega_{o_n} = \omega_o$$

When the above conditions hold, the n hyperfine components of the absorption completely overlap and Equation (6) reduces to:

$$\beta = \int_0^\infty \left[1 - \exp\left(- \frac{Sb}{\pi} \frac{\sum X_i}{(\omega-\omega_o)^2}\right)\right] \quad d\omega \qquad (7)$$

This is exactly the integral which yields the square root absorption law for a single absorption line since $X = \sum_{i=1}^{n} X_i$. Therefore:

$$\beta = 2\sqrt{SbX} \qquad (8)$$

when the hyperfine components completely overlap.

If the n hyperfine components are entirely separated and the center of the line is totally absorbed, then Equation (6) can be replaced by the sum of n separate integrals. Each of these integrals represents the total absorption of a particular hyperfine line with its center at a particular ω_{o_i}. The total absorption now can be written as:

$$\beta = \sum_{i=1}^{n} \int_0^\infty \left[1 - \exp\left(- \frac{SbX_i}{\pi} \left(\frac{1}{\omega-\omega_{o_i}}\right)^2\right)\right] \quad d\omega$$

which reduces to

$$\beta = \sum_{i=1}^{n} 2\sqrt{SbX_i} \qquad (9)$$

where again it has been assumed that S and b are the same for each hyperfine line.

In the case that the components are equally intense, $X_i = X/n$, and the total absorption reduces to:

$$\beta = 2\sqrt{nSbX} \tag{10}$$

If the components are not equally intense, the total absorption for an absorption line made up of n completely separated hyperfine components is larger than the total absorption of an absorption line with no hyperfine splitting by the factor, $\sum_{i=1}^{n} \sqrt{X_i} \Big/ \sqrt{\sum_{i=1}^{n} X_i}$.

APPENDIX G

DETERMINATION OF SELF-BROADENING EFFECTS IN AN EQUILIBRIUM LIQUID-VAPOR SYSTEM

Consider an atomic gas absorbing at wave number ω, whose concentration is such that the center of the absorption line is totally absorbed. Assume there is no foreign gas present. Moreover, consider the ratio, r_b, the square of the total absorption with self-broadening divided by the square of the total absorption without self-broadening. Since the center of the absorption line is totally absorbed,

$$r_b = \frac{\beta^2_{self}}{\beta^2_{no\ self}} = \frac{4S\ (b_N + b_S)\ X}{4\ S\ b_N\ X} \tag{1}$$

At a particular optical density, X,

$$r_b = 1 + {}^{b_S}/_{b_N} \tag{2}$$

$$\text{since} \qquad b_S = \frac{C_s\ p}{T^{\frac{1}{2}}} \tag{3}$$

$$\text{when} \qquad C_s = \frac{\sigma_s^2}{\pi c} \left(\frac{2\pi}{R} \times \frac{2}{M_1}\right)^{\frac{1}{2}} \tag{4}$$

It follows that:

$$r_b - 1 = \frac{C_s}{b_N} \quad \frac{p}{T^{\frac{1}{2}}} \tag{5}$$

$$T^{\frac{1}{2}}\ (r_b - 1) = \frac{C_s}{b_N} \quad p \tag{6}$$

$$\log_{10}\left(T^{\frac{1}{2}}\ (r_b - 1)\right) = \log_{10} \frac{C_s}{b_N} + \log_{10}\ p \tag{7}$$

If the absorbing gas is in equilibrium with a condensed phase and Δc_p is constant $\log_{10} p = -\frac{2 \times \text{SLOPE}}{T} + \frac{\Delta c_p}{R} (\log_{10} T) + C_I$

$$\text{and} \qquad \log_{10}\ T^{\frac{1}{2}}(r_b - 1) = -\frac{2 \times \text{SLOPE}}{T} + \frac{\Delta c_p}{R}\ \log_{10} T + C_I + \log_{10}\ {}^{C_s}/_{b_N}$$

$$\text{or} \qquad \log_{10}\left(T^{\left(\frac{1}{2} - \frac{\Delta c_p}{R}\right)}(r_b - 1)\right) = -\frac{2 \times \text{SLOPE}}{T} + C_I + \log_{10} \frac{C_s}{b_N} \tag{8}$$

but $$T^{\frac{1}{2}} \beta_{\text{no self}} = 2\sqrt{Sb_N \frac{p\ell a}{R}} \qquad (9)$$

and since $$S = \frac{\lambda_o^2}{8\pi c\tau} \frac{g_2}{g_1} \quad \text{and} \quad b_N = \frac{1}{4\pi c\tau} \qquad (10)(11)$$

it follows that:

$$\log_{10} T^{(\frac{1}{2} - \frac{\Delta c_p}{R})} \beta_{\text{no self}} = -\frac{\text{SLOPE}}{T} + \frac{C_I}{2} + \tfrac{1}{2}\log_{10} \frac{a\ell\lambda_o^2}{8\pi^2 c^2 \tau^2} \frac{g_2}{g_1} \frac{1}{R} \qquad (12)$$

By choosing the proper value for the intercept,

$$\frac{C_I}{2} + \tfrac{1}{2}\log_{10} \frac{a\ell\lambda_o^2}{8\pi^2 c^2 \tau^2} \frac{g_2}{g_1} \frac{1}{R} ,$$

of the line representing the hypothetical zero helium pressure total absorption data showing no self-broadening, the slope of the line, $\log_{10}(T^{(\frac{1}{2} - \frac{\Delta c_p}{R})}(r_b - 1))$ versus 1/T can be made equal to -2xSLOPE. Thus the procedure involves choosing various intercepts for the $\beta_{\text{no self}}$ equation until one has been found which makes the slope of the $\log_{10}(T^{(\frac{1}{2} - \frac{\Delta c_p}{R})}(r_b - 1))$ line equal to -2xSLOPE.

Equation (12) now gives the correct values for the total absorption without self-broadening, $\beta_{\text{no self}}$. If the lifetime of the excited state, τ, is also know, C_I can be evaluated from the intercept of Equation (12), C_s from Equation (8), and σ_s^2 from Equation (4).

APPENDIX H

SAMPLE CALCULATIONS

1. Reduction of the 746 mm Hg Helium Pressure Data

Consider a data point from Run 69 taken at T = 1088°K and P_{He} = 746 mm Hg. Three measurements of the absorption line were made. The observed value of A/I_o, $(A/I_o)_t$, equals:

$$(A/I_o)_t = \frac{1}{9}\left(\frac{14.85}{1.000} + \frac{15.10}{0.994} + \frac{14.67}{0.999}\right) = 4.970 \frac{\text{in.}^2}{\text{cu.}}$$

The above expression is divided by 3 x 3 because the numbers tabulated in Appendix I are 3 times the area of the absorption line.

The hyperfine correction factor for this value was found to be 1.027 from Figure 4, using:

$$\beta = (A/I_o)_t \frac{\text{in.}^2}{\text{cu.}} \Big/ 0.568 \frac{\text{in.}^2}{\text{cu.cm}^{-1}} = 8.75 \text{ cm}^{-1},$$

The corrected value for $(A/I_o)_t$ is: $(A/I_o)_t = (A/I_o)_t / 1.027 = 4.84 \frac{\text{in.}^2}{\text{cu.}}$

To correct for self-broadening, $(A/I_o)_0$, the observed value of A/I_o at T = 1090°K and P_{He} = 0 is calculated to be:

$$(A/I_o)_0 = \frac{1}{12}\left(\frac{1.87}{1.023} + \frac{2.11}{1.067} + \frac{1.90}{1.058} + \frac{2.10}{1.012}\right) = 0.640 \frac{\text{in.}^2}{\text{cu.}}$$

The hyperfine correction factor is found from Figure 4 to be 1.54. Therefore the corrected value of $(A/I_o)_0$ is:

$$(A/I_o)_0 = \frac{0.640}{1.54} = 0.416 \frac{\text{in.}^2}{\text{cu.}}$$

The value of A/I_o representing collision broadening alone, $(A/I_o)_f$, is now calculated from Equation (12). Using the corrected values of $(A/I_o)_t$ and $(A/I_o)_0$. $(A/I_o)_f^2 = \left[(A/I_o)_t^2 - (A/I_o)_0^2\right]^{\frac{1}{2}} = 4.82 \text{ in}^2/\text{cu}$

2. Calculation of $\Delta H_{v, Bi}$

It is shown in the text that the following equation represents total absorption values resulting from collision broadening alone:

$$\log_{10} T^{(\frac{3}{4} - \frac{\Delta c_p}{2R})} \beta = \frac{-\text{SLOPE}}{T} + \frac{C_I}{2} + \tfrac{1}{2} \log_{10} \left(\frac{4S\ C_p\ P_I a\ell}{R}\right)$$

Therefore:

$$\log_{10} T^{(\frac{3}{4} - \frac{\Delta c_p}{2R})} \left(A/I_o\right)_f = -\frac{\text{SLOPE}}{T} + \frac{C_I}{2} + \tfrac{1}{2} \log_{10} \left(\frac{4x(0.568)^2 C_p P_I\ a\ell}{R}\right)$$

Every corrected data point at P_{He} = 746 mm Hg taken above T = 972°K was used to calculate the least square line relating $\log T^{(\frac{3}{4} - \frac{\Delta c_p}{2R})} \left(A/I_o\right)_f$ and $1/T$. For the data point discussed above;

$$\log_{10} T^{(\frac{3}{4} - \frac{\Delta c_p}{2R})} \left(A/I_o\right)_f = \log_{10} \left[1088\ (1.4115)\ 4.810\right]$$

$$= 4.9659$$

and $1/T = 0.9191 \times 10^{-3}\ °K^{-1}$

The least square line through the corrected P_{He} = 746 mm Hg data, was found to be

$$\log T^{1.4115} \left(A/I_o\right)_f = \frac{-5,260.62}{T} + 9.8041$$

since $5260.62 = \text{SLOPE} = \dfrac{\Delta H_V - \Delta c_p T}{2 \times 2.303 \times R}$,

The heat of vaporization is calculated to be:

$$\Delta H_V = 2 \times 2.303 \times R \times \text{SLOPE} - \Delta c_p T$$

$$= 9.14 \times 5260.62 - 2.63T \text{ cal/gm mole } °K$$

$$= 48,100 - 2.63T,$$

where: $\Delta c_p = c_{p(v)} - c_{p(\ell)} = 4.97 - 7.60 = -2.63$

3. Calculation of Activities

Consider anatomic bismuth data point taken above the 47.4 mole % Bi lead-bismuth alloy at T = 1041°K, P_{He} = 746 mm Hg.

In the same manner as for the P_{He} = 746 mm Hg data point for pure bismuth, it was found that: $\left(A/I_o\right)_f = 1.945$, using the observed data points, $(A/I_o)_t = 2.206$, $(A/I_o)_0 = 0.357$ and the corresponding hyperfine correction factors, 1.130 and 1.75.

To calculate the activity of bismuth, $\left(A/I_o\right)_f^*$ at T = 1041°K must be calculated from the least square line for the pure bismuth data,

$$\log_{10} T^{1.4115} \left(A/I_o\right)_f^* = \frac{-5260.62}{T} + 9.8041$$

$$\text{At } T = 1041°K, \quad \left(A/I_o\right)_f^* = 3.12$$

Now from Equation (31) the activity of Bi,

$$a_{Bi} = \left(\left(A/I_o\right) \Big/ \left(A/I_o\right)^*\right)^2$$

$$= \left(1.945/3.12\right)^2 = 0.390$$

4. Correction of the Zero Helium Pressure Data for Self-Broadening

Before the zero helium pressure data is corrected for self-broadening it must first be corrected for hyperfine structure. Again consider a data point from Run 69, the one taken at T = 1187°K, P_{He} = 0.

$$\left(A/I_o\right)_t = 1.663$$

$$\beta = \frac{\left(A/I_o\right)_t}{0.568} = 2.93$$

Therefore the hyperfine correction function, F = 1.200

$$\text{and } \left(A/I_o\right)_{self} = \frac{1.663}{1.200} = 1.386 = 0.568\beta = 0.568 \times 2\sqrt{S(b_N + b_S)X}$$

since self-broadening affects the value of this data point.

If no self-broadening were present

$$\left(A/I_o\right)_{\text{no self}} \text{ would equal } 0.568 \times 2 \sqrt{S(b_N X)}$$

and $\log T^{\left(\frac{1}{2} - \frac{\Delta c_p}{2R}\right)} \left(A/I_o\right)_{\text{no self}}$ would equal

$$\frac{-\text{SLOPE}}{T} + \frac{C_I}{2} + \frac{1}{2}\log_{10}\left(\frac{4Sb_N \ell a}{R}(0.568)^2\right).$$

Also since

$$r_b = \left(\left(A/I_o\right)_{self} \Big/ \left(A/I_o\right)_{\text{no self}}\right)^2 = 1 + \frac{b_S}{b_N} = 1 + \frac{C_s p}{b_N T^{\frac{1}{2}}},$$

$\log_{10} T^{\left(\frac{1}{2} - \frac{\Delta c_p}{R}\right)} (r_b - 1)$ should equal $\frac{2 \times \text{SLOPE}}{T} + C_I + \log_{10} \frac{C_s}{b_N}$

Therefore, by trial and error, a value of

$$\frac{C_I}{2} + \frac{1}{2} \log_{10} \left(\frac{4 Sb_N \ell a}{R} (0.568)^2 \right)$$ is choosen so that the r_b's calculated from the $\left(A/I_o\right)_{\text{self}}$'s and the $\left(A/I_o\right)_{\text{no self}}$'s yield a line with slope - 2 x SLOPE when $\log_{10} T^{\left(\frac{1}{2} - \frac{\Delta c_p}{R}\right)} (r_b - 1)$ is plotted against $1/T$.

For example, assuming

$$C_I/2 + \frac{1}{2} \log_{10} \left(\frac{4 Sb_N \ell a}{R} (0.568)^2 \right) = 7.969$$

yields for the data point at T = 1187°K, $\left(A/I_o\right)_{\text{no self}} = 0.898$

and $r_b = 2.384$

This data point with the others taken at $P_{He} = 0$ and the above assumed intercept yields a value for the slope of

$T^{(1.823)} (r_b - 1)$ vs $1/T$ of - 10,576 whereas -2 x SLOPE = 10,521.

This agreement was considered sufficient and the equation for the non-self-broadened bismuth data at $P_{He} = 0$ were represented by the equation:

$$\log_{10} T^{(1.1615)} \left(A/I_o\right)_{\text{no self}} = \frac{-5260.62}{T} + 7.969$$

The MAD computer program for performing this trial and error calculation is the first program listed at the end of this appendix.

5. The Calculation of the Bismuth Vapor Pressure and the Lifetime of the Excited State for the 3067Å Line

The simultaneous calculation of τ and the vapor pressure depends on knowledge of the corrected zero helium pressure total absorption values. The equation representing these values is used to find an extrapolated value of the total absorption which obeys the square root absorption

law at a temperature where absorption data have been taken which are proportional to the first power of the vapor concentration.

Data taken in the temperature range 770 - 870°K, at P_{He} = 746 mm Hg, $(A/I_o)_{LIN}$, indicate that A/I_o is proportional to the first power of the concentration. At T = 796°K a representative value of $\left(A/I_o\right)_{LIN}$ is 0.0861 $in.^2/cu.$

Extrapolation using the equation for $\left(A/I_o\right)_{no\ self}$ obtained in section 4 yields a value at T = 796°K of:

$$\log_{10}\left(A/I_o\right)_{no\ self} = \frac{-5260.62}{796} + 7.969 - 1.1615 \log_{10}(796)$$

$$\left(A/I_o\right)_{no\ self} = 0.00980$$

This is the extrapolated value of A/I_o which obeys the square root absorption law.

Thus:
$$4b_N = \frac{\beta^2_{SQRT}\,cm^{-2}}{\beta_{LIN}\,cm^{-1}} = \frac{4SbX}{SX} = \frac{\left(\frac{\left(A/I_o\right)_{no\ self}\ in.^2/cu.}{0.568\ in^2/cu/cm^{-1}}\right)^2}{\frac{\left(A/I_o\right)_{LIN}\ in.^2/cu.}{0.568\ in^2/cu/cm^{-1}}}$$

$$= \frac{(0.00980)^2}{(0.568)(0.0861)} = 1.96 \times 10^{-3}\ cm^{-1}$$

Since $b_N = \frac{1}{4\pi c\tau}$

$$\tau = \frac{1}{\pi c 4 b_N} = \frac{1}{1.96 \times 10^{-3}\ cm^{-1} \times \pi \times 3 \times 10^{10}\ cm/sec}$$

$$= 5.4 \times 10^{-9}\ sec$$

Also $b_N = 4.91 \times 10^{-4}\ cm^{-1}$

and
$$S = \frac{\lambda_o^2}{8\pi c\tau}\frac{g_2}{g_1} = \frac{(3.067 \times 10^{-5}\ cm)^2}{8\pi \times 3 \times 10^{10}\ cm/sec \times 5.4 \times 10^{-9}\ sec} \times \frac{1}{2}$$

$$= 1.15 \times 10^{-13}\ cm$$

Now the intercept of the vapor pressure equation C_I, can be calculated since it is known that the intercept of the equation for $\left(A/I_o\right)_{no\ self}$ equals

$$\frac{C_I}{2} + \frac{1}{2}\log_{10}\left(\frac{4Sb_N\ell a}{R}(0.568)^2\right).$$

Therefore

$$C_I = 2 \times \left[7.969 - \frac{1}{2}\log_{10}\left(\frac{4Sb_N \ell a}{R} \times (0.568)^2\right)\right]$$

$$= 15.938 - \log_{10}\left[\frac{4 \times 1.15\times10^{-13}\text{cm} \times 4.91\times10^{-4}\text{cm}^{-1} \times 4.6\text{cm} \times 6.02\times10^{-13}\text{gmmole}^{-1} \times \left(0.568\ \frac{\text{in.}^2}{\text{cu/cm}}\right)^2}{82.05\ \text{cm}^3\text{atm/gm mole °K}}\right]$$

$$= 15.938 - 6.400 = 9.538$$

And the equation for the vapor pressure of atomic bismuth is:

$$\log_{10} p_{Bi} = \frac{-5260.62}{T} + 9.538 - 1.323 \log_{10} T$$

where: $$-1.323 = \frac{c_p(v) - c_p(\ell)}{R}$$

This calculation was also performed by the 709 computer using the first MAD program listed at the end of this appendix.

6. Calculation of τ For the Pb 2833Å Line

The lead total absorption data at $P_{He} = 0$ following the square root absorption law were corrected for hyperfine structure and self-broadening using the hyperfine correction function and the self-broadening correction method discussed in Appendix G. These corrections were illustrated in section 4 of this appendix. τ was then calculated directly from the equation for the total absorption, using the vapor pressures of lead tabulated in Stull and Sinke.

$$\left(A/I_o\right)_{\text{no self}} = 0.568\ \text{in}^2/\text{cu/cm}^{-1}\ 2\sqrt{Sb_N X}$$

$$+ 0.568 \times 2\left(\frac{\lambda_o^2}{8\pi c\tau}\ \frac{g_2}{g_1} \times \frac{1}{4\pi c\tau}\ \frac{pa\ell}{RT}\right)^{\frac{1}{2}}$$

$$\tau = \frac{1.136}{(A/I_o)_{\text{no self}}}\left(\frac{\lambda_o^2}{32\pi^2 c^2}\ \frac{g_2}{g_1}\ \frac{pa\ell}{RT}\right)^{\frac{1}{2}}$$

The corrected A/I_o values are given by the equation

$$\log_{10} T^{(1.003)}(A/I_o)_{\text{no self}} = \frac{-5109.61}{T} + 7.356$$

where: $1.003 + \left(\frac{1}{2} - \frac{\Delta c_p}{2R}\right)$

Therefore at T = 1200°K, $p_{Pb} = 6.60 \times 10^{-4}$ atm, $\left(A/I_o\right)_{\text{no self}} = 1.02$, and

$$\tau = \frac{1.136}{1.02 \text{ in.}^2/\text{cu/cm}^{-1}} \left(\frac{(2.833\times10^{-5})^2 \text{cm}^2 \times 3 \times 6.60\times10^{23} \text{ gm mole}^{-1} \times 4.6 \text{ cm}}{32\pi^2 \times (3\times10^{10})^2 \text{cm}^2/\text{sec}^2 \times 82.05 \frac{\text{cc atm}}{\text{gmmole°K}} \times 1200°\text{K}} \right)^{\frac{1}{2}}$$

$$= 1.39 \times 10^{-8} \text{ sec.}$$

7. Calculation of σ_I^2 and σ_s^2 for Bi 3067 Line

In making the correction for self-broadening the equation

$$\log_{10}\left(T^{\left(\frac{1}{2} - \frac{\Delta c_p}{R}\right)}(r_b - 1)\right) = \frac{-2 \times \text{SLOPE}}{T} + C_I + \log_{10}\frac{C_s}{b_N}$$

was calculated to be

$$\log_{10}\left(T^{(1.823)}(r_b - 1)\right) = -\frac{10576}{T} + 14.5812$$

therefore:

$$C_I + \log_{10}\frac{C_s}{b_N} = 14.5812$$

and since $C_s = \frac{\sigma_s^2 a}{\pi c}\left(\frac{2\pi}{R} \times \frac{2}{M}\right)^{\frac{1}{2}}$

$$\sigma_s^2 = b_N \times \frac{\pi c}{a\left(\frac{2\pi}{R} \times \frac{2}{M}\right)^{\frac{1}{2}}} \times 10^{(14.5812 - C_I)}$$

$$\sigma_s^2 = \frac{1}{4\pi c \tau\, a} \left(\frac{\pi c}{\left(\frac{2\pi}{R} \times \frac{2}{M}\right)^{\frac{1}{2}}}\right) 10^{(14.5812 - C_I)}$$

Therefore since

$$\tau = 5.4 \times 10^{-9} \text{ sec}$$

and $C_I = 9.538$

$$\sigma_s^2 = \frac{10^{(5.0432)} \text{atm}^{-1}\text{°K}^{\frac{1}{2}} \times 9.87 \times 10^{-7} \text{ atm/dyne/cm}^2}{\left(\frac{4\pi}{8.3144 \times 10^7 \frac{\text{gm cm}^2}{\text{sec}^2\text{gmmole°K}} \times 207.4 \frac{\text{gm}}{\text{gmmole}}}\right)^{\frac{1}{2}}}$$

$$\times \frac{10^{16} \text{ Å}^2/\text{cm}^2}{4 \times 5.4 \times 10^{-9}\text{sec} \times 6.02 \times 10^{23}\text{gmmole}^{-1}}$$

$$\sigma_s^2 = 3100 \text{Å}^2$$

To calculate the helium collision cross-section, a corrected value of $(A/I_o)_f$ taken at 746 mm Hg must also be known as well as corrected value for $(A/I_o)_{\text{no self}}$ taken at $P_{He} = 0$.

Consider a data point taken at P_{He} = 746 mm Hg taken at T = 1239°K.

$$(A/I_o)_f = 15.42 \text{ in}^2/\text{cm}$$

At t = 1239°K, from the equation for $A/I_{o_{\text{no self}}}$, the value at P_{He}=0 is

$$(A/I_o)_{\text{no self}} = 1.34 \text{ in}^2/\text{cu}$$

But $$\left(\frac{(A/I_o)_f}{(A/I_o)_{\text{no self}}}\right)^2 = \frac{Sb_C X}{Sb_N X} = \frac{b_C}{b_N}$$

$$= \left(\frac{15.42}{1.34}\right)^2 = 132$$

Therefore $b_C = b_N (132)$

and since $$b_C = \frac{\sigma_I^2}{\pi c} \times N_I \times \left(2\pi RT \left(1/M_1 + 1/M_2\right)\right)^{\frac{1}{2}}$$

and $$b_N = \frac{1}{4\pi c\tau}$$

$$\sigma_I^2 = \frac{132}{4\pi c\tau} \times \frac{\pi c}{N_I} \times \left[\frac{1}{2\pi RT \left(1/M_1 + 1/M_2\right)}\right]^{\frac{1}{2}}$$

For T = 1239°K and P_{He} = 0.982 atm = 746 mm Hg.

$$N_I = \frac{P_{He}\, a}{RT} = \frac{0.982 \text{ atm} \times 6.02 \times 10^{23} \text{ gmmole}^{-1}}{82.05 \frac{\text{cc atm}}{\text{gmmole °K}} \times 1239°K}$$

$$N_I = 5.82 \times 10^{18} \text{ atoms/cc}$$

Thus $$\sigma_I^2 = \frac{1}{4 \times 5.4 \times 10^{-9} \text{ sec}} \times \frac{1}{5.82 \times 10^{18} \text{cm}^{-3}} \times 10^{16} \text{ Å}^2/\text{cm}^2 \times 132$$

$$\times \left[\frac{1}{2\pi \times 8.3144 \times 10^7 \frac{\text{gm cm}^2}{\text{sec}^2 \text{gm mole °K}} \times 1239°K \left(1/209 + 1/4\right) \frac{\text{gmmole}}{\text{gm}}}\right]^{\frac{1}{2}}$$

$$\sigma_I^2 = 25.3 \text{Å}^2$$

8. Sample Error Calculations

Error in τ for Bi 3067Å line

From section 5,

$$4\,b_N = \frac{1}{\pi c \tau} = \frac{\beta^2_{SQRT}}{\beta_{LIN}} = \frac{(A/I_o)^2_{no\ self}}{(0.568)(A/I_o)_{LIN}}$$

Therefore

$$\tau = \frac{1}{\pi c} \times 0.568 \times \frac{(A/I_o)_{LIN}}{(A/I_o)^2_{no\ self}}$$

Since a least square line has been calculated for $\log_{10} T^{(\frac{1}{2} - \frac{\Delta c_p}{2R})}$ $(A/I_o)_{no\ self}$ vs $1/T$, it has been assumed that $\log_{10} (A/I_o)_{no\ self}$ is normally distributed. Therefore, the error in log τ was assumed to be normally distributed. Assuming this kind of distribution assures that the error limits on τ will never be negative. Taking the logarithm of the above equation yields:

$$\log_{10}\tau = \log_{10} \frac{0.568}{\pi c} + \log_{10} (A/I_o)_{LIN} - 2 \log_{10}(A/I_o)_{no\ self}$$

Since this is a linear equation, the estimated variance of $\log_{10}\tau$, $s^2_{\log\,\tau}$, is given by:

$$s^2_{\log_{10}\tau} = s^2_{\log_{10} (A/I_o)_{LIN}} + 4\, s^2_{\log_{10}(A/I_o)_{no\ self}}$$

$s_{\log_{10}(A/I_o)_{LIN}}$ was estimated from the data scatter to be $\pm$ 0.033.

$s_{\log_{10}(A/I_o)_{no\ self}}$ was calculated from the equation for the estimated standard deviation of a point from the least square line determined for the corrected zero helium pressure data.

$$s^2_{point} = s^2_{yr}\left[1 + \frac{1}{n} + \frac{x - \bar{x}}{s(x^2)}\right]$$

where: s^2 is the variance of a point, $\log_{10}T^{1.1615}(A/I_o)_{no\ self}$,

s^2_{yr} is the residual variance of $\log_{10}T^{1.1615}(A/I_o)_{no\ self}$,

x is $1/T$, $\bar{x}$ is the mean $1/T$, and $s(x^2) = \frac{\sum(x - \bar{x})^2}{n}$

For the line $T^{1.1615}(A/I_o)_{no\ self}$ vs $1/T$, it was found that:

$$s^2_{point} = 0.000514 + 4.12\left(1/T - \frac{0.890}{1000}\right)^2.$$

But $s^2_{\log_{10}(A/I_o)_{no\ self}} = s^2_{\log_{10}(T^{1.1615}(A/I_o)_{no\ self})}$

Therefore since τ was calculated using linear data taken at $T = 796°K$, the variance of $\log_{10}(A/I_o)_{no\ self}$ at that temperature is:

$$s^2_{\log_{10}(A/I_o)_{no\ self}} = 0.000514 + \frac{4.12}{1000}(1.256 - 0.890)^2$$

$$= 0.000514 + 0.000552$$

$$= 0.001066$$

Now the variance of the $\log_{10}\tau$ can be calculated

$$s^2_{\log_{10}\tau} = (0.0033)^2 + 4 \times 0.001066$$

$$= 1.09 \times 10^{-3} + 4.26 \times 10^{-3}$$

$$= 5.35 \times 10^{-3}$$

therefore $s_{\log_{10}\tau} = \pm 0.073$ and the 95% confidence limits are given by:

$$\pm 2s = \pm 0.146$$

Consequently $\log_{10}\tau = \log_{10} 5.4 \times 10^{-9} = -8.268 \pm 0.146$

From the uncertainty in the logarithm, the limits on τ were calculated to be:

$$\tau = 5.4\ {}^{+2.3}_{-1.7} \times 10^{-9} \text{ sec.}$$

```
            MAD(MICHIGAN ALGORITHM DECODER) PROGRAM FOR SELF-BROADENING
                                        CORRECTIONS


            DIMENSION X(50),Y(50)
            DIMENSION T(50),BETA(50),RECIPT(50),LINVAR(50),LOOP2(3)
            INTEGER NPOINT ,I,J,N,RUN,JMAX
   BEGIN    READ FORMAT CONST, SLOPE,INCEPT,DLCPOR,INCREM,JMAX,N,RUN
            READ DATA, NPOINT,HC, HEXP
            READ FORMAT DATA1,BETA(1)...BETA(N)
            READ FORMAT DATA2,T(1)...T(N)
            PRINT FORMAT TOP, RUN
             PRINT COMMENT $4       AREA/IZERO  DATA$
               PRINT RESULTS BETA(1)...BETA(N)
            PRINT FORMAT CHECK2,T(1)...T(N)
            PRINT FORMAT CHECK3,SLOPE,INCEPT,DLCPOR,INCREM,JMAX,N
            PRINT RESULTS NPOINT, HC, HEXP
            K=1
            L=1
            INCEP1=INCEPT
            THROUGH LOOP2, FOR J=1,1,J.G.JMAX
            PRINT FORMAT HEAD
            THROUGH LOOP1, FOR I=1,1,I.G.N
            BETANC=10.P.(-SLOPE/T(I)+INCEPT+(DLCPOR/2-0.5)/2.30259*ELOG.
           1 (T(I)))
            BRDRAT=(BETA(I)/BETANC).P.2.
             WHENEVER BRDRAT.LE.1,BRDRAT=1.001
            LINEXP=T(I).P.(0.5-DLCPOR)*(BRDRAT-1.)
            LINVAR(I)=ELOG.(LINEXP)/2.30259
            RECIPT(I)=1./T(I)
   LOOP1    PRINT FORMAT TABL ,T(I),RECIPT(I),BE3AT(I),BETANC,BRDRAT,LINEX
           1P,LINVAR(I)
            THROUGH END1, FOR I=1,1,I.G.NPOINT
            Y(I)=LINVAR(I)
 END1       X(I)=RECIPT(I)
           R   BEGINNING OF LEAST SQUARES PROGRAM
            SUMX = 0.0
            SUMY = 0.0
            SUMXY = 0.0
            SUMX2 = 0.0
            SUMY2 = 0.0
            THROUGH END4, FOR I=1,1,I.G.NPOINT
            SUMX = SUMX + X(I)
            SUMY = SUMY + Y(I)
            SUMXY = SUMXY + X(I)*Y(I)
            SUMY2 = SUMY2 + Y(I)*Y(I)
 END4       SUMX2 = SUMX2 + X(I)*X(I)
            MEANX = SUMX/NPOINT
            MEANY = SUMY/NPOINT
            SOSX = SUMX2-SUMX.P.2/NPOINT
            SOSY = SUMY2 - SUMY.P.2/NPOINT
            SOSXY = SUMXY-SUMX*SUMY/NPOINT
            R = SOSXY/SQRT.(SOSX*SOSY)
            B = SOSXY/SOSX
            A = MEANY-B*MEANX
            VARYR = (SOSY-B*SOSXY)/(NPOINT-2)
            VARB = VARYR/SOSX
```

```
          R  SELF-BROADENING PROGRAM CONTINUED
          R
          R
          R
           STDDVB = SQRT.(VARB)
           MAXDEV = 0.0
           MSD = 0.0
           PRINT FORMAT TITLE
           THROUGH END7, FOR I=1,1,I.G.NPOINT
           DEV = Y(I)-(A+B*X(I))
           MSD = MSD+DEV.P.2/NPOINT
           WHENEVER I.E.1
           HIX = X(I)
           LOWX = X(I)
           OR WHENEVER X(I).G.HIX
           HIX = X(I)
           OR WHENEVER X(I).L.LOWX
           LOWX = X(I)
           END OF CONDITIONAL
           WHENEVER .ABS.(DEV).G..ABS.(MAXDEV)
           MAXDEV = DEV
END7       END OF CONDITIONAL
           CAL = 0.0
           VARLIN = VARYR*(1./NPOINT+(CAL-MEANXD.P.2/SOSX)
           VARPT = VARYR+VARLIN
           STDDVP = SQRT.(VARPT)
           PRINT FORMAT TABLE,  CAL, VARLIN, VARPT, STDDVP
           THROUGH END8, FOR CAL = LOWX,0.1*(HIX-LOWX), CAL.G.HIX
           VARLIN = VARYR*(1./NPOINT+(CAL-MEANX).P.2/SOSX)
           VARPT = VARYR+VARLIN
           STDDVP = SQRT.(VARPT)
END8       PRINT FORMAT TABLE,  CAL, VARLIN, VARPT, STDDVP
           PRINT FORMAT FIT, A, B, VARB, STDDVB= VARYR, MSD, MAXDEV, R
          R
           VECTOR VALUES FIT = $S40,11HINTERCEP3 =F35.6/S40,7HSLOPE =F39
          1.6/S40,19HVARIANCE OF SLOPE =F27.6/S40,26HSTANDARD DEVIATION
          2SLOPE =F17.6/S40,27HVARYR (RESIDUAL VARIANCE) =F19.6/S40,
          323HMEAN SQUARE DEVIATION =F23.6/S40,19HMAXIMUM DEVIATION =F27
          4.6/S40,25HCORRELATION COEFFICIENT =F21.6*$
           VECTOR VALUES TITLE = $1H4,S35,48HRE2ULTS OF REGRESSION ANALY
          1SIS-LEAST SQUARES FIT//S15,1HX,S12,16HVARIANCE OF LINE,S12,
          2                          13HVARIANCE OF Y,S12,27HSTANDARD DEVI
          3ATION OF POINT*$
           VECTOR VALUES TABLE = $F22.6,F20.6,F27.6,F33.6*$
          R  END OF LEAST SQUARES PROGRAM
           PRINT RESULTS INCEPT
           WHENEVER B .G. -0.99*SLOPE*2.
             WHENEVER INCEP1.G.INCEPT,K=2.1*L
             INCEP1=INCEPT
             INCEPT=INCEPT+INCREM/K
           OR WHENEVER B.L. -1.01 *SLOPE*2.
              WHENEVER INCEP1.L.INCEPT,L=2.1*K
             INCEP1=INCEPT
             INCEPT=INCEPT-INCREM/L
           OTHERWISE
           READ FORMAT SPECTR, BETAPL,BETAPH,TLOW,THIGH,LAMBDA,G2OG1,
          1  LENGTH,PINERT,MW1,MW2,CINSTR
           PRINT COMMENT $1$
```

```
R  SELF-BROADENING PROGRAM CONTINUED
R
 PRINT RESULTS        BETAPL,BETAPH,TLOW,THIGH,LAMBDA,G2OG1,
1  LENGTH,MW1,MW2,CINSTR,PINERT
 RTO=10.P.(-2.*SLOPE/TLOW+2.*INCEPT+(DLCPOR-1.0)/2.30259
1*ELOG.(TLOW))/BETAPL
 PINCEP =2.*INCEPT-ELOG.(RTO*RTO*LAMBDA*LAMBDA/8.*G2OG1*LENGTH
1  *7.34E05)/2.30259
 TAU=CINSTR/(3.14159*3.0E10*RTO)
 KCOL=1./(4.*3.14159*TAU)*10.P.(A-PINCEP  )/3.0E10
 SSSELF=KCOL*6.*3.14159/3.37*(MW1/2.).P.0.5
 RATSR=BETAPH/(10.P.(-SLOPE/THIGH+INCEPT+(DLCPOR/2.-0.5)/
1  2.30259*ELOG.(THIGH)))
 SSPRES =    1 /4./TAU*2./3.37*SQRT.(THIGH/(1./MW1+1./MW2))/
1 PINERT*(RATSR.P.2-1.0)/1.0E10
 PRINT FORMAT RESULT ,SLOPE,PINCEP,DLCPOR,TAU,SSSELF,SSPRES
 TRANSFER TO BEGIN
LOOP2  END OF CONDITIONAL
 VECTOR VALUES CONST=$4F15.6,3I5*$
R  SLOPE,INCEPT,DLCPOR,INCREM,JMAX,N,RUN
R
 VECTOR VALUES DATA1=$(7F10.7)*$
R  BETA(I)...BETA(N)
R
 VECTOR VALUES DATA2=$(7F10.1)*$
R  T(1)...T(N)
R
R
 VECTOR VALUES CHECK2=$1H4,I6HTEMPERATURE DATA//(S10,10F10.1)
1  *$
R
 VECTOR VALUES TOP=$1H1,S25,65HTHE TREATMENT OF ZERO INERT GAS
1 PRESSURE DATA FOR SELF BROADENING//S56,3HRUN,I3*$
R
 VECTOR VALUES CHECK3=$1H4,S10,6HSLOPE=,F14.6,S10,10HINTERCEPT
1=,F10.6,S10,11HDELTA CP/R=,F9.4,S10,10HINCREMENT=,F8.3//S20,
2 5HJMAX=,I3,S20,2HN=,I3*$
R
 VECTOR VALUES HEAD=$1H1,S3,9HTEMP DEG K,S7,6H1/TEMP,S9,7HAREA
1/IZ,S7,9HA/I NO BD,S7,8HBRDRATIO,S6,8HT (BR-1),S5,
2  13HLOG(T (BR-1))*$
R
 VECTOR VALUES TABL =$/F10.1,E20.6,2E15.6,2E15.6,F15.6*$
R  T(I),RECIPT(I),BETA(I),BETANC,BRDRAT,LINEXP,LINVAR(I)
R
 VECTOR VALUES SPECTR =$7F10.6/3F10.6,E15.6*$
R  BETAPL,BETAPH,TLOW,THIGH,LAMBDA,G2OG1,LENGTH,PINERT,MW1,
R  MW2,CINSTR
R
 VECTOR VALUES RESULT=$1H4,S10,11HLOG P = -2*,F15.5,3H/T ,
0 2H+ ,F10.6,S1,
1 F10.5,6H*LOG T///  S45,4HTAU=,S11,E15.6/S35,30HSIGMA SQUARED
2 SELF BROADENING=,S10,F10.4/S30,35HSIGMA SQUARED COLLISION BR
3OADENING=,S10,F10.4*$
 END OF PROGRAM
```

MAD PROGRAM TO CALCULATE THE HYPERFINE CORRECTION FUNCTION

```
          DIMENSION BETA(30), DELTA(10), G(10)= GR(10)
          INTEGER I,J,IMAX,NHFC
START     READ DATA, IMAX NHFC,MUMAX,DMUMIN,BE3A(1)...BETA(IMAX),
         R  DELTA(1)...DELTA(NHFC),G(I)...G(NHFC)
          PRINT COMMENT $1
         1 HYPERFINE CORRECTION FUNCTION$
          PRINT COMMENT $8$
          PRINT RESULTS IMAX,NHFC,MUMAX,DMUMIN=DELTA(I)...DELTA(NHFC),
         1 G(1)...G(NHFC)
          THROUGH LOOP6, FOR J=1,1,J.G.NHFC
LOOP6     GR(J)=SQRT.(G(J))
          THROUGH LOOP3,FORI=1,1,I.G.IMAX
          FD=0.3
          H=3.0
          Y=BETA(I).P.2/4.0/3.14159
          THROUGH LOOP3, FOR DELMU=.02*BETA(I),-DELMU/2, DELMU.L.DMUMIN
         1 .OR.(FD/H.G.0.995.AND.FD/H.L.1.005)
          H=FD
          GE = 0.8
          THROUGH LOOP4,FOR MU=0.0,2*DELMU, MU.G.MUMAX.OR. GE.L.0.0005
          EXPEN=0.
          EXPON=0.
          EXPO=0.
          EXPE=0.
          GE=0.0
          GO=0.0
          GEN=0.0
          GON=0.0
          THROUGH LOOP5,FORJ=1,1,J.G.NHFC
          WHENEVER .ABS.((-MU-DELTA(J))/(BETA(I)*GR(J))) .L. 0.06
          GEN = 1.0
          OTHERWISE
          EXPEN=EXPEN+G(J)/((-MU-DELTA(J)).P.2)
          END OF CONDITIONAL
          WHENEVER .ABS.((-MU-DELMU-DELTA(J))/(BETA(I)*GR(J))).L.0.06
          GON = 1.0
          OTHERWISE
          EXPON=EXPON+G(J)/((-MU-DELMU-DELTA(J)).P.2)
          END OF CONDITIONAL
          WHENEVER .ABS.((MU-DELTA(J))/(BETA(I)*GR(J))).L.0.06
          GE  = 1.0
          OTHERWISE
          EXPE=EXPE+G(J)/((MU-DELTA(J)).P.2)
          END OF CONDITIONAL
          WHENEVER .ABS.((MU+DELMU-DELTA(J))/(BETA(I)*GR(J))).L.0.06
          GO  = 1.0
          OTHERWISE
          EXPO=EXPO+G(J)/((MU+DELMU-DELTA(J)).P.2)
LOOP5     END OF CONDITIONAL
          WHENEVER GE  .NE. 1.0, GE=1.0-EXP.(-Y*EXPE)
          WHENEVER GO .NE. 1.0, GO=1.0-EXP.(-Y*EXPO)
          WHENEVER GEN .NE. 1.0, GEN=1.0-EXP.(-Y*EXPEN)
          WHENEVER GON .NE. 1.0, GON=1.0-EXP.(-Y*EXPON)
          WHENEVER MU.E. 0.

         R  HYPERFINE CORRECTION PROGRAM CONTINUED
         R
         R
          GENO = 1.0
          OTHERWISE
          GENO=1.0-EXP.(-Y/MU/MU)
          END OF CONDITIONAL
          GONO=1.0-EXP.(-Y/(MU+DELMU)/(MU+DELMU))
          WHENEVER MU.E.0
          FD=(GE+GEN+4*(GO+GON))/3.0
            FZ=1./3.*GENO+4./3.*GONO
          OTHERWISE
          FD=FD+(2.*(GE+GEN)+4*(GO+GON))/3.0
          FZ=FZ+(2.*GENO+4.*GONO)/3.
  LOOP4   END OF CONDITIONAL
          FD=(FD-(GE+GEN+4.*(GO+GON))/3.0)/BETA(I)*DELMU
            FZ=(FZ-1./3.*GENO-4./3.*GONO)/BETA(I)*DELMU*2.
          FC=FD/FZ
          AOIOC=FC/1.76*BETA(I)
 LOOP3    PRINT RESULTS MU,DELMU, FD,FZ,FC,BETA(I),AOIOC
          TRANSFER TO START
          END OF PROGRAM
```

APPENDIX I

RAW DATA

RUNS 61,62 BISMUTH ABOVE U-UBI HELIUM PRESSURE = 746 MM HG CELL LENGTH = 4.6 CM

INPUT DATA FOR RUN

RUN	SET	HE PRESS (MM)	TEMP (°K)	3x AREA	IZERO
61	2000-1	748	1265	3.480000	.928000
				3.460000	.923000
				3.430000	.925000
61	2000-2	745	1266	3.320000	.943000
				3.390000	.948000
				3.390000	.940000
61	1950-1	746	1241	2.860000	.958000
				2.990000	.949000
				2.920000	.955000
61	1950-2	745	1240	2.650000	.963000
				3.050000	.970000
				2.860000	.958000
61	1950-3	745	1255	3.310000	.978000
				3.210000	.970000
				3.290000	.970000
61	1850-1	745	1206	2.330000	1.012000
				2.040000	1.020000
				2.180000	1.018000
61	1850-2	746	1224	2.580000	.974000
				2.300000	.954000
				2.490000	.975000
61	1850-3	746	1222	2.570000	.995000
				2.620000	1.003000
				2.540000	1.010000
61	1800-1	746	1195	1.720000	.966000
				1.670000	.974000
				1.760000	.973000
61	1800-2	749	1190	1.750000	1.022000
				1.780000	1.020000
				1.620000	1.012000
61	1850-4	747	1211	2.090000	.999000
				2.050000	.995000
				2.290000	1.002000
				2.010000	1.008000
				2.210000	1.021000
61	1850-5	745	1212	2.200000	1.007000
				2.060000	1.007000
				2.070000	1.024000
				2.010000	.990000
				2.210000	.993000

Runs 61, 62, U-UBi, Cont'd

61	1900-4	745	1244	3.130000	.986000
				2.980000	.978000
				2.990000	.968000
				3.090000	1.009000
				3.040000	.970000
61	1750-1	747	1167	1.360000	.993000
				1.170000	.990000
				1.220000	.995000
				1.310000	.987000
				1.140000	.986000
62	2000-1	745	1282	4.180000	.988000
				4.290000	.982000
				4.270000	.995000
				4.220000	.982000
62	1900-1	746	1232	2.410000	.942000
				3.040000	.944000
				2.710000	.942000
				2.490000	.940000
62	1900-2	745	1231	2.680000	.990000
				2.550000	.937000
				2.670000	.990000
62	1800-1	746	1181	1.800000	.937000
				1.520000	.920000
				1.720000	.927000
				1.620000	.928000
62	1800-2	746	1178	1.480000	.938000
				1.550000	.923000
				1.680000	.932000
62	1825-1	746	1187	1.600000	.931000
				1.470000	.948000
				1.540000	.960000
62	1825-2	745	1184	1.430000	.968000
				1.380000	.963000
				1.520000	.968000
62	1825-3	745	1184	1.560000	.948000
				1.550000	.943000
				1.420000	.944000
62	1950-3	746	1237	2.590000	.930000
				2.680000	.951000
				2.540000	.930000
62	1750-1	746	1146	.620000	.962000
				.790000	.968000
				.660000	.991000
				.740000	.989000
62	1950-1	747	1234	4.670000	.961000
				4.660000	.964000
				4.540000	.957000
62	1950-2	746	1237	2.900000	.900000
				3.050000	.899000
				2.950000	.902000

RUN 69 PURE BISMUTH HELIUM PRESSURE = 000 MM HG CELL LENGTH = 4.6 CM

INPUT DATA FOR RUN

RUN	SET	HE PRESS (MM)	TEMP (°K)	3x AREA	IZERO
69	2000AB	0	1283	12.380000	.996000
				12.730000	.946000
				12.440000	.974000
				12.690000	.991000
				13.700000	1.031000
				11.790000	.986000
69	1955A	0	1275	12.090000	1.050000
				11.110000	.996000
				10.740000	.996000
69	1900AB	0	1238	7.470000	.990000
				8.210000	.992000
				8.390000	1.034000
				8.280000	.992000
				7.740000	1.000000
69	1850A	0	1221	6.390000	.999000
				6.330000	1.000000
				6.490000	.974000
				6.740000	1.041000
69	1800AB	0	1197	5.100000	.995000
				4.680000	.998000
				5.360000	.987000
				5.300000	1.030000
				4.950000	1.006000
				3.940000	.841000
69	1750A	0	1173	4.110000	1.000000
				4.100000	.981000
				4.200000	1.079000
				4.090000	1.016000
69	1700A	0	1135	2.930000	1.020000
				3.000000	1.001000
				3.150000	.985000
				2.770000	.950000
69	1650A	0	1127	2.690000	.997000
				2.780000	1.024000
				2.980000	1.030000
				3.060000	1.055000
				3.240000	1.053000
69	1600A	0	1090	1.870000	1.023000
				2.110000	1.067000
				1.900000	1.058000
				2.100000	1.012000
69	1550A	0	1063	1.820000	1.045000
				1.800000	1.028000
				1.670000	1.000000
				1.730000	1.041000

Run 69, ATOMIC BISMUTH, Cont'd

69	1500A	0	1030	1.330000	1.022000
				1.340000	1.038000
				1.290000	1.045000
				1.440000	1.070000
				1.420000	1.090000
69	1450A	0	1009	1.090000	1.022000
				1.050000	1.030000
				1.150000	1.040000
				1.050000	1.011000
69	1400A	0	981	1.010000	1.000000
				1.120000	.987000
				1.150000	.987000
				.980000	.968000
				.940000	.980000
69	1350A	0	955	.970000	.997000
				.980000	1.001000
				1.050000	1.009000
				.960000	.990000
69	1300A	0	930	.870000	1.012000
				.910000	1.015000
				.840000	.995000
				.850000	1.006000
				.900000	1.024000
69	1250A	0	904	.690000	1.007000
				.780000	1.025000
				.810000	1.010000
				.890000	1.011000
				.840000	1.008000
69	1200A	0	879	.710000	1.002000
				.670000	1.005000
				.730000	1.004000
				.690000	1.008000
				.710000	1.003000
69	1150A	0	851	.580000	1.000000
				.540000	1.000000
				.560000	1.003000
				.620000	1.008000
				.610000	1.015000
69	1175A	0	842	.480000	1.005000
				.510000	.991000
				.530000	.980000
				.550000	.972000
69	1100A	0	825	.330000	1.019000
				.360000	1.018000
				.350000	1.013000
				.380000	1.010000
				.350000	1.001000

Run 69, ATOMIC BISMUTH, Cont'd

69	1075A	0	812	.270000	.991000
				.290000	1.010000
				.250000	1.005000
				.290000	.998000
				.280000	.928000
69	1050A	0	796	.180000	.974000
				.230000	.986000
				.190000	.981000
				.180000	.982000
				.230000	.988000
				.220000	.983000
69	1025A	0	784	.190000	1.014000
				.140000	1.013000
				.155000	1.016000
				.180000	1.018000
69	1000A	0	770	.073000	1.028000
				.070000	1.036000
				.065000	1.037000

RUN 69 PURE BISMUTH HELIUM PRESSURE = 350 MM HG CELL LENGTH = 4.6 CM

INPUT DATA FOR RUN

RUN	SET	HE PRESS (MM)	TEMP (°K)	3x AREA	IZERO
69	2000C	350	1283	46.740000	1.033000
				40.040000	.973000
69	1950B	350	1273	35.500000	.961000
				36.310000	.970000
				38.540000	.994000
69	1900C	350	1239	30.830000	.914000
				29.140000	.923000
69	1850B	350	1223	27.700000	1.021000
				28.570000	1.042000
				28.650000	1.020000
69	1800C	350	1187	24.130000	.960000
				21.170000	.970000
				22.300000	.962000
69	1750B	350	1172	18.700000	1.017000
				19.520000	.980000
				18.940000	.981000
				18.880000	.975000
69	1700B	350	1136	14.230000	.955000
				14.420000	.928000
				14.000000	.930000
69	1650B	350	1125	15.420000	1.072000
				13.960000	1.020000
				12.700000	.982000
				14.430000	1.013000
69	1600B	350	1088	10.850000	.997000
				10.870000	.999000
				10.590000	.998000
69	1550B	350	1062	8.430000	1.003000
				8.230000	1.000000
				8.300000	1.000000
69	1500B	354	1030	6.650000	.997000
				6.720000	.988000
				6.730000	.983000
69	1450B	350	1009	5.060000	.908000
				4.970000	.908000
				5.240000	.910000
				5.230000	.910000
69	1400B	350	981	4.540000	1.004000
				4.740000	1.010000
				4.730000	1.010000

69	1350B	350	956	3.190000	.922000
				3.210000	1.003000
				3.580000	1.005000
				3.640000	.983000
69	1300B	350	929	2.730000	1.025000
				2.830000	1.024000
				2.860000	1.021000
69	1250B	350	905	2.080000	1.026000
				2.020000	1.025000
				2.170000	1.028000
				2.010000	1.014000
69	1200B	350	880	1.580000	.998000
				1.590000	1.000000
				1.600000	.996000
69	1150B	350	851	1.020000	1.021000
				1.060000	1.012000
				1.020000	1.014000
				1.080000	1.010000
69	1175B	350	841	.790000	.912000
				.820000	.905000
				.760000	.916000
				.790000	.923000
				.770000	.925000
69	1100B	350	824	.570000	1.021000
				.570000	1.021000
				.530000	1.031000
				.580000	1.036000
				.560000	1.026000
69	1075B	350	812	.360000	.986000
				.420000	.988000
				.480000	.992000
				.300000	.990000
				.440000	.987000
				.350000	.983000
69	1050B	350	796	.290000	.960000
				.220000	.957000
				.220000	.956000
				.270000	.963000
				.250000	.962000
				.240000	.959000
				.280000	.957000
69	1025B	350	783	.155000	1.000000
				.145000	1.000000
				.160000	1.000000
				.150000	1.000000
69	1000B	350	770	.090000	1.068000
				.100000	1.068000
				.105000	1.066000
				.110000	1.064000
				.080000	1.061000
				.090000	1.065000
				.115000	1.069000
				.105000	1.061000

RUN 69 PURE BISMUTH HELIUM PRESSURE = 746 MM HG CELL LENGTH = 4.6 CM

INPUT DATA FOR RUN

RUN	SET	HE PRESS (MM)	TEMP (°K)	3x AREA	IZERO
69	1900D	746	1239	50.470000	1.042000
69	1850C	746	1223	40.540000	1.002000
				40.500000	1.010000
				44.860000	1.020000
69	1800D	745	1189	35.810000	1.034000
				34.780000	1.038000
				37.530000	1.033000
69	1750C	747	1172	27.770000	1.000000
				27.740000	.994000
				28.010000	.974000
69	1700C	746	1136	21.720000	.972000
				21.780000	.971000
69	1650C	746	1125	20.200000	1.050000
				19.680000	1.015000
				20.460000	1.007000
69	2000D	746	1284	56.190000	.938000
69	1950C	746	1271	53.180000	.992000
				55.030000	.995000
69	1600C	746	1088	14.850000	1.000000
				15.100000	.994000
				14.670000	.999000
69	1550C	746	1063	11.600000	.978000
				11.800000	.979000
				11.790000	.984000
69	1500C	748	1032	10.410000	1.000000
				9.130000	.940000
				8.720000	.942000
				10.120000	.928000
69	1450C	746	1010	7.560000	.975000
				7.540000	.978000
				7.370000	.980000
69	1400C	746	980	6.020000	1.020000
				6.100000	1.028000
				6.140000	1.022000
69	1350C	746	958	4.640000	.983000
				4.970000	.976000
				4.980000	.983000
				4.710000	.981000

	69	1300C	746	929	3.820000	1.006000
					3.730000	1.008000
					3.780000	1.005000
					3.630000	1.001000
	69	1250C	746	905	2.910000	1.003000
					2.690000	.998000
					2.800000	1.003000
					2.790000	.999000
	69	1200C	746	880	2.030000	.995000
					2.000000	.997000
					1.940000	1.000000
					2.140000	1.006000
	69	1150C	746	852	1.150000	.996000
					1.100000	.973000
					1.140000	.966000
	69	1175C	746	840	.960000	1.013000
					1.040000	.948000
					.910000	.970000
					1.000000	.904000
					.980000	1.028000
	69	1100C	747	824	.650000	1.013000
					.590000	1.007000
					.630000	1.004000
	69	1075C	745	812	.380000	.975000
					.390000	.996000
					.380000	.995000
					.380000	.995000
					.400000	.994000
					.400000	.984000
	69	1050C	746	795	.250000	.928000
					.250000	.940000
					.240000	.965000
					.230000	.975000
					.280000	.983000
					.240000	.980000
	69	1025C	747	784	.220000	1.045000
					.155000	1.045000
					.180000	1.035000
					.180000	1.013000
					.215000	.981000
					.190000	1.050000
	69	1000C	747	771	.083000	1.070000
					.105000	1.060000
					.070000	1.068000
					.075000	1.068000
					.090000	1.066000
					.105000	1.073000
					.105000	1.068000
					.075000	1.072000
					.070000	1.062000

RUN 69 PURE DIATOMIC BISMUTH HELIUM PRESSURE = 000 MM HG CELL LENGTH = 4.6 CM

INPUT DATA FOR RUN

RUN	SET	HE PRESS (MM)	TEMP (°K)	3x AREA	IZERO
69	1900B	0	1238	1.114000	.308000
				.932000	.237000
				.877000	.256000
69	1850A	0	1221	.625000	.164000
				.640000	.169000
				.628000	.180000
69	1800A	0	1187	.965000	.263000
				.967000	.280000
				.927000	.262000
69	1800B	0	1187	.997000	.293000
				1.160000	.328000
				1.131000	.297000
69	1800D	0	1189	1.032000	.140000
				1.038000	.145000
				1.034000	.143000
69	1750A	0	1173	1.120000	.403000
				.785000	.289000
				.842000	.292000
69	1700D	0	1136	.675000	.321000
				.677000	.321000
				.706000	.335000
69	1650A	0	1127	.932000	.495000
				.936000	.479000
				.949000	.514000
				.909000	.512000
69	1600A	0	1090	.722000	.513000
				.727000	.525000
				.759000	.540000
69	1500A	0	1030	.638000	.542000
				.643000	.558000
				.604000	.523000
69	1450D	0	1010	.580000	.535000
				.605000	.544000
				.609000	.556000
				.539000	.498000

RUN 70 PURE LEAD OPTICAL PATH LENGTH= 46 mm HELIUM PRESSURE=000MM AREA/IZERO VS 1/TEMP

INPUT DATA FOR RUN

RUN	SET	HE PRESS (MM)	TEMP (°K)	3x AREA	IZERO
70	2000A	0.	1285.	10.070000	0.965000
				9.640000	0.960000
				10.080000	0.959000
70	1900A	0.	1233.	6.440000	0.980000
				6.060000	0.982000
				6.080000	0.980000
				6.130000	0.962000
70	1800A	0.	1180.	3.400000	0.991000
				3.470000	0.985000
				3.500000	0.975000
				3.630000	0.975000
70	1700A	0.	1128.	1.970000	0.989000
				2.140000	0.988000
				2.040000	0.990000
				2.180000	0.987000
70	1600A	0.	1075.	1.290000	0.996000
				1.310000	0.992000
				1.340000	0.991000
				1.230000	0.983000
70	1500A	0.	1032.	1.040000	1.024000
				1.040000	1.019000
				1.090000	1.015000
				1.110000	1.010000
				1.120000	1.005000
70	1400A	0.	979.	0.790000	0.982000
				0.800000	0.985000
				0.770000	1.005000
				0.800000	1.028000
70	1300A	0.	931.	0.670000	1.047000
				0.680000	1.050000
				0.620000	1.049000
				0.650000	1.048000
				0.670000	1.041000
70	1200A	0.	876.	0.650000	1.053000
				0.590000	0.952000
				0.630000	1.048000
				0.550000	1.012000
70	1150A	0.	853.	0.430000	0.976000
				0.470000	0.970000
				0.500000	0.927000
				0.680000	0.932000
				0.590000	0.985000
				0.440000	1.000000

Run 70, ATOMIC LEAD, Cont'd

	70	1100A	0.	816.	0.300000	0.991000
					0.300000	0.990000
					0.340000	0.999000
					0.360000	0.997000
					0.330000	0.992000
					0.370000	0.998000
					0.380000	0.997000
	70	1050A	0.	808.	0.290000	1.018000
					0.340000	1.018000
					0.280000	1.022000
					0.260000	1.022000
					0.280000	1.030000
					0.270000	1.025000
	70	1000C	0.	783.	0.260000	1.024000
					0.200000	1.021000
					0.170000	1.021000
					0.160000	1.017000
					0.170000	1.013000
					0.220000	1.006000

RUN 70 PURE LEAD OPTICAL PATH LENGTH= 46 mm HELIUM PRESSURE=746MM AREA/IZERO VS 1/TEMP

INPUT DATA FOR RUN

RUN	SET	HE PRESS (MM)	TEMP (°K)	3x AREA	IZERO
70	2000B	746.	1286.	67.809999	0.900300
				65.719999	0.901300
70	1900B	746.	1234.	51.380000	0.938300
				48.050000	0.934300
70	1800B	746.	1179.	33.240000	0.941300
				32.570000	0.937300
				30.990000	0.940300
70	1700B	747.	1127.	22.120000	0.954300
				22.320000	0.953300
				22.290000	0.952300
70	1600B	745.	1075.	14.340000	0.965300
				14.680000	0.964300
				15.110000	0.967300
70	1500B	747.	1032.	10.360000	0.986300
				9.750000	0.971300
				10.080000	0.969300
				10.170000	0.969300
70	1400B	746.	979.	5.990000	1.021300
				6.300000	1.026300
				6.140000	1.018300
				6.440000	1.012300
70	1300B	745.	931.	3.440000	1.050300
				3.420000	1.044300
				3.550000	1.045300
				3.670000	1.040300
12 70	1200B	746.	876.	1.840000	1.020300
11				1.820000	1.020300
				1.850000	1.019300
10				1.910000	1.015300
9 70	1150B	747.	853.	1.360000	0.965300
				1.380000	0.985300
8				1.340000	1.000300
				1.320000	0.996300
7				1.360000	0.980300
6 70	1100B	745.	818.	0.710000	1.014300
				0.630000	1.006300
5				0.660000	1.011300
				0.650000	1.015300
4				0.660000	1.010300

ATOMIC LEAD, Cont'd

Run 70, ATOMIC LEAD, Cont'd

70	10508	745.	809.	0.530000	1.023000
				0.550000	1.020000
				0.560000	1.013000
				0.530000	1.015000
				0.500000	1.018000
70	10000	746.	783.	0.250000	1.025000
				0.260000	1.025000
				0.300000	1.030000
				0.310000	1.027000
				0.310000	1.028000
				0.260000	1.022000

RUN 71 PB IN BI-PB HELIUM PRESSURE = 000 MM HG Cell Length = 4.6 cm

INPUT DATA FOR RUN

RUN	SET	HE PRESS (MM)	TEMP (°K)	3xAREA	IZERO
71	2000C	0	1243	3.830000	.990000
				4.110000	.985000
71	1850A	0	1192	2.200000	.869000
				2.390000	.970000
				2.430000	.947000
				2.680000	.965000
71	1775A	0	1150	1.610000	.966000
				1.500000	.960000
				1.640000	.965000
71	1700A	0	1109	1.290000	1.033000
				1.390000	1.023000
				1.340000	1.015000
71	1625A	0	1070	.940000	.928000
				.840000	.970000
				.900000	.980000
				.900000	.984000
71	1550A	0	1040	.940000	.995000
				.820000	1.000000
				.920000	.995000
				.870000	.997000
71	1475A	0	1007	.850000	.995000
				.860000	.997000
				.810000	.983000
71	1400A	0	967	.640000	.910000
				.580000	.911000
				.690000	.912000
				.530000	.921000

RUN 71 PB IN BI-PB HELIUM PRESSURE = 746 MM HG CELL LENGTH 46 MM

INPUT DATA FOR RUN

RUN	SET	HE PRESS (MM)	TEMP (°K)	3x AREA	IZERO
71	2000D	746	1238	34.460000	.975000
				34.380000	.985000
71	1850B	746	1192	25.170000	.902000
				23.260000	.805000
				26.930000	.889000
71	1775B	746	1145	16.580000	1.034000
				17.370000	1.033000
				18.400000	1.024000
71	1700B	746	1108	13.220000	.970000
				13.440000	.970000
				13.090000	.974000
71	1625B	746	1070	9.470000	.974000
				9.580000	.980000
				9.590000	.976000
				10.090000	.970000
71	1550B	746	1041	7.430000	.990000
				7.710000	.995000
				8.050000	.998000
				7.980000	.996000
71	1475B	746	1005	5.730000	1.010000
				5.970000	1.011000
				5.540000	1.007000
				5.860000	1.005000
71	1400B	746	967	3.850000	.960000
				3.630000	.972000
				3.890000	.970000
				3.890000	.967000

RUN 71 BI IN BI-PB HELIUM PRESSURE = 000 MM HG. Cell Length = 4.6 cm

INPUT DATA FOR RUN

RUN	SET	HE PRESS (MM)	TEMP (°K)	3xA$_R$EA	I$_Z$ERO
71	2000A	0	1243	4.070000	.991000
				4.210000	.992000
				4.450000	.955000
71	1850A	0	1192	2.750000	.943000
				2.820000	.942000
				2.690000	.932000
				2.600000	.920000
71	1775A	0	1150	2.050000	.998000
				2.130000	.990000
				1.910000	.949000
71	1700A	0	1109	1.520000	.957000
				1.420000	.961000
				1.510000	.962000
71	1625A	0	1070	1.200000	1.015000
				1.240000	1.012000
				1.300000	1.024000
				1.220000	.939000
71	1550A	0	1040	1.090000	1.009000
				1.140000	1.008000
				1.050000	1.012000
				1.050000	1.010000
71	1475A	0	1007	.970000	1.019000
				.960000	1.022000
				1.010000	1.025000
				1.050000	1.020000
71	1400A	0	976	.940000	1.030000
				.880000	1.027000
				.900000	1.024000
				.900000	1.015000

RUN 71 BI IN BI-PB HELIUM PRESSURE = 746 MM HG CELL LENGTH 46 MM

INPUT DATA FOR RUN

RUN	SET	HE PRESS (MM)	TEMP (°K)	3x AREA	IZERO
71	2000B	748	1236	29.690000	1.008000
				30.760000	.964000
				29.090000	1.007000
				30.560000	.979000
71	1850B	748	1192	20.900000	.993000
				20.980000	1.007000
				21.370000	.993000
71	1775B	746	1145	14.240000	.963000
				13.970000	.974000
				14.070000	.972000
71	1700B	746	1108	10.500000	.986000
				10.490000	.983000
				10.990000	.993000
71	1625B	746	1070	7.560000	1.022000
				8.180000	1.018000
				7.560000	1.020000
				8.010000	1.017000
71	1550B	746	1041	6.690000	1.010000
				6.580000	1.009000
				6.620000	1.006000
				6.770000	1.003000
71	1475B	746	1005	5.270000	.981000
				5.450000	.985000
				5.100000	.983000
				4.960000	1.015000
71	1400B	746	967	3.590000	1.021000
				3.820000	1.029000
				3.860000	1.038000
				3.540000	1.018000

RUN 71 BI2 IN BI-PB HELIUM PRESSURE = 000 MM HG CELL LENGTH 46 MM

INPUT DATA FOR RUN

RUN	SET	HE PRESS (MM)	TEMP (°K)	IZERO	I NU
71	2000B	0	1243	1.006000	.616000
				1.026000	.622000
				1.031000	.646000
71	1850A	0	1192	.797000	.616000
				.804000	.625000
				.805000	.629000
71	1775A	0	1150	.623000	.553000
				.632000	.547000
				.642000	.545000
				.587000	.519000
71	1700A	0	1109	.932000	.848000
				.928000	.850000
				.940000	.859000
71	1625A	0	1070	.833000	.805000
				.837000	.804000

RUN 71 BI2 IN BI-PB HELIUM PRESSURE = 746 MM HG CELL LENGTH 46 MM

INPUT DATA FOR RUN

RUN	SET	HE PRESS (MM)	TEMP (°K)	IZERO	I NU
71	2000E	748	1236	.763000	.520000
				.735000	.493000
				.747000	.483000
71	1850B	746	1192	.795000	.630000
				.740000	.582000
				.735000	.589000
				.715000	.565000
71	1775B	746	1145	.881000	.775000
				.888000	.770000
				.889000	.790000
71	1700B	746	1108	.866000	.815000
				.878000	.809000
				.854000	.808000
71	1625B	746	1070	.834000	.799000
				.852000	.808000
				.850000	.812000

RUN 72 SI HELIUM PRESSURE = 0 MM HG CELL LENGTH 46 MM

INPUT DATA FOR RUN

RUN	SET	HE PRESS (MM)	TEMP (°K)	3x AREA	IZERO
72	19238	0	1233	9.240000	1.015000
				8.430000	1.019000
				7.200000	1.013000
				7.690000	1.026000
72	18506	0	1.98	5.760000	.981000
				5.340000	1.044000
				6.067000	1.022000
72	17756	0	1465	3.810000	1.020000
				4.180000	1.022000
				3.790000	1.010000
				4.100000	1.043000
72	17008	0	1132	2.700000	1.011000
				2.690000	1.008000
				2.720000	1.000000
72	16258	0	1058	1.910000	1.023000
				1.870000	1.019000
				1.930000	1.026000
72	15508	0	1079	1.370000	.990000
				1.400000	.995000
				1.340000	1.000000
				1.320000	.996000
72	14758	0	1006	1.100000	1.010000
				1.040000	1.010000
				1.100000	1.017000
				1.160000	1.007000
72	14008	0	971	.900000	1.000000
				.950000	1.008000
				.970000	1.011000

RUN 72 BI IN PURE BI HELIUM PRESSURE = 746 MM HG CELL LENGTH 46 MM

INPUT DATA FOR RUN

RUN	SET	HE PRESS (MM)	TEMP (°K)	3x AREA	IZERO
72	1925F	746	1235	48.970000	.960000
				45.160000	.954000
				51.200000	.975000
72	1850B	747	1202	40.340000	1.073000
				39.000000	1.072000
				38.120000	1.070000
72	1775F	747	1165	27.440000	.983000
				27.210000	.999000
				28.060000	1.000000
72	1700B	747	1145	18.680000	.977000
				18.210000	.989000
72	1625F	748	1089	14.090000	.940000
				14.000000	.998000
				13.800000	1.001000
72	1500B	746	1042	9.850000	1.003000
				9.680000	1.002000
				9.750000	1.000000
				9.680000	1.003000
72	1475B	748	1009	7.640000	1.011000
				7.600000	1.012000
				7.170000	1.009000
				7.130000	1.013000
72	1400B	748	972	5.420000	1.021000
				5.290000	1.020000
				5.520000	1.021000

RUN 72 BI2 IN PURE BISMUTH HELIUM PRESSURE = 0 MM HG CELL LENGTH 46 MM

INPUT DATA FOR RUN

RUN	SET	HE PRESS (MM)	TEMP (°K)	IZERO	I NU
72	1925A	0	1233	.935000	.178000
				.955000	.198000
72	1925A	0	1233	.990000	.253000
				.900000	.227000
72	1850A	0	1198	1.185000	.316000
				1.005000	.278000
				1.029000	.283000
72	1775A	0	1163	.810000	.333000
				.792000	.329000
				.814000	.339000
72	1700A	0	1123	.835000	.514000
				.786000	.450000
				.900000	.450000
72	1625A	0	1083	.796000	.597000
				.796000	.593000
				.798000	.592000
72	1550A	0	1043	.930000	.797000
				.936000	.794000
				.937000	.792000
				.935000	.810000
72	1475A	0	1008	.682000	.631000
				.675000	.630000
				.671000	.622000
				.669000	.625000
72	1400A	0	971	.870000	.830000
				.832000	.797000
				.877000	.850000

RUN 72 BI2 IN PURE BISMUTH HELIUM PRESSURE = 746 MM HG CELL LENGTH 46 MM

INPUT DATA FOR RUN

RUN	SET	HE PRESS (MM)	TEMP (°K)	IZERO	I NU
72	1925F	748	1235	.950000	.218000
				.995000	.248000
				.955000	.230000
72	1850B	747	1202	.835000	.213000
				.883000	.235000
				.895000	.237000
72	1775F	747	1165	.983000	.395000
				.973000	.390000
				.966000	.375000
				1.002000	.398000
72	1700B	747	1145	.861000	.502000
				.890000	.503000
				.885000	.514000
72	1625F	748	1089	.854000	.624000
				.835000	.622000
				.850000	.625000
72	1500B	746	1042	.680000	.593000
				.683000	.600000
				.679000	.600000
				.687000	.600000
72	1475B	748	1009	.659000	.619000
				.660000	.609000
				.657000	.613000
72	1400B	748	972	.908000	.880000
				.905000	.872000
				.907000	.871000
				.893000	.858000

RUN 73 BI ABOVE PURE BISMUTH HELIUM PRESSURE = 746 MM HG CELL LENGTH = 46 MM

INPUT DATA FOR RUN

RUN	SET	HE PRESS (MM)	TEMP (°K)	3x AREA	IZERO
73	1925A	751	1231	44.030000	.935000
				43.930000	.952000
				46.360000	.947000
73	1850	749	1216	42.260000	1.000000
				43.990000	1.001000
				44.040000	1.002000
73	1775	748	1179	32.210000	.986000
				31.940000	.983000
				32.690000	.982000
73	1700	747	1144	23.250000	.990000
				23.990000	.984000
				23.510000	.983000
73	1625	745	1104	16.390000	1.002000
				16.010000	.995000
				16.050000	.987000
73	1550	749	1067	11.710000	.995000
				11.710000	.998000
				12.270000	.998000
				11.830000	.998000

RUN 73 BI2 ABOVE PURE BISMUTH HELIUM PRESSURE = 746 MM HG CELL LENGTH = 46 MM

INPUT DATA FOR RUN

RUN	SET	HE PRESS CMMD	TEMP C°K)	IZERO	I NU
73	1925A	751	1231	.758000	.173000
				.732000	.185000
				.715000	.180000
				.735000	.183000
73	1850	749	1216	.490000	.133000
				.498000	.121000
				.483000	.133000
				.493000	.122000
73	1775	748	1179	.631000	.225000
				.628000	.220000
				.648000	.231000
				.638000	.221000
73	1700	747	1144	.787000	.393000
				.794000	.395000
				.779000	.386000
				.777000	.397000

BIBLIOGRAPHY

1. Almy, G. M. and Sparks, F. M., Phys. Rev., 44, 365-75 (1933).

2. Bell, G. D., Davis, M. H., King, R. B., and Routly, P. M., Astrophys, J., 127, 775 (1958).

3. Brackett, E. and Brewer, L., University of California Radiation Laboratory, Report 3712 (March 8, 1957).

4. Brodersen, Svend, J., Op. Soc. Am., 44, 22 (1954).

5. Cosgarea, A., Hucke, E. E., and Ragone, D. V., Acta Met., 9, No. 3, 225 (1961).

6. Elasser, W. M., Harvard Meteorological Studies, No. 6, Harvard University, 1942.

7. Engler, Hans D., Zeit. f. Phys., 144, 343 (1956).

8. Gonser, U., Zeit. Physik. Chem. (Frankfurt), 1, 1-20 (1954).

9. Heitler, W., Quantum Theory of Radiation, 3rd ed., Oxford University Press, 1954.

10. Herbenar, A. W., Siebert, C. A., and Duffendack, O. S., Trans. AIME, 188, 323 (1950).

11. Hirst, L. L. and Olson, A. R., J. Am. Chem. Soc., 51, 2398 (1929).

12. Kostkowski, H. J. and Bass, A. M., J. Op. Soc. Am., 46, No. 12 (1956).

13. Landenburg, R. and Levy, S., Zeit. f. Phys., 65, 189 (1930).

14. Minkowski, R., Zeit. f. Phys., 36, 839 (1926).

15. Mitchell, A. C. S., and Zermansky, M. W., Resonance Radiation and Excited Atoms, Cambridge University Press, 1961.

16. Penner, S. S., Quantitative Molecular Spectroscopy and Gas Emissivities, Addison-Wesley Publishing Co., Inc., 1959.

17. Plass, G. N., J. Op. Soc. Am., 48, No. 10, 690 (1958).

18. Rice, P. A., Balzhiser, R. E., and Ragone, D. V., Thermodynamics of the Uranium-Bismuth System, International Atomic Energy Association's Symposium on Nuclear Materials, May 1962.

19. Rodebush, W. H. and Dixon, A. L., J. Am. Chem. Soc., 47, 1036 (1925).

20. Rodebush, W. H. and Dixon, A. L., Phys. Rev., 26, 851 (1925).

21. Scatchard, G. and Westland, R. A. Jr., J. Am. Chem. Soc., 75, 4189 (1953).

22. Scatchard, G. and Boyd, R. H., J. Am. Chem. Soc., 78, 3889 (1956).

23. Schutz, Wilhelm, Zeit. f. Astrophys., 1, 300 (1930).

24. Van der Held, E. M. F., Zeit, f. Phys., 70, 508 (1931).

25. Vidale, G. L., Technical Information Series, Reports Nos. R60SD330, R60SD331, R60SD333, R60SD390, Space Sciences Laboratory, General Electric Missile and Space Vehicle Dept., Philadelphia, Pa., 1960.

26. Wagner, C. and Engelhard, G. Zeit. Physik. Chem., 159, 241 (1932).

27. Yoshiyama, S., J. Chem. Soc. Japan, 62, No. 8, 204-7 (1941).

28. Stull, D. R. and Sinke, G. C., Thermodynamic Properties of the Elements, American Chemical Society, Washington, D. C., 1956.

29. Mrozowski, S., Phys. Rev., 62, 526 (1942).

UNIVERSITY OF MICHIGAN
3 9015 03525 0953